

**SIMULATION BASED DESIGN OF LITHIUM ION BATTERY  
CONFIGURATION USING BAYESIAN OPTIMIZATION**

A Thesis  
Presented to  
The Academic Faculty

by

Dong Yeon Yoo

In Partial Fulfillment  
Of the Requirements for the Degree  
Master of Science in Mechanical Engineering

Georgia Institute of Technology  
August 2018

Copyright © 2018 by Dong Yeon Yoo

**SIMULATION BASED DESIGN OF LITHIUM ION BATTERY  
CONFIGURATION USING BAYESIAN OPTIMIZATION**

Approved by:

Dr. Yan Wang, Advisor  
School of Mechanical Engineering  
*Georgia Institute of Technology*

Dr. Hailong Chen  
School of Mechanical Engineering  
*Georgia Institute of Technology*

Dr. Seung Woo Lee  
School of Mechanical Engineering  
*Georgia Institute of Technology*

Date Approved: May 18<sup>th</sup>, 2018

## ACKNOWLEDGEMENTS

First of all, I would like to sincerely thank my advisor, Dr. Yan Wang, for his knowledge and insightful guidance that have provided me with the basis and direction for this work. He has constantly provided me with the motivation to push my knowledge further in this specific field and have always had answers to my questions. His endless support and trust during my undergraduate and graduate studies at Georgia Tech has made the completion of my degree possible.

I would also like to thank my thesis committee members, Dr. Hailong Chen and Dr. Seung Woo Lee, for their time reviewing my master's thesis as well as for their valuable feedback during my defense. I also want to express my gratitude to all members in Dr. Wang's Multi-Scale Systems Engineering Research Group, especially Anh Tran, for their feedback during weekly presentation meetings. I have grown to become a better presenter as I have gained confidence in communicating my knowledge to others. I want to emphasize that Anh Tran's support regarding this work on Bayesian optimization for the past two semesters have been crucial and helpful. He was never hesitant to help and answer my questions. I will always remember your help and support.

Finally, I would like to thank my parents who have provided me with everything in life - without them, I would not be where I am right now. They have provided me with wings when I was struggling on the ground - I could not ask for better parents. Lastly, I thank my girlfriend, Jeyoung Oh, for all the emotional support during times of my hardship as well as academic advice as someone who is already on track to pursue a career in academia. You have been present during my struggle, so you deserve to be present during my success. Thank you everyone.

# TABLE OF CONTENTS

<b>ACKNOWLEDGEMENTS .....</b>	<b>iii</b>
<b>LIST OF TABLES .....</b>	<b>vi</b>
<b>LIST OF FIGURES .....</b>	<b>vii</b>
<b>SUMMARY .....</b>	<b>x</b>
<b>CHAPTER 1. INTRODUCTION .....</b>	<b>1</b>
<b>CHAPTER 2. BACKGROUND.....</b>	<b>5</b>
2.1. Manufacturing of Lithium Batteries.....	6
2.2. Design Parameters in Battery .....	10
2.3. Electrode.....	11
2.3.1. Thickness .....	11
2.3.2. Surface-to-Volume Ratio, Density, and Porosity .....	18
2.3.3. Particle Size .....	25
2.3.4. Tortuosity .....	30
2.3.5. Cathode-Anode Area Ratio.....	31
2.3.6. Cathode-Anode Mass Ratio .....	32
2.3.7. Surface Texture.....	33
2.3.8. Volumetric Expansion Ratio.....	34
2.3.9. Cathode-Anode Layout and Configuration.....	34
2.3.10. Geometry-Materials Correlation .....	40
2.4. Electrolyte .....	41
2.4.1. Electrolyte-Electrode Configuration.....	41
2.4.2. Ion Transport Path.....	42
2.4.3. Separator Membranes .....	43
2.5. Current Collector.....	44
2.5.1. Geometry.....	44
2.5.2. Electrode-Collector Configuration.....	49
2.6. Modeling and Simulation Tools.....	49
2.7. Electrochemical, Thermal, and Mechanical Models.....	50
2.8. Application of Commercial Simulation Packages .....	51
2.9. Atomistic Modeling.....	51
2.10. Equivalent Circuit Model .....	52
2.11. Design Optimization.....	53

2.11.1.	Optimization Methods with Multiple Design Parameters.....	53
2.11.2.	Sensitivity Informed Optimization.....	54
2.11.3.	Sequential Quadratic Programming .....	55
2.11.4.	Direct Search Method.....	56
2.11.5.	Particle Swarm Optimization .....	57
2.11.6.	Surrogate Based Optimization .....	58
2.11.7.	Optimization via Sensitivity Analysis.....	61
2.11.8.	Hybrid Optimization .....	64
2.12.	Other Design Objectives.....	64
2.12.1.	Capacity Fade .....	65
2.12.2.	Cell Temperature Distribution .....	67
2.13.	Topology Optimization.....	68
2.14.	Multi-Objective Optimization .....	73
<b>CHAPTER 3. SIMULATION-BASED DESIGN OPTIMIZATION METHODOLOGY...</b>		<b>77</b>
3.1.	Battery Electrochemistry.....	77
3.2.	Bayesian Optimization .....	79
3.3.	Gaussian Process .....	80
3.4.	Acquisition Functions .....	82
3.5.	Parallelization of Bayesian Optimization.....	85
<b>CHAPTER 4. DEMONSTRATION AND OPTIMIZATION RESULTS .....</b>		<b>87</b>
4.1.	One-Dimensional (1D) Model Simulation.....	87
4.2.	Two-Dimensional (2D) Model Simulation .....	94
4.2.1.	2D Model with Variable Electrode-Electrolyte Interface.....	97
4.2.2.	2D Model with Multiple Electrodes .....	108
<b>CHAPTER 5. CONCLUSION AND FUTURE WORKS .....</b>		<b>114</b>
5.1.	Accomplishments and Contribution.....	114
5.2.	Future Work .....	116
<b>REFERENCES.....</b>		<b>118</b>

## LIST OF TABLES

Table 2.1 List of design parameters for each battery component .....	10
Table 2.2. Averaged specific capacities at different cycling rates of 2-4 $\mu\text{m}$ and 5-10 $\mu\text{m}$ $\text{LiCoO}_2$ particle size distribution [51]. .....	28
Table 2.3. Different particle size distributions [52]. .....	30
Table 4.1. For each case, different values have been assigned for the above parameters [35]. ...	96

## LIST OF FIGURES

Figure 1.1 Block diagram of a battery cell that shows flow of electrons from anode to cathode through an external load [28].	1
Figure 2.1. Current lithium ion battery manufacturing processes [28, 29].	9
Figure 2.2. (a)-(c) Simulated discharge curves and (d) rate performance under various discharge rates and NMC electrode thicknesses [30].	13
Figure 2.3. Comparison of discharge capacities and volumetric energy density of full cells containing 70 $\mu\text{m}$ , 105 $\mu\text{m}$ , 155 $\mu\text{m}$ , 205 $\mu\text{m}$ , 255 $\mu\text{m}$ and 305 $\mu\text{m}$ thick electrodes at different C-rates [31].	14
Figure 2.4. Curve graph that shows how specific energy is related to electrode thickness where three porosity values in relation to the DOE goal is shown [41].	20
Figure 2.5. Values of porosity and their effects in terms of electronic and ionic conductivity [46].	21
Figure 2.6. Rate capability and cycle performance of $\text{LiCoO}_2$ cathodes with thickness (T) of (a) 20 $\mu\text{m}$ , (b) 35 $\mu\text{m}$ and (c) 50 $\mu\text{m}$ for different densities (D) [44].	22
Figure 2.7. Specific discharge capacity from $\text{LiMn}_2\text{O}_4$ powders of different particle sizes [49].	26
Figure 2.8. $\text{LiMn}_2\text{O}_4$ capacity-voltage curves with varying particle size at 0.2 $\text{mA}/\text{cm}^2$ [53].	26
Figure 2.9. $\text{LiCoO}_2$ particle size effect on cycle stabilities: (O) 2-4 $\mu\text{m}$ , and ( $\Delta$ ) 5-10 $\mu\text{m}$ [51].	28
Figure 2.10. Different coin cells with varying electrode area ratios [59].	32
Figure 2.11. (Top panels) Four different cathode-anode array arrangements with their respective isopotential lines and current densities at electrode surfaces. Electrode areas are constant for each arrangement [65].	36
Figure 2.12. Possible three dimensional (interdigitated, trench, concentric, aperiodic) battery architectures [66].	37
Figure 2.13. Concentration profile development in the 3D-trench design. Top electrode: positive. Bottom electrode: negative. (left) Conductivities for both electrodes are 1 S/m, (right) Conductivities are 1 S/m for negative and 0.01 S/m for positive [66].	38
Figure 2.14. The number of digits vary while the area of each component remains constant [68].	40
Figure 2.15. Voltage as a function of delivered capacity for varied porosity $\epsilon$ with scan rate of a) 0.15C and b) 5C [72].	44

Figure 2.16. Different placements and geometries of current collector tabs (unit: mm) [73].	46
Figure 2.17. Electrode-collector configurations: (a) types A–F, (b) type G, and (c) type H [85].	49
Figure 2.18. Energy density as a function of positive electrode thickness and porosity [131].	57
Figure 2.19. Design objective for different microstructures: $b=1.6$ , $q=2.5, 7.5, 15, 25, 40$ [161].	71
Figure 2.20. The Pareto front for the multi-objective optimal topologies for volume fraction of Base cell (A) and shifted base cell with higher Pareto weights (B) [162].	73
Figure 4.1 One-dimensional solid-state lithium battery showing the electrolyte, positive electrode and the interfaces in between	87
Figure 4.2. Four battery models discharged for $t=50s$ with different thicknesses are compared as initial study of thickness parameter effects: a) $L_{negative}=2.5\mu m$ ; $L_{separator}=135\mu m$ ; $L_{positive}=2.5\mu m$ (1.79% : 96.4% : 1.79%); b) $L_{negative}=5\mu m$ ; $L_{separator}=130\mu m$ ; $L_{positive}=5\mu m$ (3.57% : 92.86% : 3.57%); c) $L_{negative}=20\mu m$ ; $L_{separator}=100\mu m$ ; $L_{positive}=20\mu m$ (14.3% : 71.4% : 14.3%); d) $L_{negative}=55\mu m$ ; $L_{separator}=30\mu m$ ; $L_{positive}=55\mu m$ (39.3% : 21.4% : 39.3%)	89
Figure 4.3. Battery voltage vs. Number of Iterations scatter plot for 1D lithium battery model using Bayesian Optimization	91
Figure 4.4. Truncated Bayesian Optimization plot for Figure 4.3 upto 200 iterations	92
Figure 4.5. Battery voltage vs. negative electrode thickness scatter plot for 1D lithium battery model using Bayesian Optimization	92
Figure 4.6. Battery voltage vs. electrolyte thickness scatter plot for 1D lithium battery model using Bayesian Optimization	93
Figure 4.7. Battery voltage vs. positive electrode thickness scatter plot for 1D lithium battery model using Bayesian Optimization	93
Figure 4.8. Geometry of solid-state battery: 10,000 nm in length and 1820 nm in thickness [35].	95
Figure 4.9. A 2D lithium ion battery geometry with uneven cathode-electrolyte interface and its corresponding discharge curve.	98
Figure 4.10. A 2D lithium ion battery geometry with uneven cathode-electrolyte interface (left) and surface electrolyte salt concentration contours (cut-off at $t=636s$ )	99
Figure 4.11. A 2D lithium ion battery geometry with uneven cathode-electrolyte interface (left) and surface electrolyte salt concentration contours (cut-off at $t=622s$ )	99
Figure 4.12. Electric potential discharge curves for Figure 4.10 (left) and Figure 4.11 (right)	100

Figure 4.13. 2D battery geometry with uneven positive electrode boundary .....	100
Figure 4.14. Electrolyte Salt Concentration and Electrical Potential (cut-off at t=628s).....	101
Figure 4.15. Electrolyte Salt Concentration and Electrical Potential (cut-off at t=1128s).....	101
Figure 4.16. Electrolyte Salt Concentration and Electrical Potential (cut-off at t=1421s).....	102
Figure 4.17. a) Electrolyte Salt Concentration and Electrical Potential with cut-off time at t=477s; b) Electrolyte Salt Concentration and Electrical Potential with cut-off time at t=984s; c) Electrolyte Salt Concentration and Electrical Potential with cut-off time at t=1571s .....	103
Figure 4.18. A three-dimensional representation of an interdigitated battery model [174]. .....	105
Figure 4.19. Variable-interface model with inconsistent electrolyte thickness .....	105
Figure 4.20. Battery voltage vs. Number of Iteration scatter plot for the Bayesian optimization of a 2D lithium battery model with variable electrode-electrolyte interface. The geometries indicate the models that generated the three highest and lowest battery voltages. ....	107
Figure 4.21. Battery Voltage vs. Number of Iterations scatter plot for 2D lithium battery model with two electrodes using Bayesian Optimization. The geometries indicate the models that generated the three highest and lowest battery voltages .....	111
Figure 4.22. Battery voltage vs. Number of Iterations scatter plot for 2D lithium battery model with four electrodes using Bayesian Optimization. The geometries indicate the models that generated the four highest and lowest battery voltages. ....	112

## SUMMARY

The performance of a lithium ion battery is determined not only by materials of electrode and electrolyte, but also by geometry and topology of the battery cell structure. Each individual component of the battery can be specified with certain design parameters, which in turn determine the performance of the complete battery. In this thesis, major geometric parameters that have major influence on battery performance are identified. Existing research studies show that design parameters associated with geometry and topology can affect battery performance. A new global optimization technique, Bayesian optimization, is utilized to search the optimum geometric parameters such as electrode thickness and electrode-electrolyte interface. Electrochemical models of lithium ion batteries are applied to predict properties. This investigation has demonstrated that Bayesian optimization is an efficient method to perform battery components and configuration design.

## CHAPTER 1. INTRODUCTION

With higher power density and longer cycle life relative to other battery types, the lithium-ion battery is the preferred major source of power for applications such as electronic devices, electric vehicles, aerospace vehicles, and many others [1, 2, 3, 4, 5]. The major components of battery include the anode, cathode, electrolyte, and the current collector, as shown in Figure 1.1. During the discharge process, lithium ion moves from anode to cathode across the electrolyte. While charging, the transport direction is reversed. The commonly used materials for electrodes include lithium ion phosphate ( $\text{LiFePO}_4$ , or LFP), lithium ion manganese oxide ( $\text{LiMn}_2\text{O}_4$ ,  $\text{Li}_2\text{MnO}_3$ , or LMO), lithium nickel manganese cobalt oxide ( $\text{LiNiMnCoO}_2$  or NMC), and lithium titanate ( $\text{Li}_4\text{Ti}_5\text{O}_{12}$  or LTO), compounded with graphite to increase conductivity [6, 7, 8]. Liquid electrolytes are typically lithium salts (e.g.  $\text{LiPF}_6$ ) in organic solvent [9]. Solid-state gel types of electrolytes have also been proposed.

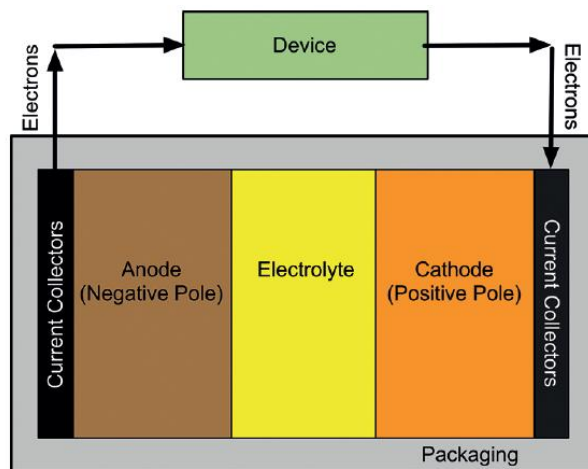


*Figure 1.1 Block diagram of a battery cell that shows flow of electrons from anode to cathode through an external load [28].*

The usage of lithium-ion batteries is ubiquitous, but there still exists research challenges designing batteries which have high power density and long lifespan, and are also safe and environmentally friendly [10, 11]. Most of the research until now emphasized on battery materials, where novel materials and compounds are introduced to enhance the performance of the four components [12, 13, 14, 15, 16] in the battery. However, materials are not the only factor that affect the battery performance. Recently, researchers have started to realize that in order to optimize battery systems, geometry and topology of the components also have profound effects on the performance of the system.

Most of the current battery systems are manufactured into a sandwich or a pouch form [17, 18, 19, 20] to maximize the surface contacts between components. There are also batteries that have components rolled up in the manufacturing process and placed inside a metal canister to form a cylindrical shape that resembles commercial alkaline batteries today. Although the pouch and cylindrical batteries appear seemingly different from the outside, the internal geometries and the way they are manufactured are identical. The efforts by the battery manufacturing industry over the years to reduce manufacturing costs and time for increased production efficiency has resulted in these batteries having a common internal structure where the thickness of each component is consistent throughout the cross-sectional area. A battery with electrodes and electrolyte of equal thickness that are stacked on top of each other to form a sandwich structure may be cost-effective and easy to produce, but it is not optimized in terms of battery performance. The recent advancements in the battery manufacturing industry to manufacture battery components using additive manufacturing process has shown a promising possibility that batteries do not necessarily need to possess a stacked sandwich shape with consistent thicknesses throughout the battery cross-

section. With the use of advanced, rapid 3D printers, complex battery shapes and dimensions, once thought to be impossible have been proven to be achievable.

Having introduced the definition of a lithium battery, its current limitations as well as a potential direction of improvement for better performance, it is important to discuss how this can be realizable. For battery design and optimization, the best combination of design parameters need to be obtained so that battery performance can be optimized. The battery design is an iterative searching process. The major research challenges of design optimization include the selection of several quantitative measures as objective functions for optimization and trade-off between them, as well as the consideration of multiple significant parameters in higher dimensional spaces. Various optimization algorithms and methods have been applied to optimize battery performance, where the best combination of design parameters is sought. Both gradient-based and gradient-free algorithms have been applied. The most commonly used objective is energy density of battery cell, where improving the performance is the most important goal. Another one is the mass or weight of battery, where reducing weight is important for applications. If multiple design objectives are involved, multi-objective optimization methods are needed.

Using a set of different input geometrical parameter values for each experimental trial may provide a holistic relationship between the parameters and the output and how varying one affects the other, but it cannot be determined whether a certain value is the best or optimized for that given situation. That is because although a minimum or a maximum input parameter may be determined but one cannot confirm whether it is local or global. A seemingly linear relationship between input and output correlation may suddenly become exponential when the input approaches zero. Multiphysics simulation software tools such as COMSOL Multiphysics simulation tools provide the option of parametric sweep that allows the user to automatically solve the model using different

input variables to find the design's optimum instead of altering the property and parameter values manually and solving the model after every change. However, this is not efficient as parametric sweep does not incorporate any optimization scheme that intelligently searches for an optimal value. It simply passes the same model through a range of a specific geometric parameter one at a time over a range of input values. Because the parametric sweep function uses a rather 'brute force' method to go through every single parameter, it is hence inefficient. To effectively determine which value of a specific geometric parameter of interest will result in the best performance, whether it is maximizing or minimizing a particular output value, an optimization algorithm is used.

The primary contribution of this thesis includes: 1) the systematic investigation of major geometry related design parameters in lithium-ion battery design, and 2) effective application of Bayesian optimization to the optimization of specific geometric parameter of a lithium ion battery. What is new in this work is the effective usage of Bayesian optimization algorithm that sequentially determines the optimal of the unknown black-box functions by determining at which input value is necessary to achieve the maximum or minimum of a particular output.

The problem or the goal to optimize a specific parameter can be considered as a complex black-box function which is unknown and the Bayesian strategy considers it as a random function and places a prior over it. A prior is a belief of the function's behavior which is used to determine a posterior distribution over the function that will eventually determine what the next value will be. Simply, the Bayesian optimization uses previous iterations of random inputs to determine a trend which to follow in order to select where to look next. It is effective in the sense that not all values need to be investigated one by one to determine the optimized value for a given battery simulation model.

## CHAPTER 2. BACKGROUND

In this literature review section of the thesis, a comprehensive discussion of structural design and optimization for battery is given, where existing studies of the effects of geometric parameters on battery performance are summarized. It is necessary to identify the important design parameters available for performance optimization and the available design optimization methods that researchers can employ. To fully investigate key parameters in order to improve battery performance, either physical experiments or computational simulations can be conducted to measure the parameters' optimum. Since repetitive physical experiments are often time consuming and expensive, computational simulations are the economical alternative. The main objective of simulation is to quickly quantify the sensitivity of design parameters on the battery performance and subsequently generate guidelines for more selective experimental investigation and validation. Various analytical and simulation models were made to analyze and predict battery performance since 1970s. Plenty of work has been done in modeling and simulation of battery behaviors and properties. These include electrochemical transport models that capture the diffusion of Li ions in porous solid electrode and liquid electrolyte solution [21, 22], thermal property where heat is generated and dissipated during charging and discharging [23, 24], and electromechanical behavior [25]. However, the studies of how to systematically perform structural design and optimization based on simulations are still limited.

The objective of this review is to provide a holistic view of important geometric and topological parameters for battery design and the methods that have been applied in design optimization. In Section 2, a review of existing work on analyzing the effect of geometric parameters in battery is given, where papers are categorized based on the design parameters. Section 3 introduces the major modeling and simulation techniques at multiple scales used in

battery designs, specifically on electrochemical, thermal, and atomistic models. In Section 6, existing work of design optimization is reviewed.

## **2.1. Manufacturing of Lithium Batteries**

The effect of thickness of lithium ion battery components have been investigated by many literature papers in the past. Changes in the thickness of the positive electrode, negative electrode and electrolyte all have an impact in both the electrochemical battery performance as well as in terms of thermal effects. The manufacturing techniques of state-of-the-art batteries today have been optimized specifically for production rate improvements and high delivery targets to meet the world's demand for lithium ion batteries. There are many types of battery manufacturing techniques that are currently implemented in various battery production plants, but the most common is focused in the manufacturing of cylindrical and pouch cells.

First is the cylindrical or the roll-up type that has an exterior form of a typical off-the-shelf alkaline battery but with lithium ion battery constituents inside. This is also often referred to as a cylindrical battery. The second common type that is widely used in portable electronics is the pouch type that has a thin form with a rectangular shape, suitable for applications such as smartphones and mobile devices. The manufacturing processes for both cylindrical and pouch type batteries share many common processes. In a typical fabrication process, the electrode materials are amalgamated in their respective combinations to form what is known as a slurry. Besides the active materials, additional materials such binders that hold the electrode in place, carbon black and graphite that enhance conductivity as well as a solvent to dissolve the binder completely are included in the slurry. Once the distribution of the constituents has reached homogeneity through a thorough and continuous mixing process, the mixture is then spread evenly as a coating over the current collector material. The active electrode materials are coated with metallic foils that act as

current collectors. As the electrode materials are slowly poured over the current collectors, it immediately goes through the compressing stage or the calendaring process through which the solvent is pressed and desiccated completely in the drying tunnel at a temperature of up to 150°C. The purpose of this process is to minimize the porosity while achieving desired target thickness.

Once each of the electrodes are bound to their respective current collectors, they are then stacked on top of each other, precisely overlapping the area of the component below, with the separator in the middle. For the cylindrical cell, bending or curving is applied to this stack and is slowly rolled into a form of a cylinder that can be placed inside the cell canister for permanent packaging. Once placed inside the canister, the electrolyte is introduced and injected inside before the pouch is finally sealed off from the external environment. For the case of the pouch cell, the stack is not rolled up, but rather cut according to desired pouch dimensions. It is then placed in a hermetic, waterproof pouch, after which electrolyte is filled. For both cases of the battery, it is important to remove any remaining air inside the cell, hence the air is completely removed inside a vacuum chamber.

Besides the previously mentioned manufacturing techniques, three other manufacturing techniques are also widely used. Spray printing using highly atomized ink through compressed gas has been shown to be able to produce batteries by Singh et al [29]. By depositing active materials through a spray, electrodes are deposited layer by layer between which the materials are quickly dried as they are deposited. Another method is stencil printing which is a method used by Gaikwad et al. [26, 27, 28] that utilizes a laser cut stencil that is predesigned into the desired shape of the final battery. Once the stencil is placed firmly over the substrate and is fixed, the active battery material is poured above it slowly until the material takes complete form of the stencil shape. Afterwards, a squeegee is used to drag the material and spread over the shape area so that the

stencil is completely and evenly filled without any void. The squeegee set parallel to the deposit bed and is slowly dragged from one end of the stencil to the other, during which the excess material is removed once the squeegee reaches the end. The thickness of the stencil can be changed to change printed layer thickness. Similar to spray printing, inkjet printing is also another common method that requires the battery's active materials to be placed inside an ink cartridge which is then used to print the material inside the cartridge chamber that is very similar to the functionality of today's conventional inkjet printers. The fine nozzle of the inkjet cartridges, often between 35 and 70  $\mu\text{m}$ , provides exceptional precision and accuracy while maintaining cost-effectiveness. One distinct advantage of inkjet printing, as compared to the existing battery manufacturing method, is the fact that there is no wasted material in the fabrication process. In a conventional battery manufacturing process, a lot of material is wasted when the electrodes on the current collectors are cut up into desired shapes and whatever material that are beyond the bounds of the battery shape are not utilized but disposed. [29].

With recent rapid advancements in the battery manufacturing industry, many attempts have been made to manufacture battery components using the additive manufacturing process. Specifically, with the use of advanced, rapid 3D printers, complex battery shapes and dimensions, once thought to be impossible, have been proven to be achievable. Sun et al. have used additive manufacturing to develop a novel 3D interdigitated battery. The stage of preparing the electrodes in the form of a slurry is similar to the existing manufacturing methods. Specifically, Sun et al. used  $\text{Li}_4\text{Ti}_5\text{O}_{12}$  (LTO) as anode material and  $\text{LiFePO}_4$  (LFP) as cathode material in the form of fine powder. These nanoparticle powders are then suspended in ethylene glycol, glycerol as well as viscosifiers, and then centrifuged together to form a homogenous colloid. Then through a 30  $\mu\text{m}$  diameter nozzle at the tip of two 3 mL barrel syringes for each of the two electrodes, the

electrodes are then printed on to the current collectors that have been patterned on a glass substrate through lithographic patterning and electron beam deposition. Achieving a varied thickness along the width or length of the complete lithium ion battery is achievable. Past literature has investigated the effects of thickness of each component and how it affects the battery's performance. However, there has been a lack of research in how cells with variable thicknesses affect performance.

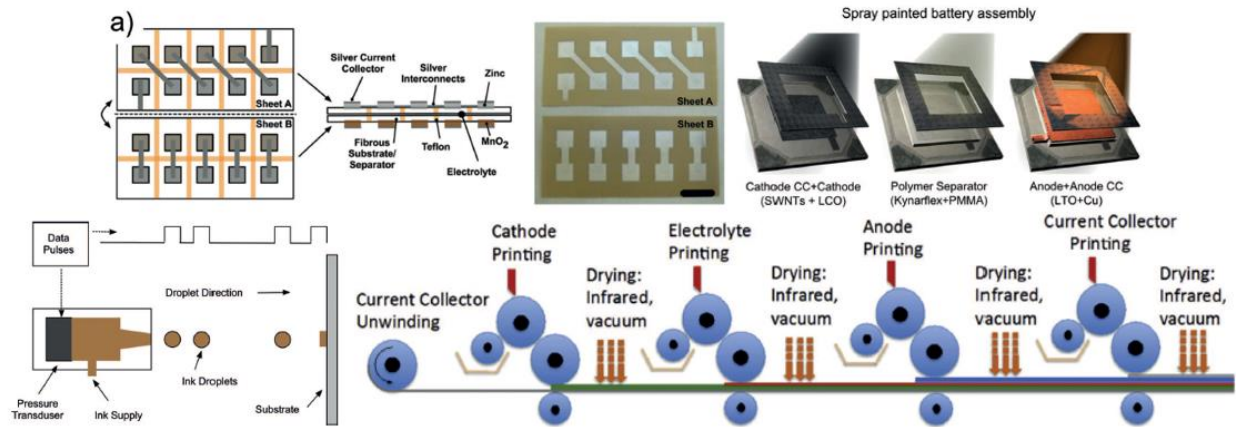


Figure 2.1. Current lithium ion battery manufacturing processes [28, 29].

There is one concept that is common in these battery manufacturing processes shown in Figure 2.1. Besides the fact that each process involves the manufacturing and combining of individual battery components, it is also common fact that each process are manufacturing the batteries so that the thickness of the three components are constant through out the battery. The cross section of a cut open lithium ion battey will look identical.

## 2.2. Design Parameters in Battery

The geometric parameters in a battery that have significant impacts on its performance include thickness, surface-to-volume ratio, cathode-anode area ratio, mass ratio, electrode density, particle size, porosity, tortuosity, current collector geometry and configurations. Among them, thickness, surface-to-volume ratio, area ratio, mass ratio, electrode densities, and particle size have been reported as crucial parameters that determine battery performance. Different geometric parameters of electrolyte, current collectors, and separators also have major effects in enhancing energy potentials. Important parameters of different components in a lithium-ion battery are listed in Table 2.1. Moreover, other design parameters which are related to material characteristics, such as lithium diffusivity, current density, and separator membranes, are also included.

*Table 2.1 List of design parameters for each battery component*

<b>Geometric Parameters</b>			<b>Other Design Parameters</b>
<b>Electrode</b>	<b>Electrolyte</b>	<b>Current Collector</b>	
<i>Thickness</i>	<i>Layer Thickness</i>	<i>Shape</i>	<i>Geometry-Materials Correlation</i>
<i>Surface-to-Volume Ratio, Density, Porosity</i>	<i>Electrode-Electrolyte Configuration</i>	<i>Location</i>	<i>Current Density</i>
<i>Cathode-Anode Area Ratio</i>	<i>Ion Transport Path</i>		<i>Separator Membranes</i>
<i>Cathode-Anode Mass Ratio</i>	<i>Shape of Solid-State Electrolyte</i>		
<i>Surface Texture</i>			
<i>Particle Size</i>			
<i>Tortuosity</i>			
<i>Electrode Layout</i>			

### **2.3. Electrode**

The battery's functionality relies heavily on the performance of each individual battery component, especially on the design parameters of electrodes because there are many parameters affecting battery performance. Meticulous attention is necessary to study the effects of each design parameter pertaining to the electrode to quantitatively analyze the overall performance. In addition, the relationship between parameters must be determined to effectively optimize the battery performance.

#### *2.3.1. Thickness*

Battery performance such as overall heat generation, energy density, and capacity fading rate is closely tied to electrode thickness. The thickness variation can change ion diffusion length and the internal resistance, affecting both the thermal and electrochemical performance [30]. The battery that consisted of a thicker electrode tends to possess higher heat and high temperatures during discharge resulting in the reduction of lifespan and capacity utilization, in addition to the introduction of potential safety risks. Zhao et al. [31] performed experimental and simulation studies to observe how electrode thickness effects thermal and electrochemical properties. During discharge, it was shown that the battery with thin electrodes displayed lower average resistance than batteries with a relatively thicker electrode. In terms of fading rate, the battery with thinner electrodes shows overlapping results for different numbers of cycles, which demonstrates consistent electrochemical reactions in ignorance of proceeding discharges. However, the discharge process stops earlier as the number of cycle increases for batteries with thicker electrodes because it possesses higher internal resistance that results in decreased power output. Thicker electrodes ultimately result in more movements of lithium ions during reaction, which leads to

generation of high ohmic heat. The highly uneven thermal response leads to degradation of performance and increase of safety risk. Although it is commonly believed that a battery with thicker electrodes would have increased amount of active materials and thus improved energy density, there are negative effects that need to be prevented including the degradation of thermal and electrochemical properties.

Electrode thickness also influences rate capabilities, power and energy densities according to Zheng et al. [32]. A thorough review of the thickness effect is crucial in formulating good quality electrodes. An increase in electrode thickness results in a higher Peukert coefficient and greater capacity loss due to diffused lithium ions. The internal resistance increases with distance, and better energy density can be achieved with a thicker electrode at the sacrifice of a lower power density. The relationship among the electrode thickness, discharge capacity, relative discharge rate (C-rate) was revealed. Zheng et al. compared the performance of conventionally fabricated nickel-manganese-cobalt cathodes with thicknesses up to 108  $\mu\text{m}$  and active material content percentage of 85%. It was shown that thinner electrodes can produce cell's capacity at much higher rate, whereas thicker electrodes exhibit a lower rate. The lithium iron phosphate cathode of 10  $\mu\text{m}$  discharges at a high rate of 100C, whereas the cathode of same material with a 108  $\mu\text{m}$  thickness discharges merely at 2C. A higher C-rate results in a lower discharge curve caused by internal resistance polarization. Thinner electrodes deliver maximum capacity at a high rate, while capacity and rate decrease in thicker electrodes despite higher capacity fading-rate. The thickness also influences the weight specific impedance, where the internal resistance increases with a greater electrode thickness.

Xu et al. [33] used electrode thicknesses between 30  $\mu\text{m}$  and 120  $\mu\text{m}$  to observe thickness effects on rate capability. In addition, thicknesses greater than 60  $\mu\text{m}$  have proven to have a

profound effect in cell utilization as the utilization declines sharply between 1C and 3C. The utilization is near zero for thicknesses of 105  $\mu\text{m}$  and 120  $\mu\text{m}$ , largely caused by increased diffusion length that inhibits ion transport.

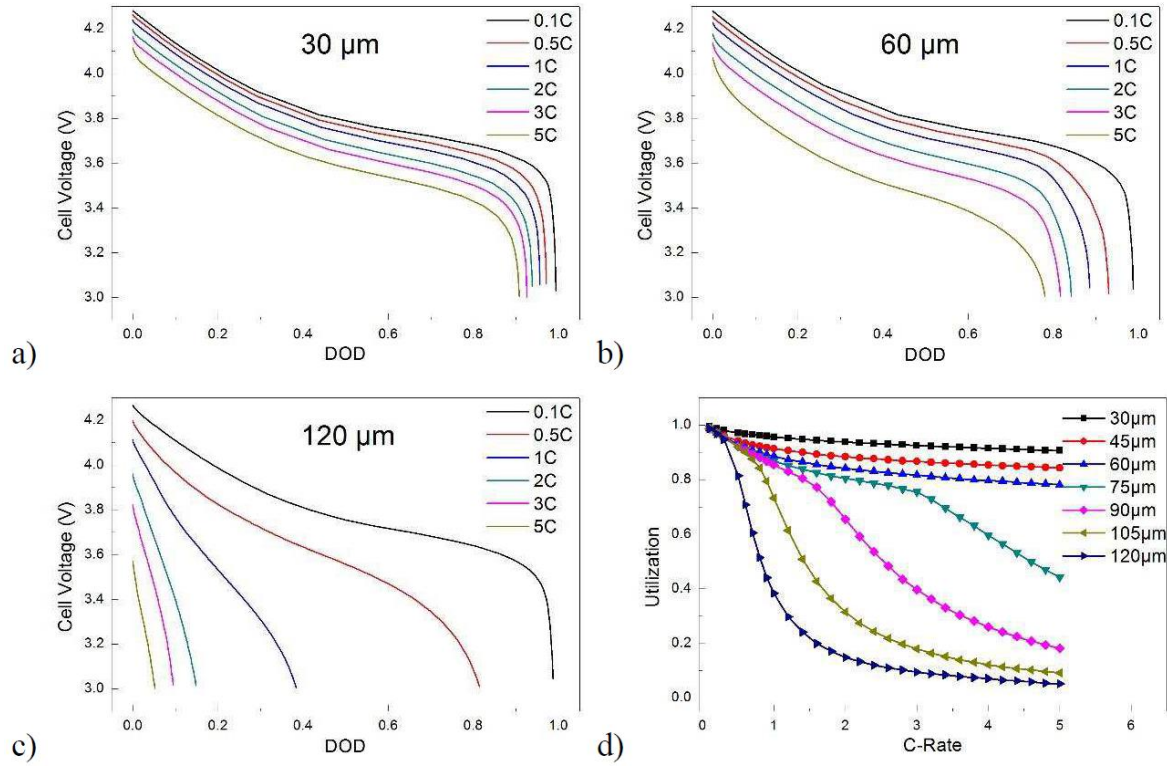


Figure 2.2. (a)-(c) Simulated discharge curves and (d) rate performance under various discharge rates and NMC electrode thicknesses [33].

Singh et al. [34] prepared and analyzed electrodes of much greater thickness with more active materials in a full cell configuration. Electrodes with post-calendering thicknesses of 70  $\mu\text{m}$ , 105  $\mu\text{m}$ , 155  $\mu\text{m}$ , 205  $\mu\text{m}$ , 255  $\mu\text{m}$ , 305  $\mu\text{m}$  were made to characterize in terms of capacity and volumetric energy density. C-rates were varied between  $C/10$  and  $C/2$  for 220 cycles during which the discharge capacities of six cells with different thicknesses were observed. As shown in Figure 2.3, at  $C/10$ , each cell displayed approximately 10% loss of its initial capacity during the first 20 cycles. For the remaining three C-rates of  $C/5$ ,  $C/3$ , and  $C/2$ , battery cells with 70  $\mu\text{m}$ , 105  $\mu\text{m}$ ,

and 155  $\mu\text{m}$  thick electrodes displayed close to no effect in the discharge capacity at every cycle, while cells with thicker electrodes gradually began to show capacity losses. The capacity of the cell with 205  $\mu\text{m}$  decreased by 13% by the end of C/2 while the cell with 255  $\mu\text{m}$  and 305  $\mu\text{m}$  showed a reduction of 36% and 65%, respectively. This indicates a capacity fade because of cell aging and lithium plating in the graphite anode layer. A similar trend can be noticed when volumetric energy densities are compared for the same cells at C-rates of C/5, C/3, and C/2, significant energy density losses can be seen for the thicker three electrodes. At C/10, each cell experienced a similar percentage loss during first 20 cycles, but no significant energy density losses were noticed for the thinnest three electrodes in C/5, C/3, and C/2. In thicker electrodes, energy density losses are significantly larger at higher C-rates.

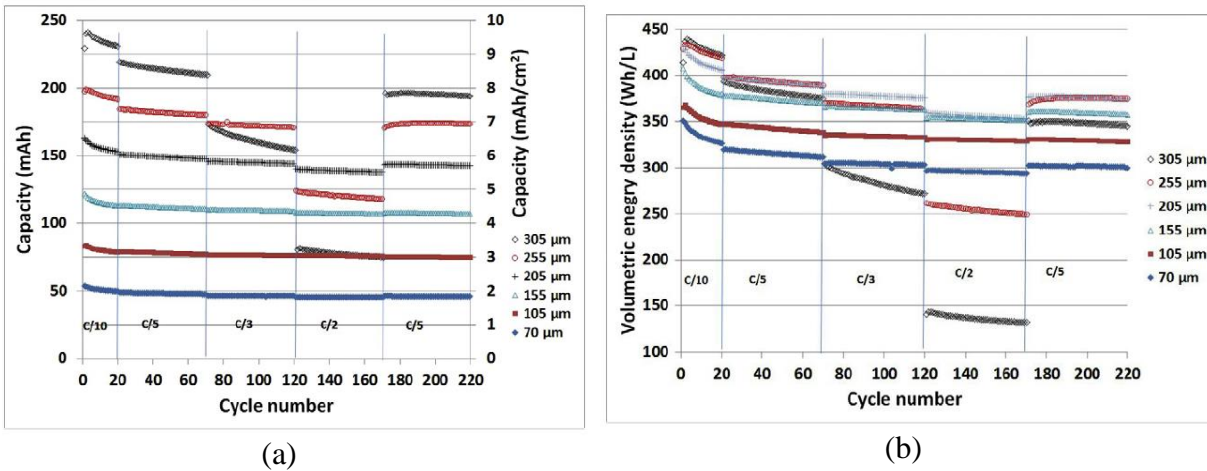


Figure 2.3. Comparison of discharge capacities and volumetric energy density of full cells containing 70  $\mu\text{m}$ , 105  $\mu\text{m}$ , 155  $\mu\text{m}$ , 205  $\mu\text{m}$ , 255  $\mu\text{m}$  and 305  $\mu\text{m}$  thick electrodes at different C-rates [34].

Du et al. [35] observed the effect of electrode thickness on volumetric density as well under different C-rates. Similar to the observations by Singh et al. [34], energy density increases as the electrode thickness increases. At a rate of C/5, energy density increases sharply initially and

plateaus at 728 Wh/L. For the rate C/2, the maximum energy density of 692 Wh/L is at 210  $\mu\text{m}$  and for 1C, the maximum energy density of 643 Wh/L is at 150  $\mu\text{m}$ . When the electrode thickness surpasses the critical thickness, the energy density declines quickly as shown by the rate of 2C where the maximum energy density of 563 Wh/L is at 120  $\mu\text{m}$ . Du et al. also observed that the increase in cathode thickness leads to a decrease in average discharge voltage, especially as the applied current increases from C/2 to 2C. The discharge voltage is lowered due to polarization and decreased capacity.

Jeong et al. [36] prepared four lithium metal polymer batteries (LMPB) with  $\text{LiFePO}_4$  cathodes with different electrode thicknesses. It was shown that the cathodes improve in capacity retention behaviors through higher density and lower thickness. The density(D)-thickness(T) of each of them are  $\text{D}1.6[\text{g}/\text{cm}^3]\text{-T}20[\mu\text{m}]$ ,  $\text{D}1.6[\text{g}/\text{cm}^3]\text{-T}40[\mu\text{m}]$ ,  $\text{D}2.0[\text{g}/\text{cm}^3]\text{-T}20[\mu\text{m}]$ , and  $\text{D}2.0[\text{g}/\text{cm}^3]\text{-T}40[\mu\text{m}]$ . The  $\text{D}2.0\text{T}20$  LMPB cell, with  $2.0 \text{ g}/\text{cm}^3$  density and 20  $\mu\text{m}$  thickness, displayed the best rate capability indicating that the rate capability is improved with higher density and lower thickness while maintaining the cell capacity up to 2C rate. The capacity only decreases at rates greater than 5C that is rather a severe state for such cells at room temperature. Choi et al. [47] observed the best rate capability at lower densities as opposed to observations made by Jeong et al., most likely due to materialistic discrepancies between  $\text{LiFePO}_4$  and  $\text{LiCoO}_2$ . This can be supported by the fact that even in liquid electrolyte, the LMPB cells display the best rate capability at higher density and lower thickness that enhances electrical conductivities and shorter lithium ion diffusion lengths.

Wang et al. [37] observed the effects of electrode thickness in a cell where current collectors are constructed of 3D metal foams. The graphite anode and nickel-manganese-cobalt cathode used copper and aluminum foam, respectively, as current collectors. Both foam current

collectors were filled with electrodes in the form of a slurry. The electrodes were prepared to have thicknesses of 1.2 mm, 0.6 mm, and 0.3 mm that are much greater than the conventional lithium ion electrodes. Four different experiments were conducted for each thickness using a unipolar and bipolar design. According to the charge/discharge curve, specific capacity is greater in electrode with 0.3 mm thickness while the voltage hysteresis during charge and discharge is smaller. Conversely, electrode resistance increases with thickness increase. Among the three thicknesses, 0.6 and 0.3 mm copper foam electrodes with up to C/5 cycling rate had the most potential for increased battery performance.

In the simulation studies by Bates et al. [38], electrochemical reaction, heat transfer, diffusion of lithium ions and electrons in the layer of electrolyte, as well as solid lithium diffusion in the positive electrode were all simulated with a 2D battery model by using COMSOL Multiphysics. Sensitivity studies were conducted with different parameter values of lithium ion diffusion rate, lithium diffusion rate, electrolyte thickness, and electrode thickness. Electrolyte potential, electric potential, lithium ion concentration in electrolyte, and solid lithium concentration in the positive electrode are primary dependent variables as the results of simulations. Particularly, while the Li-ion diffusion, lithium diffusion and electrolyte thickness were kept constant, the positive electrode thickness was reduced from 500 nm to 250 nm at multiple C-rates. When measured in terms of the discharge curve in which the electric potential declines over time, the reduced thickness resulted in the maximal activity or complete discharge to be reached much quicker at each C-rate. In terms of lithium ion concentration over the distance along the electrolyte, the concentration gradient rapidly increased at higher C-rates but the concentration was adjusted to 3000~19000 mol/m<sup>3</sup> from 2000~20000 mol/m<sup>3</sup> of the control case. At the low C-rate of 6.4, the reduction in thickness of the positive electrode had little effect. When positive electrode thickness

was halved, a complete discharge was reached much faster than other cases. Higher C-rates results in solid lithium polarization in positive electrode. Also, only at higher C-rates, reduction of electrode thickness influenced the solid lithium concentration range to have higher minimum concentration, mostly due to reduced diffusion distance in the electrode. However, it is suggested that lithium-ion solid state battery should be operated under lower discharge currents due to the possibility of high internal heating and poor rechargeability. Bates et al. concluded that the concentration of polarization is high at higher C-rates, and this would result in a lower performance as lithium would stack up at the positive electrode and less lithium ions would be present between electrode and electrolyte.

In experimental studies by Yu et al. [39], the optimal ranges for lithium iron phosphate ( $\text{LiFePO}_4$ /graphite) batteries are discussed.  $\text{LiFePO}_4$  has been widely chosen as a preferred material because it is less expensive, safe, less toxic and has long cycle life. The parameters they experimented include conductor ratio, electrode thickness, and electrode density. Experiments showed that adding a proper amount of acetylene black would enhance the electron conduction which would then increase the energy density. The conductor ratio is important because it determines how much of the capacity is lost during the first cycle of discharge. It was concluded that thicker and denser electrodes lose capacity more greatly at higher current rates, while they improve the intrinsic discharge capacity. Thus, it was recommended that thicker and denser electrodes be used in applications such as energy storage system because such system requires large energy density running at low current rate. For other applications, a proper range of electrode thickness for high discharge capacity at higher current rates was recommended.

### 2.3.2. *Surface-to-Volume Ratio, Density, and Porosity*

Although thinner electrodes result in greater surface-to-volume ratio (SVR), investigation of SVR as an independent design parameter can be useful, especially when the geometry of electrodes is more complex and porous. The effect of electrode porosity and density on the battery discharging capacity has been studied by many researchers. Shim and Striebel [40] investigated how pressed and unpressed natural graphite electrodes differ in terms of thickness and density. Natural, carbon-coated, and synthetic graphite are mixed with binder and compressed into electrodes with different densities. Low density reduced both reversible and irreversible capacity due to the decrease in porosity and active electrode surface area as a result of compression along with decreased charge and discharge. In the opposite case when density increases, more capacity is retained until  $0.9 \text{ g/cm}^3$  after which a decline occurs.

Shim and Striebel [41] also investigated that when the anode density was increased with compression, the first-cycle reversible and irreversible capacities decreased. The anode that was compressed in varied compression rates was flaky natural graphite, and it was found that pressing the electrode decreases the anode porosity as well as active areas. Larger particles are formed due to agglomeration between layers by surface attraction. The intercalation became less reversible with increased electrode density, while parameters such as current cycling, cyclic voltammetry and electrochemical impedance were constant.

Smekens et al. [42] experimentally investigated the influence of compression of positive electrodes on cell performance. Compression is applied during the calendaring process by two cylindrical rolls that ultimately exert the necessary pressure on the electrode to achieve the desired thickness and density. Three groups of ten cells with  $\text{Li}_x\text{Ni}_{1/3}\text{Mn}_{1/3}\text{Co}_{1/3}\text{O}_2$  based positive electrode and graphite based negative electrode have been produced, each group having a different positive

electrode density of 3.2 g/cm<sup>3</sup>, 3.0 g/cm<sup>3</sup>, and 2.8 g/cm<sup>3</sup>. The 1C current rate is set at 600 mA. The calendering process decreases the contact resistance, and electrodes with higher density have higher volume fraction of carbon binder domain in pore space that improves particle binding. Experimental results by Smekens et al. for the electrodes with three different densities show that at lower current rates, rates of 0.5C and 1C, higher density cell shows slightly higher capacity than the low-density cell. The three electrodes display roughly a similar capacity but at higher rates of 4C and 5C, the difference becomes significant. The high-density cell shows much lower discharge capacities than the low-density cell due to lower porosity as well as deteriorated tortuosity caused by calendering. Calendering of electrodes results in a less porous structure, but it improves electrode thickness uniformity and is required to increase the electrode volumetric capacity [43]. Srinivasan and Newman [44] applied electrochemical and kinetics models through experiments to simulate and optimize the effect of electrode porosity and thickness for maximum specific energy in a given discharge time. The positive electrode porosity of  $\epsilon=0.19$  at a thickness of 410  $\mu\text{m}$  was found to generate maximum specific energy. In the numerical simulation study by Yu et al. [39], it was shown that the ion transport in denser electrodes is more difficult because it reduces diffusivity and conductivity. The distance from the separator and electrode was also considered. Lithium ion concentration was noticed to decrease significantly when the distance increases.

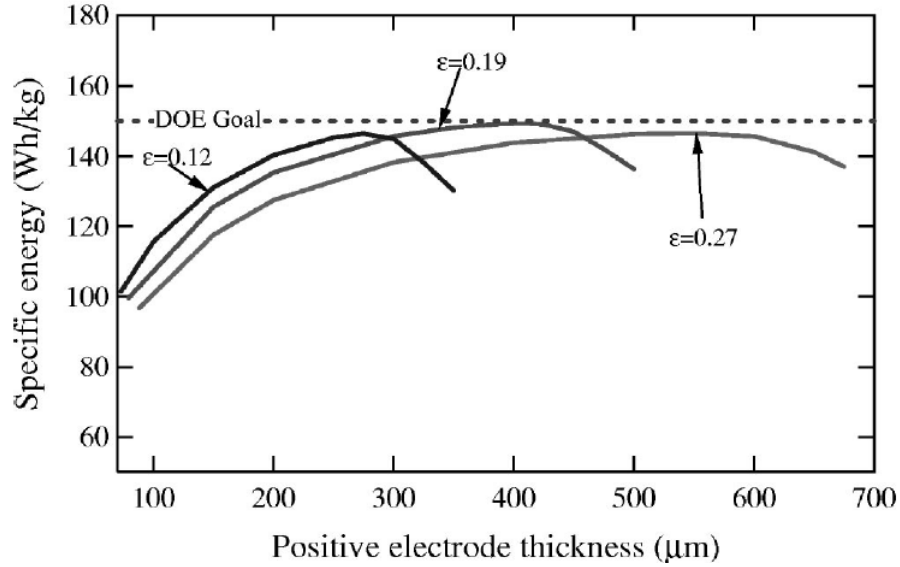


Figure 2.4. Curve graph that shows how specific energy is related to electrode thickness where three porosity values in relation to the DOE goal is shown [44].

Based on an ion diffusion simulation model and experimental results, Chen et al. [45] demonstrated that the cathode porosity affects both the ionic and electrical conductivity. Polydisperse structures of the cathode using an elastic collision model was used to predict the two types of conductivities. It was shown that as porosity is increased from 30% to 50%, ionic conductivity could be increased by two-fold, whereas electronic conductivity could be reduced by more than half. In order to optimize the design, a trade-off between ion diffusivity and electrical conductivity needs to be made.

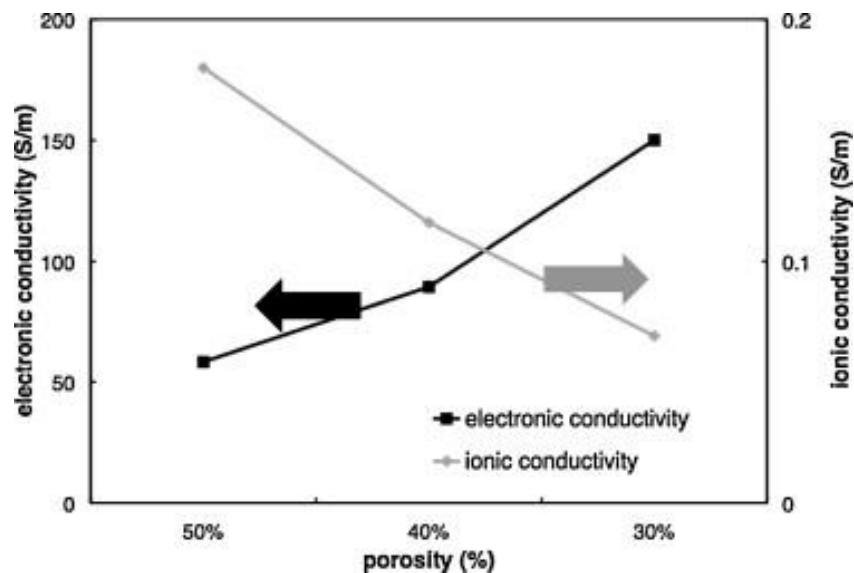


Figure 2.5. Values of porosity and their effects in terms of electronic and ionic conductivity [46].

As the porosity is reduced, the percentage of the active material in the solid is increased which translates to higher electronic conductivity, but this in turn slows down the movement of ion that inhibits reaction and reduced specific energy. Optimization of these parameters are necessary depending on the application. Bitsch et al. [46] also identified increasing electronic conductivity due to porosity decrease. By having more octanol in electrode slurry increased the dry film porosity. Specifically, large carbon black agglomerates are formed and prevent the formation of conductive pathways inside the electrode. The electrodes with porosities of 53%, 66%, and 63% have shown electronic conductivities of  $3119 \text{ S}\cdot\text{m}^{-1}$ ,  $510 \text{ S}\cdot\text{m}^{-1}$  and  $865 \text{ S}\cdot\text{m}^{-1}$ , respectively. However, when preparing the capillary suspension slurry, it is easier and more effective to increase the conductivity than a decrease in porosity by increasing the mixing speed.

Choi et al. [47] experimentally compared electrical conductivity, rate capacity, cycle performance with different  $\text{LiCoO}_2$  cathode densities.  $\text{LiCoO}_2$  cathodes with five densities ( $D=1.5, 2.0, 2.5, 3.0, 3.5 \text{ g}\cdot\text{cm}^{-3}$ ), each having thickness  $T=20 \mu\text{m}, 35 \mu\text{m},$  and  $50 \mu\text{m}$ , were manufactured for analysis. It was shown that reduced porosity can lead to degradation of rate capacity and

cyclability. When the thickness is set constant at  $50\ \mu\text{m}$ , it was seen that the electric resistivity decreases while the density is increased. Simultaneously, as expected, the electric conductivity increases with increase in density, which is congruent to the discussion by Chen et al. [45]. The density effect on rate capability is shown in Figure 2.6 for three different thicknesses. Under the same thickness, as discharge current density is raised from  $0.1\text{C}$  to  $20\text{C}$ , the gradually decreasing trend in capacity retention drops significantly at current densities of  $5\text{C}$  and higher. Higher density cathodes showed greater drops than cathodes with lower density. Figure 2.6 also displays how density affects cycle performance for the three thickness values. At a thickness of  $20\ \mu\text{m}$ , no capacity fading can be seen regardless of density. However, with increasing thickness, the effect of increased density amplifies as capacity retention is better at lower densities. None of the cathodes with  $50\ \mu\text{m}$  managed to retain its capacity at the  $50^{\text{th}}$  cycle. It can be concluded that porosity is a significant parameter that is responsible for the reduced performance of cathodes.

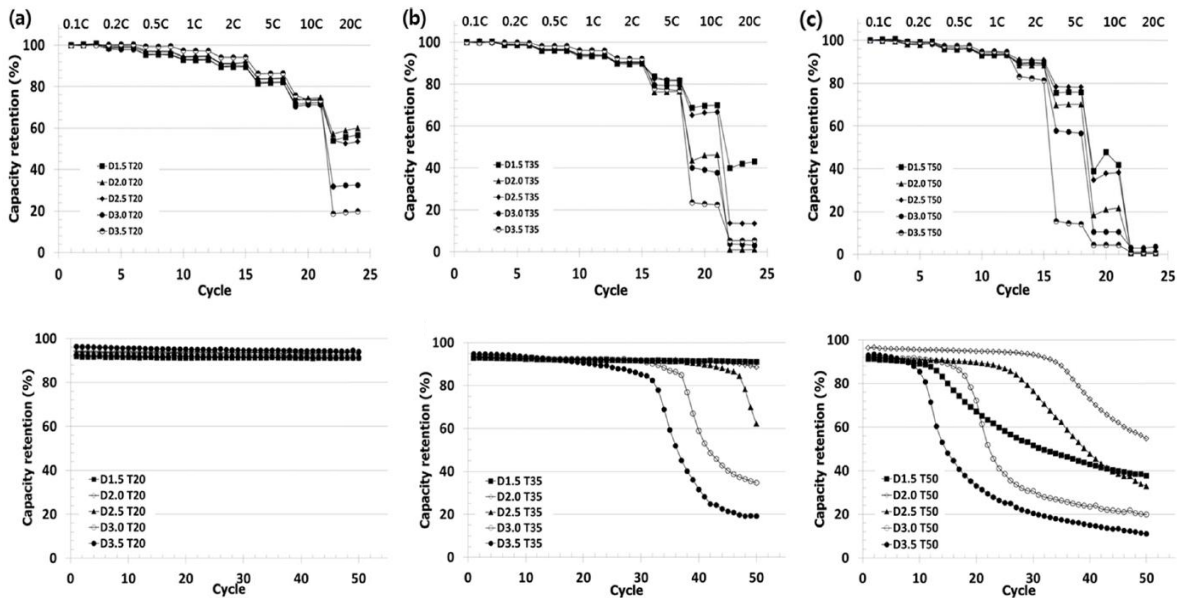


Figure 2.6. Rate capability and cycle performance of  $\text{LiCoO}_2$  cathodes with thickness ( $T$ ) of (a)  $20\ \mu\text{m}$ , (b)  $35\ \mu\text{m}$  and (c)  $50\ \mu\text{m}$  for different densities ( $D$ ) [47].

Das et al. [48] conducted a study about the benefits of micro- and nano-structured electrodes which include increased ion transfer from electrode to electrolyte due to a greater electrode surface area. Simulations using integrated Li-ion Battery Module in COMSOL Multiphysics show the impact of electrode SVR on energy capacity and heat generation. By keeping the electrode and electrolyte volumes constant, the number of electrodes in the interdigitated pattern increases while reducing the relative variation of lithium ion concentration. The devised interdigitated pattern includes a current collector in each leg of the electrodes. The saturation of lithium ion concentration was observed to be more rapid in the thinner electrode. Large SVR values yield increased power, energy density and longer discharge duration. By increasing number of electrodes, power consumption of each current collector leg decreased while the total power consumption remained constant. Results show that heat dissipates more properly with increased electrode number. The observed maximum temperature increase was 28.85 K for two pairs of electrodes, while it was 12.85 K for five pairs of electrodes. It was shown that increasing the number of electrodes and current collectors helps heat dissipation and prevents temperature rise. Hence, increasing the effective SVR of the battery is an effective way to reduce the temperature increase during discharge.

Suthar et al. [49] observed higher energy density in the thinner and less porous electrode with a smaller Bruggeman coefficient, but with very short discharge capacity. In addition, radial and tangential stresses were both higher for thinner and less porous electrodes even higher at greater Bruggeman coefficients. In the second scenario, it was shown that higher porosity at the anode-separator interface generates improved capacity with reduced stress that translates to a favorable capacity fade. Meanwhile, the linear positive porosity gradient demonstrated faster voltage elevation, and even faster with higher Bruggeman coefficient. Through this study, it was

concluded that thinner and less porous electrodes provide better capacity, given a columnar tortuosity.

To resolve the issue of quick degrading of performance at the electrode-electrolyte interface, Liu et al. [50] showed that an increase in porosity leads to improvement of conductivity and lithium ions diffusivity inside electrodes using a double-layered porosity-graded electrode. Using spinel  $\text{LiNi}_{0.5}\text{Mn}_{1.5}\text{O}_4$  (LNMO) powder over other materials such as  $\text{LiMn}_2\text{O}_4$  and  $\text{LiFePO}_4$  for its high specific energy and theoretical capacity, CR2032 coin cells were fabricated with mixed with acetylene black and carbon super P along with a polyvinylidene fluoride binder to form the cathode. LNMO half cells and full cells were charged and discharged between 3.7 V to 4.7 V and 4.1 V to 5.2 V, respectively, and were then compared to the conventional full cell. Using electrochemical impedance spectroscopy, the Nyquist impedance plots were produced that showed that the change in porosity resulted in change in the ratio of electron-transfer rate as well as the diffusion coefficient. The increased porosity improved conductivity and diffusivity while capacity fade was reduced by 8.285% (full cell) and 5.29% (half-cell). This can be explained with presence of greater porosities in the top layer of the porosity-graded cathode that leads to more uniform and decreased solid-electrolyte interphase (SEI) formation that leads to decreased hindrance of lithium ion diffusion that is common in conventional cathodes.

Dai et al. [51] tried to maximize energy density as a function of the positive electrode's thickness and porosity. The maximum energy density of a  $\text{LiMnO}_4$ /graphite cell was determined for a given discharge time with its corresponding optimal thickness and porosity. The maximum energy density that could be produced is 184.2 Wh/kg at porosity 0.23  $\mu\text{m}$  and thickness 160  $\mu\text{m}$  respectively. Then two models, one with constant porosity and the other with varied porosities, were compared to investigate the advantage of constant and varied porosity designs. However,

insignificant improvements in terms of specific energy and volumetric energy density have been noticed across the time of discharge. The specific energy of the varying-porosity design was only 2.8% higher while the energy density was 3.1% better. For optimal values of thickness and active material loading, the two porosity designs exhibit similar cell performance. In addition, by varying the Bruggeman exponent from 3 to 1, Dai et al. was raised the energy density by 25%, but was not able to differentiate the performances of the two porosity models. The only difference that could be identified between the two porosity designs could be seen in the porosity profiles along the positive electrode for different discharge C-rates, in which the porosity was greater for the varying-porosity design near the electrode-separator interface. With increasing C-rate, the difference was greater with the varying-porosity design having a greater porosity.

### 2.3.3. Particle Size

The effect of particle size in cathodes on electrochemical performance was investigated by Lu et al. [52].  $\text{LiMn}_2\text{O}_4$  was initially used as the cathode material, but it showed low charge capacity and large capacity fading during cycling. It was found that the capacity and cyclability can improve with higher crystallinity and smaller particle size. Cathodes of different particle sizes were prepared and examined in a two-electrode cell with lithium foil as the negative electrode with  $\text{LiPF}_6$  electrolyte. In Figure 2.7. It is apparent that the capacity increases significantly with decreasing average particle size. Moreover, the cathode with particle size of  $19.9 \mu\text{m}$ , the smallest size, displayed the highest coulomb efficiency and the best electrochemical performance. This is because reduced particle size leads to greater overall surface area and more lithium ions. Smaller particles could also increase the interfacial contact area within electrolytes and increase coulomb efficiency. It was decided that size of particle of the cathode powders not only improves capacity,

but also improves coulomb efficiency due to large interface area that increases the number of lithium ions for diffusion. In addition, particle sizes also affect the charge and discharge patterns.

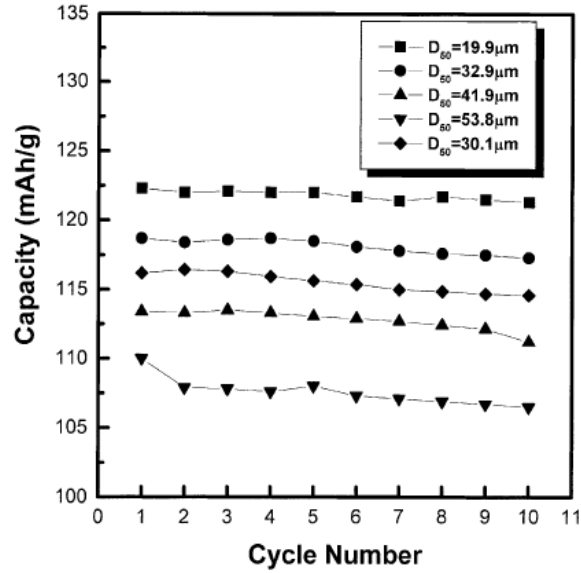


Figure 2.7. Specific discharge capacity from  $\text{LiMn}_2\text{O}_4$  powders of different particle sizes [52].

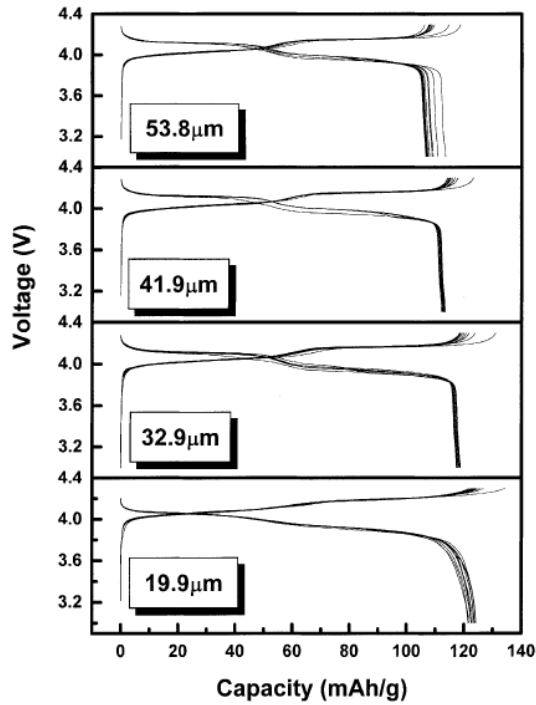


Figure 2.8.  $\text{LiMn}_2\text{O}_4$  capacity-voltage curves with varying particle size at  $0.2 \text{ mA/cm}^2$  [53].

The particle size also influences the thermal behavior of lithium ion cells. People have found that flaming of batteries occur due to buildup of pressure and venting when overcharged. Botte et al. [53] used galvanostatic charge/discharge behavior based on a pseudo 2D model with spherical solid-phase particles that excluded any volumetric expansions and contractions during cycling. When the temperature of a cell elevates, the side reactions such as the decompositions of electrodes and electrolyte are most likely to occur. The negative electrode was selected as the main target because of its decomposition at relatively low temperature. When the cell was discharged until 2.2 V of the cutoff voltage, the model with a bigger particle size in the negative electrode reached cutoff voltage more rapidly than that of a smaller particle size. This was due to an increased limitation on solid-state diffusions and an increased overpotential. This meant that the ohmic heat generation is larger, which leads to higher temperature. When three different particle sizes of the negative electrode were tested with the relaxation of 20 additional minutes after reaching at the cutoff voltage, the electrodes with larger particle sizes heated up faster as expected. However, it was shown that the final temperature of smaller particles after the relaxation of 20 minutes was higher than that of larger particles because the cell with a smaller particle size did not reach the cutoff voltage as fast as the cell with a larger particle size. In addition, it was demonstrated that the cell discharged at lower current density reached higher temperature. The importance of optimization of particle size was addressed in this study that the cell with 15  $\mu\text{m}$  of particle size reached at 135 °C, which is the melting point of the separator. In summary, larger particles lead to a higher heating rate while smaller particles lead to higher temperatures in the cell. This study marked the significance of electrode particle size and considered it as an important parameter that affects the cell's thermal behavior, especially in negative electrode. However,

further studies on positioning particles and accurate values of thermodynamic factors such as self-heating and total heat are required to verify the predictions.

Sheu et al. [54] investigated how size of  $\text{LiCoO}_2$  particles affects cell performance and rate capabilities. Two  $\text{LiCoO}_2$  electrodes, one with a particle size distribution of 2-4  $\mu\text{m}$  and another with a greater 5-10  $\mu\text{m}$ , were prepared in the form of a coin cell using lithium cobalt oxide, acetylene black and polyvinylidene fluoride. The cycle stability is more stable for the electrode with smaller particle size distribution for all C-rates. However, in terms of rate capability, no difference was noticed between the two electrodes with different particle size distributions.

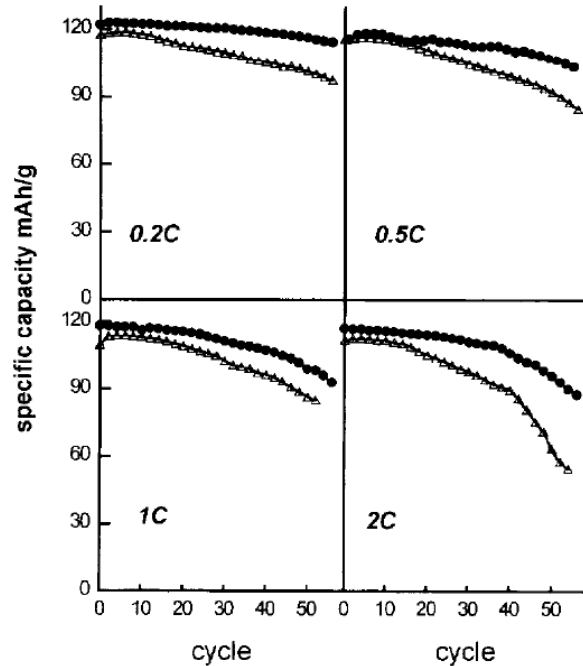


Figure 2.9.  $\text{LiCoO}_2$  particle size effect on cycle stabilities: (O) 2-4  $\mu\text{m}$ , and ( $\Delta$ ) 5-10  $\mu\text{m}$  [54].

Table 2.2. Averaged specific capacities at different cycling rates of 2-4  $\mu\text{m}$  and 5-10  $\mu\text{m}$   $\text{LiCoO}_2$  particle size distribution [54].

C-rate	0.2C	0.5C	1C	2C
2 - 4 $\mu\text{m}$	122.1 (100%)	119.2 (98%)	118.4 (97%)	117.1(96%)
5 - 10 $\mu\text{m}$	119.1 (100%)	117.0 (98%)	115.1 (97%)	114.0 (96%)

Most of existing studies on particle sizes have focused on uniform distribution of particle sizes. However, Taleghani et al. [55] denoted how significant the variance in particle size is in development of lithium-ion batteries. Under this study, mono-modal, bi-modal, and three-particle size distributions, as shown in Table 2.3, were compared to observe their effects on lithium-ion battery performance. The models were generated with COMSOL Multiphysics to observe how the battery discharges. A few assumptions were made in this study. The most important one is that the bi-modal and three-particle models were only applied to the positive electrode and the negative electrode was applied with mono-modal distribution. In addition, the mass and specific surface area in bi-modal and three-particle models were set as identical as the ones in the mono-modal model. An increase in volume fractions of the smallest particle sizes increased the cell voltage, while the total polarization was decreased for both bi-modal and three-particle models. Furthermore, Taleghani et al. investigated how the effect of particle size distribution becomes significant at higher discharge rates than at lower discharge rates. The mono-modal model produced the best cell voltage compared to the other two models. Particle size distribution may become a significant design parameter along with particle arrangements to optimize battery performance.

Table 2.3. Different particle size distributions [55].

Particle Size Distribution		Radius ( $\mu\text{m}$ )	Volume Fraction Ratio
<b>Mono-modal</b>		8.67	1
<b>Bi-modal</b>	Case 1	8.5	0.49
		8.84	0.51
	Case 2	2.34	0.135
		15	0.865
<b>Three-particle model</b>	Case 1	4	0.265
		15	0.734
		7	0.001
	Case 2	4	0.15
		15	0.57
		7	0.28
	Case 3	4	0.1
		15	0.5
		7	0.4

#### 2.3.4. Tortuosity

Newman [56] stated that porosity should be decreased instead of increasing the electrode thickness to reach a balance between increasing capacity and increasing mass and ohmic potential drop. The optimum porosity increases with increase in positive electrode density, but at the same time reduces the optimum electrode thickness since these changes can compensate for the increased mass. Longer discharge times allow not only thicker electrodes, but also smaller porosities to get more capacity into a given volume without incurring a large ohmic penalty. With basis on Newman's model, many attempts were made to characterize and quantify the tortuosity of battery components in addition to porosity. Shen [57] defines tortuosity as a value that is computed by dividing the length between the pixels on one end of a given pore structure and the closest pixel on the other end by the shortest distance between the two ends of a given pore structure.

Thorat et al. [58] developed different methods to quantify tortuosity in the separator and the electrode while Shearing et al. [59] generated a negative electrode sample into voxels that was

initially characterized by X-ray tomography, and then further sub-divided them by nine to analyze tortuosity. For each division, volume specific surface area and tortuosity was determined and was concluded that less tortuous regions had high volume-specific surface area. Kehrwald et al [60] improved on Newman's model by investigating how homogenous tortuosity affects the electrochemistry and predicted that a decline in capacity and life resulted from inhomogeneity.

Lim et al. [61] modelled microstructures and compared geometric characteristics between an anode that is freshly prepared with one that has gone through intensive cycling process, specifically the parameters of porosity and tortuosity that are important factors of battery performance. Quantitatively, it was determined that porosity increased by 0.04 and tortuosity declined by 0.25 after cycling, showing a clear difference between the new and aged electrode in which the percentage of active material lost during the process of cycling was 5.6%. This can be associated with greater abundance of pores with bigger size at post-cycling that resulted in reduced specific surface area. Although capacity fading occurred up to a ten percent because of cycling, it can be inferred from the lower tortuosity value that lithium ions are transported more easily.

### 2.3.5. *Cathode-Anode Area Ratio*

The area ratio between the electrodes (N/P ratio) and its effect on the battery's electrochemical performance was studied by Son et al. [62]. In this study, five cells with N/P area ratio between 0.56 and 2.25 were fabricated, and their initial coulomb efficiencies and charge/discharge capacities were monitored. The coulomb efficiency dropped by 11% with increased decomposition reaction when the anode area increased  $1.41 \text{ cm}^2$ , forming a larger solid electrolyte interface. The opposite case with a larger cathode was also studied, in which the discharge capacity decrease to an extent where the coulomb efficiency plunged to 63%. This resulted from lithium dendrite formation on anode surface and cell bottom, making the battery

with a larger anode a better option. Lastly, when the cathode and the anode were set to have identical diameters, at N/P ratio of one to one, the discharge capacity was retained at initial value as the coulomb efficiency quickly saturated. The cell displayed slightly more rapid capacity fading after thirtieth cycle due to insufficient anode capacity.

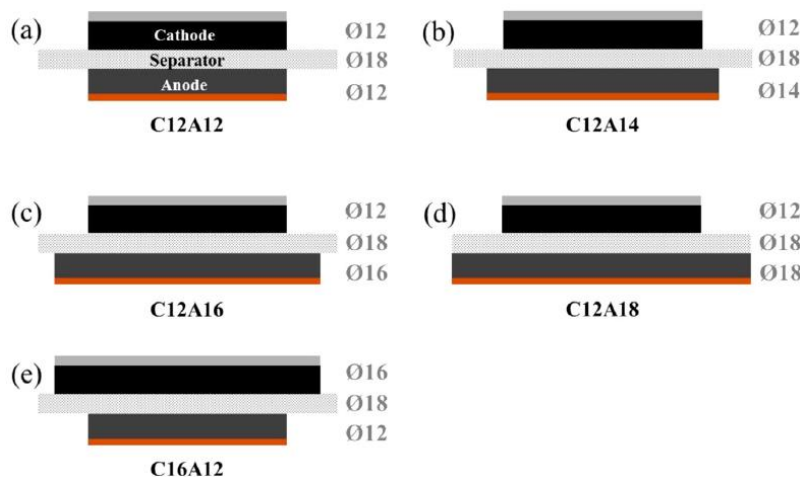


Figure 2.10. Different coin cells with varying electrode area ratios [62].

### 2.3.6. Cathode-Anode Mass Ratio

Another design parameter that is of interest in quantifying battery performance is the electrode mass ratio as the lithium ion amount determine capacity and Xue et al. [63] varied this ratio to study its impact on performance. First, using the chemical reaction equation, a theoretical mass ratio of 1.35 was calculated, from which the ratio was varied. Although the theoretical mass ratio dictates that the ratio should ideally be 1.35, the actual mass ratio should be larger due to electrolyte decomposition. When ratio was lowered to 1.23, it was clear that the lithium ions were insufficient to provide sufficient capacity with high anode potential, indicating poor performance. In the opposite case with abundant lithium ions, at a value of 4.20, the anode potential level was found to be negligible but raised with increased cycling due to decreased lithium reversibility.

After investigating the two extreme cases of mass ratios, a value of 2.73 was selected to observe the performance. This value displayed a larger capacity as compared to the two other cases as the anode potential remained above zero. An intermediate mass ratio value of 2.73 provided larger capacity with the anode potential near zero after charging and 0.5V after discharging, indicating the necessity of a carefully optimized mass ratio to achieve acceptable capacity and cycle life. Clearly, the electrode mass ratio has an influence on performance, but only three examples of ratios are not sufficient and an optimization method must be employed to determine the optimum mass ratio.

Similarly, Kim et al. [64] studied the lithium plate effect and degradation with different electrode mass ratios. The capacity ratios of negative to positive electrodes used were 1.10, 1.20, and 1.30 that are maintained by increasing the thickness and anode loading level. In terms of discharging capacity, all three cases have shown significant capacity fading at charging voltages greater than 4.40V with a declining trend as the number of cycle increased.

### 2.3.7. *Surface Texture*

The surface texture and roughness of electrodes also affect battery performance. Kohler and colleagues [65,66] studied the effect of electrode's microscale surface texture on the power density and chemical stresses. SnO<sub>2</sub> and LiCoO<sub>2</sub> films were deposited with radio frequency magnetron sputtering in argon, and 3D micro textures with conical shape were added using projected excimer laser radiation. The shape, size, height, orientation, and density of the cones can be controlled by adjusting laser pulse. The results show that as aspect ratio of the cones increases, the corner effect from the tip of the conical structure improves the intercalation rate of the lithium, but reduces the percentage of the useful delivered charge, as compared to a thin film electrode. This is because of the intercalation inhomogeneity from the conical topology. In the Ragone plot,

as the C-rate increases with fixed aspect ratio, the power and energy density decrease due to the tip focusing effect. It has been found that the aspect ratio that maximizes the average discharge stress is found to be 0.32. In general, when the aspect ratio of conical structure increases, the intercalation of lithium ions at the tip increases as well.

### 2.3.8. *Volumetric Expansion Ratio*

Ikeshita et al. [67] investigated effects of volumetric expansion and contraction of active electrode materials during charge-discharge cycles on the charge capacity through multi-physics simulations. The volumetric expansion ratio is incorporated in consideration of geometric parameter variations including electrode thickness, surface area, mass ratio, and tortuosity. The galvanostatic charge curves shows that at constant C-rate, increased volumetric expansion ratio leads to lower capacity. In terms of normalized reaction rate distribution in the electrode, the increase in volumetric expansion ratio showed an increased reaction rate that is close to the anode separator during charging. Lastly, the relationship between the C-rate and the charge capacity was investigated for two electrode thicknesses of  $L=60$  and  $L=80$ . The charge capacity, defined as the final capacity in the charge curve, decreased 27% for  $L=60$  compared to the non-expanding example. The charge capacity declined 40% for  $L=80$ . It is concluded that larger anode expansion ratios correlated with lower charge capacities through the analysis of various distributions in the electrode. Ikeshita et al. showed that it is important to consider the dynamics of geometry caused by the volumetric expansion of active materials during electrode design.

### 2.3.9. *Cathode-Anode Layout and Configuration*

One of the drawbacks in 3D cell architecture is the non-uniform current density. Hart et al. [68] demonstrated the difficulty of obtaining uniform current densities through simulation

predictions of the current and potential from different configurations of electrodes. In simulation models, cathode and anode rods with current collectors were placed densely to increase energy and power density. But such design has non-uniform current density which leads to poor utilization of the electrode materials. This lowers not only the utilization rate, but also the cell efficiency, electrode stability, and heat dissipation. Four configurations were tested, as shown in Figure 2.11. The first one has the electrode arrays in parallel, where rows of cylindrical electrodes are arranged in a rectangular alternating grid. High current flow between neighboring electrode pairs was observed but the current flow decreases between adjacent electrodes of the same type. The second design consists of alternating cathodes and anodes, where each anode is enclosed by four cathodes and vice-versa. It could be noticed that the current densities were more uniform, hence the current density becomes more uniform as there are more electrodes of opposite polarity in the vicinity. In the third design, there are six cathodes in the vicinity of every anode, creating a hexagonal formation. This results in an even current density at the anode but not at the cathode. The last array configuration does not use cylindrical electrodes but use triangular shaped electrodes that generated greater cell capacity and power, but has a significantly reduced primary current uniformity. From the four models, it was shown that increasing power and energy density is easier to achieve than a uniform current distribution in 3D cells. Electrode configurations play a critical role.

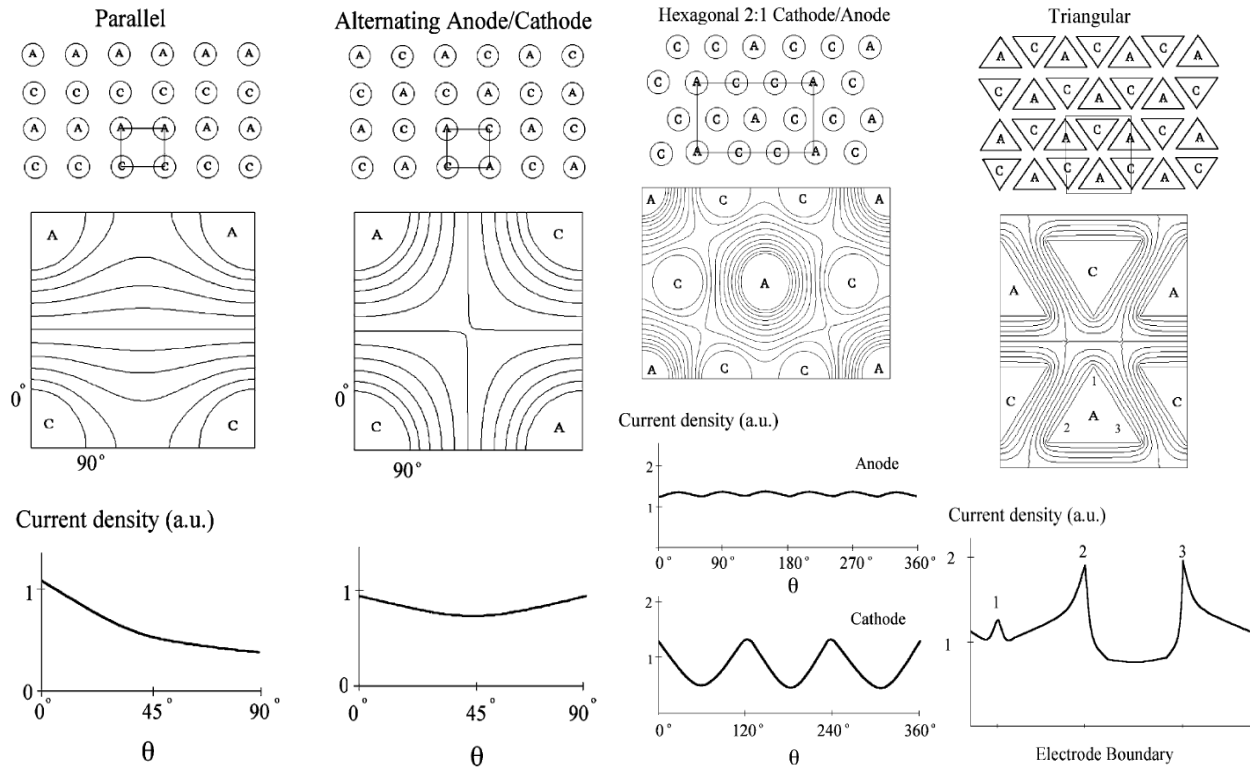


*Figure 2.11. (Top panels) Four different cathode-anode array arrangements with their respective isopotential lines and current densities at electrode surfaces. Electrode areas are constant for each arrangement [68].*

Zadin et al. [69] studied the effects of alternating positive electrode conductivity and electrode plate height. By performing finite element analysis on the trench design, the most useful electronic conductivity values of the electrodes were found using the concentration gradient development and discharge curves. Several 3D designs illustrated in Figure 2.12 were studied. It was shown that the difference in current density between two electrodes could be reduced by simply changing the position of the anode and cathode. The homogeneity of the current can be optimized by utilizing different number of cathodes and anodes. The authors suggested that computer modeling can be useful to achieve uniform electrochemical activities on the electrode surface in a complex 3D battery. The results show that in the trench design, delithiation and

lithiation of electrodes both start from the tip of each electrode. As the battery discharges further, there is faster depletion as well as accumulation of lithium ions at the tip region. This causes inhomogeneous current density distribution from difference in size between the tips and their corresponding opposite sides. Even though the parameters were set to be delithiated and lithiated simultaneously, the varying reaction rate at the tips causes the current to find a different route and terminates the electrochemical process. Hence, the simulation reflects only 80% of the theoretical capacity. This suggests that if two electrodes have a large difference in conductivity, then the height of another electrode could be reduced to optimize electrode material usage. However, there is still a possibility that shorter electrodes would result in capacity loss because material usage is decreased by losing the benefits of having it 3D.

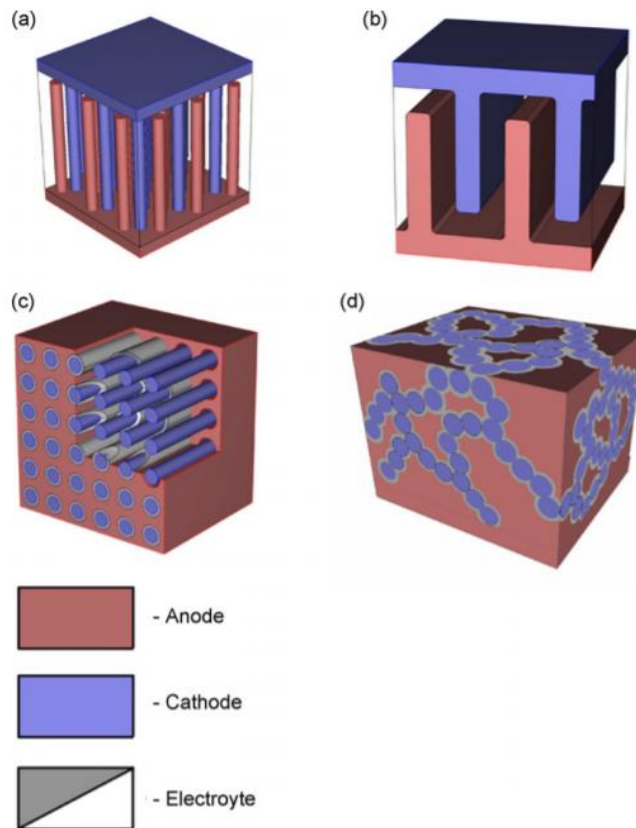


Figure 2.12. Possible three dimensional (interdigitated, trench, concentric, aperiodic) battery architectures [69].

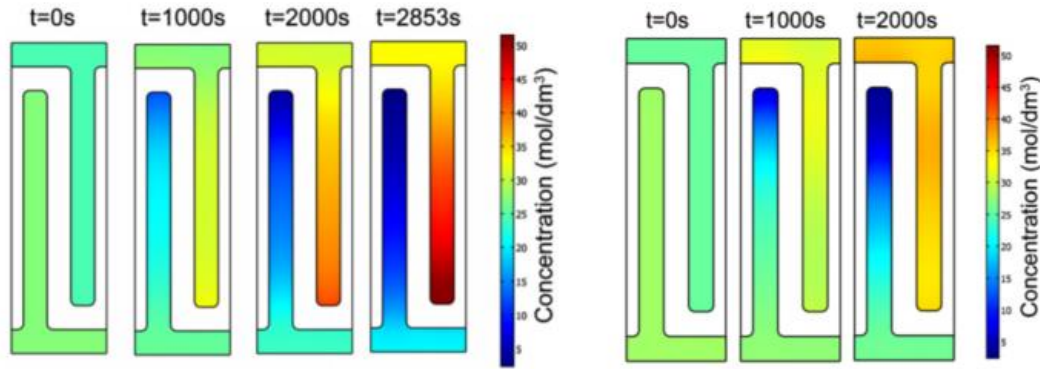


Figure 2.13. Concentration profile development in the 3D-trench design. Top electrode: positive. Bottom electrode: negative. (left) Conductivities for both electrodes are 1 S/m, (right) Conductivities are 1 S/m for negative and 0.01 S/m for positive [69].

Using computer simulations, Miranda et al. [70] investigated different geometries of lithium-ion batteries. The designs used are horseshoe, spiral, ring, antenna, and gear as well as a conventional and an interdigitated pattern. Theoretical model simulations were used to study these seven different designs while the core components of the battery such as the electrode are constant in terms of area. In this work, the effects of different geometries are quantitatively compared using theoretical simulations while the areas of its components are constant for a low, medium, and high discharge rate. First, the current collector positions were investigated that resulted in greater delivered capacities with decreasing maximum distance between the current collectors due to a shortened path for ions to travel and lower ohmic losses. In horseshoe geometry, at a high discharge rate of 500C, the length of the side of the battery leads to a reduction of ohmic resistance that results in increased capacity values. On the other hand, capacity loss could be observed when thicker separator, which makes longer paths for electrons, and less surface contact area between electrodes were implemented in the design. The ring design can be characterized by its radius, so the radius was increased from  $20 \mu\text{m}$  to  $93.9 \mu\text{m}$  and the capacity value increased. But for a radius

greater than  $93.9 \mu\text{m}$ , the performance of the battery gradually decreased. When digitated shapes were introduced to the ring geometry and turning it into a gear geometry, the performance was increased due to increased contact surface area. Using computer simulations for the different geometries, it is easy to obtain performance data for each design. The use of optimization for a broader range of battery designs and patterns are necessary.

Miranda et al. [71] emphasized the importance of computer simulations and evaluations before experimental implementation because they can demonstrate how certain changes in a particular parameter can impact key aspects of a battery. By maintaining the area of electrodes and separator constant, other parameters such as number, thickness, and length of digits were varied, as shown in Figure 2.14, to determine which set of parameters produce an optimized battery performance. The areas of different components were maintained constant because this allows true comparison while keeping amount of active material equal. It was demonstrated that the battery with conventional geometry without a digitated pattern showed a delivered capacity of  $0.7 \text{ Ah}\cdot\text{m}^{-2}$  while the battery with 8 digits showed a capacity of  $323.77 \text{ Ah}\cdot\text{m}^{-2}$ . The results imply that by keeping equal digit length for each different digit thickness, larger thickness improves delivered capacity because this creates a truncated path for ions to migrate between electrodes.

Increasing the digit length also increases the delivered capacity due to greater contact surface between electrodes while the ion pathways are decreased. By increasing the thickness and the digit length, ohmic losses associated with charge transport during the discharge process is reduced. The paper concludes that the interdigitated geometry significantly increases the capacity if compared to the conventional battery geometry the areas for all components were set constant.

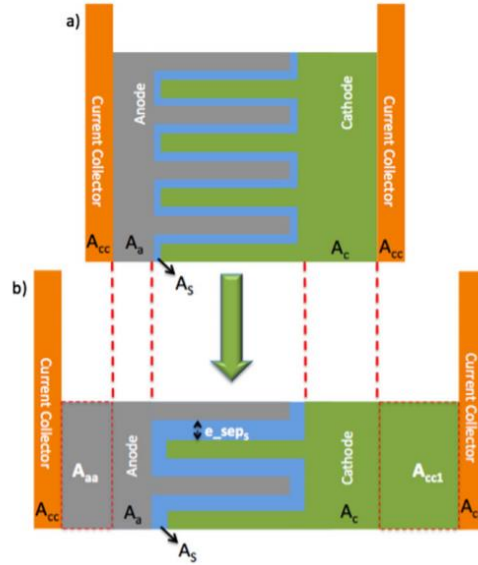


Figure 2.14. The number of digits vary while the area of each component remains constant [71].

### 2.3.10. Geometry-Materials Correlation

Geometry and material properties of electrodes are highly correlated. The effects of electrical conductivity, lithium diffusivity, and reaction rate constants of active electrode materials were studied by Chabot et al. [72] to determine electrode performance sensitivity. The effects of these properties were examined through many cell designs such as different thickness of electrode, volume fraction of active electrode material, and initial electrolyte salt concentration. Multi-physics models were built in COMSOL. The results indicated that lithium diffusivity has minor impact on cells composed of thicker electrode or higher volume fractions. The effect of lithium diffusivity in both electrodes remain unchanged when certain diffusivity level is reached. However, reducing the lithium diffusivity could cause a decrease in cell performance.

The results also showed that the electrical conductivity affects the cell with thicker electrode more as it means there is a lengthier path for electrons. The reaction rate constant plays a slightly more important role when the cell is composed of thin or lower volume fraction of

electrodes. In an active negative electrode, the lithium diffusivity greatly influences the cell performance because cell-specific energy was observed to be enhanced up to 11% by increasing the lithium diffusivity by one order of magnitude. In both active electrodes, it was shown that increasing reaction rate could enhance the specific energy and power by 4%. This study has shown the importance of considering the material properties such as electrical conductivity, lithium diffusivity, and reaction rate constant during structural design for the best cell performance.

## **2.4. Electrolyte**

For safety and environmental concerns, solid state lithium-ion batteries need to use electrolytes that do not experience phase change or do not release toxic gasses when disposed. Lithium ions are transported through the electrolyte during charge and discharge cycles and while electrolyte is in contact with both cathode and anode, a separator must electronically separate the two electrodes. Ceramic or polymeric materials are commonly used as separators between electrodes in applications using liquid electrolyte. The ion conduction can be achieved through a membrane when polymer electrolyte is used.

### *2.4.1. Electrolyte-Electrode Configuration*

Kennell and Evitts [73] studied two different electrolyte-electrode configurations by simulations. The first geometry has the electrolyte extending beyond the electrode edges, while the second configuration has the cathode extending further than the anode edge. In other words, not only electrodes could have different lengths, the electrolyte-electrode interfaces can also have different contact areas. The simulation study showed that the extension of electrolyte does not significantly impact the behavior of the electrodes while the effective conductivity was increased in the edge region. However, when the second design was studied, the concentration gradient of lithium and

current distribution were found to be affected significantly. When electrode width was assumed to be not electro-active, the extension of the electrolyte resulted in less current densities in the electrode edges, and resulted in reduced potential gradient. On the other hand, when the width of electrodes was assumed to be electro-active, more electric current was generated in the anode edge region than the cathode edge region since materials with higher equilibrium potential are used for the anode. The cathodic current density is reduced at the cathode tip, while there is only little reduction on the anode side. To balance this, the extension of cathode over anode was tested. The result showed that less excessive current was generated towards the anode edge region as time passed because anode's stoichiometric coefficient decreased. However, it was addressed that this extension has a possibility to cause large electric potential drops and ohmic losses in the beginning phase of cell charging within the electrolyte. As charging continues, the equilibrium potential gradient would become less and cause lower cathodic reaction rate at the elongated section as well as lithium deposition.

#### 2.4.2. *Ion Transport Path*

The effect of trench depths in the electrolyte layer was studied by Zadin et al. [74] with simulations. The geometry of trench affects the ion transport path. Common electrode and electrolyte materials were used for the trench. It was assumed that diffusion and conductivities coefficients as well as electrode volumes are constant, while side reactions were negligible and electrolyte is electro-neutral. Multi-physics models were built in COMSOL, and simulations were conducted with varied electrode conductivities, length, and curvature radius. When depth of trench was gradually decreased from 100  $\mu\text{m}$  to 10  $\mu\text{m}$ , the electrode surface area decreased greatly. To maintain current density, electrodes with higher conductivity can be used to compensate the decreased surface area. It was shown that the depth of the trench does not have an effect on the

high concentration gradient on the upper and lower electrode plates. High values of concentration gradient indicate that the material is over exploited. The trench design leads a design with highly non-uniform current densities that can be improved with rounded ends instead of sharp corners.

#### 2.4.3. *Separator Membranes*

In some battery designs, separator membrane is used, which is located between two electrodes in the form of a polymer matrix inside an electrolyte solution. The option of whether or not to use membranes affects lithium-ion battery performance. Miranda et al. [75] simulated ion diffusion and electrode conductivities electrodes and electrolyte. The electrolyte is a P(VDF-TrFE) copolymer since it has high ionic conductivity and good stability. To optimize performance through simulation, the parameters of membranes that were studied are thickness, the Bruggeman exponent, and porosity. Results showed that when low discharge rate is a low 0.15C, there is no effect in the change of porosity percentage. But at a high rate of 5C, a decrease in degree of porosity decreases voltage, especially for a porosity of 50% and below. At the same time, tortuosity amount at different porosity values was studied. The separator thickness has no influence on the delivered capacity at low rate of 0.15C. But with an increased rate of 5C, the increase in thickness decreases the delivered battery capacity.

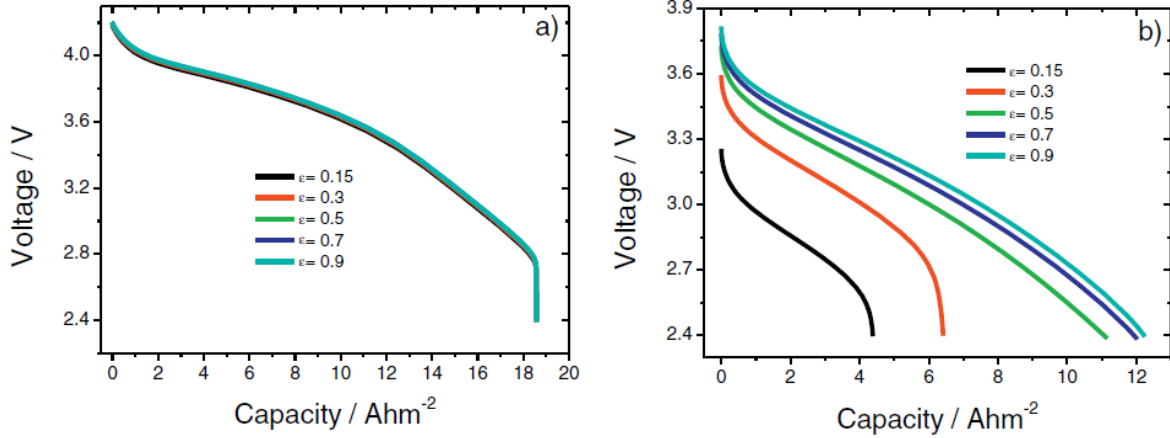


Figure 2.15. Voltage as a function of delivered capacity for varied porosity  $\epsilon$  with scan rate of a)  $0.15C$  and b)  $5C$  [75].

## 2.5. Current Collector

Current collector is also an intrinsic part of lithium-ion batteries as current collector provides a conducting path to minimize the resistance of a battery. It can also affect other components of the battery. Therefore, material selection as well as geometric parameters of the current collector are significant in determining battery performance.

### 2.5.1. Geometry

It is important to consider how the temperature fluctuates or how deep the battery is discharged within a current collector, which both are determined by the geometry. For instance, there exists a trade-off about the thickness of current collector as smaller cross-sectional area results in greater ohmic loss, whereas a thicker current collector results in poor specific energy. In the simulation study by Kosch et al. [76], aluminum and copper were used for current collectors, respectively. Using a multi-physics model in COMSOL, it was observed that the peak temperature starts from near the current collector tabs, and then migrates into the middle, and then to the bottom

of the battery as the discharge continues. Four different current collector designs were studied. Two designs have both the current collectors aligned at the top, whereas other two have the current collectors aligned on two sides of the cell. In the study, various tab sizes and three different current collector thicknesses were applied. It was found that the tab sizes play a more significant role in minimizing depth-of-discharge imbalance than current collector thickness, since the smallest tab sizes resulted in a maximum depth-of-discharge imbalance. However, larger tabs allow lower temperature increase along the cell so there is a need for optimization between the two objectives. However, when the current collectors were positioned each side, the influence of current collector thickness was slightly higher than that of the tab sizes on the depth-of-discharge imbalance. In addition, current collectors on opposite sides generated lower overpotential losses, a more uniform depth-of-discharge distribution, and less heat. This study provided a new way of energy density optimization by alternating the current collector geometries, but interactions with other components in the battery should be also considered for optimized energy density with realistic boundary conditions such as non-uniform heat generation.

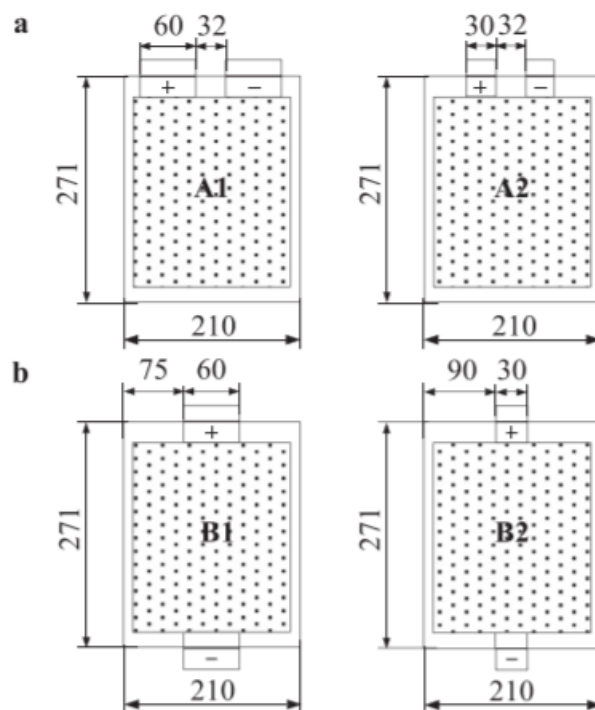


Figure 2.16. Different placements and geometries of current collector tabs (unit: mm) [76].

Electrodes with thicknesses between 300  $\mu\text{m}$  and 600  $\mu\text{m}$  were used by Yang et al. [77] to investigate the size effects of metal foam current collectors. A 3D metal foam was produced plating Ni on polyurethane and using heat treatment to remove polyurethane [78]. 3D porous current collectors have also shown superior performance with aluminum plating as performed by Wang et al [79] by reducing charge-transfer resistances and having a large contact area between active materials and current collector. When foil-type and foam-type current collectors are compared in a charge-discharge curve, not much difference of overvoltage in the plateau region can be seen at low current rate. But with increased current rate, the internal resistance is 14  $\Omega$  for the metal foam and 111  $\Omega$  for the foil [80]. Three NiCrAl alloy foams with sizes of 450, 800, and 1200  $\mu\text{m}$  were produced in the investigation by Yang et al. [77]. Once the electrode material was spread on the metal foam, thickness of each electrode was 330, 430, 540  $\mu\text{m}$ , respectively, with the respective

amount of active material as 32.5, 46.5, and 56.3 mg·cm<sup>-2</sup>. The cell capacities for all three sizes of metal foam gradually decreased with increasing current density. Among the three, the foam with the largest size had the greatest capacity at low current density. But the order changes at current density of 3 mA·cm<sup>-2</sup>, where the foam with larger size starts to display lower capacity than the one with smaller size. As current density increases more, the capacity difference among the three electrodes also reduces. On the other hand, with increasing current rate or C-rate, the three metal foams of varying cell size showed no difference in specific capacity at lower rates. While all three cells displayed poor rate performance, the cell using the largest 1200 μm size showed the worst performance among the three. However, this performance is better than the aluminum foil current collectors when compared in a C-rate vs. Capacity graph, as the cell capacity using metal foam was decreased much less with increasing C-rate compared to the aluminum foil [81]. Differences were also seen in comparison of the charge-discharge curves at a lower current density. No difference in power performance was noticed in the plateau region due to identical over-potential. But at a higher current density, the over-potential of the cell with 1200 μm cell size metal foam increased much more rapidly than the other two smaller metal foams.

In another work by Yang et al. [82], electrodes using Ni alloy foam current collector were pressed or put through calendaring to produce a different density than an unpressed electrode. Electrodes with 4 w.t.% carbon black were compared with charge-discharge curves at 4 mA (0.5C), AC impedance curves, and cyclic voltammetric curves. Significant difference in performance for pressed and unpressed electrodes was observed. The voltage drop at the plateau region of the charge-discharge curve and the calculated internal resistance were much higher for the unpressed electrode. The high internal resistance in the unpressed electrode was explained using the AC impedance analysis, where the charge transfer resistance is shown to be four times greater than

that of the pressed electrode despite the higher capacity. However, the effective redox area is also larger for the unpressed electrode because as calendering process doubles the density of the pressed electrode, it effectively makes the transport paths more torturous with decreased cell space, leading to diffusion limitation [83]. Despite having a larger redox area, the unpressed electrode has poorer conductivity and requires higher energy to transfer the same amount of lithium as the pressed electrode. Yang et al. resolved the drawbacks of both pressed and unpressed electrodes by introducing more carbon black to 14 w.t.%. This increases conductivity effectively and reduces the internal resistance for the unpressed electrode. The conductive additive has a positive influence on both electrical conductivity and porosity [84], but lowers the packing density [85]. Carbon black, typically in the range of 10 and 100 nm, is commonly used by cell manufacturers as it is not only cheap, but also has large contact surface area [86]. For the pressed electrode, the introduction of inactive material decreases the thickness and density, hence reducing the diffusion limitation. The additional carbon black in the pressed and unpressed electrodes shows little difference in the voltage drop in the charge-discharge and impedance curves.

In addition to electrical and thermal properties, current collectors need to have proper geometry to mechanically overcome the stress from lithium ion diffusion. Zhang et al. [87] investigated the stress distribution within current collectors. It was seen that current collectors of large electrodes with symmetric structure undergo uniform tensile stress, whereas those with asymmetric structure experience bending and thus non-uniform stresses. If the current collectors are too thin, they will not be able to bear the stress at the interface and potentially cause safety issues. As long as the minimum requirement of strength is satisfied, it is necessary to minimize the current collector thickness to an extent that materials having small elastic modulus can effectively reduce stress level.

### 2.5.2. Electrode-Collector Configuration

The effects of size and the placement of current collectors were examined by Kwon et al. [88]. Different electrode-collector configurations were compared. The current collectors for anode and cathode are made from copper and aluminum, respectively. The placement of the current collecting tabs on electrodes significantly influenced the potential distribution and current density distribution. The potential gradient reaches maximum in areas near the tab, where all of the current flows from tab to whole electrode plate. A simple one-dimensional (1D) battery model was used in the study, assuming that gradients of the variables are negligible in the two directions parallel to the current collectors. This simplification works for small-scale batteries because potential drops along the collector and the ohmic drop affects the current distribution.

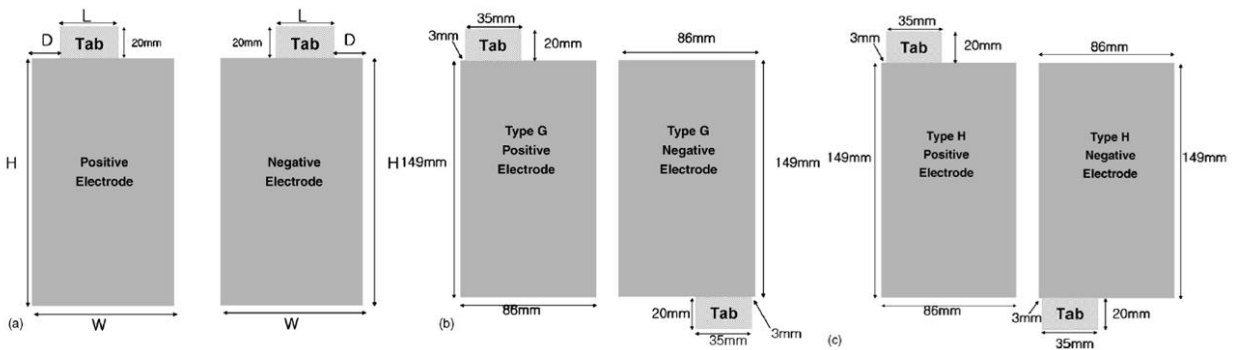


Figure 2.17. Electrode-collector configurations: (a) types A–F, (b) type G, and (c) type H [88].

## 2.6. Modeling and Simulation Tools

Various simulation models for battery were developed in the past two decades to understand and predict lithium ion diffusion process, thermal and mechanical effects in charge-discharge cycles, and even atomistic scale phenomena. Simulation models allow us to design and optimize battery much more efficiently than relying on physical experiments. Simulation based design optimization is a cost-effective approach to quickly check feasibility of design and search

the optimum. Comprehensive reviews of simulation models for battery are available, including electrochemical processes [89, 90], electrical circuits [91], thermal modeling [92, 93], and atomistic scales [94]. Instead of providing a comprehensive review here, we only highlight the available modeling and simulation tools for battery design so that readers can have an overview.

## **2.7. Electrochemical, Thermal, and Mechanical Models**

To model electrical currents at a molecular level, the diffusion of lithium ion needs to be explicitly captured. Doyle et al. [95, 96] developed a 1-D electrochemical model in which the lithium ion diffusion in the electrolyte solution is captured by the evolution of ion concentration, which is also combined with the kinetics that occur at the electrode-liquid interface in the Butler-Volmer form. Sikha et al. [97] built a 1-D model of charge density diffusion in both solid and liquid electrolyte phase. The diffusion in the solid phase follows the Fick's law of diffusion, whereas the mass balance in solution phase is similar to the one in Doyle et al. [95]. Kennell and Evitts [98] developed a 2D transport model for diffusion of species, coupled with Laplacian equation of electrical potential. The edge effect of electrodes was investigated with this model. With porosity in consideration, Arunachalam et al. [99] developed a mesoscale mass and charge transport model in electrode and electrolyte phases from the homogenization of a microscale model for porous electrodes. Recently, Zhang and Tartakovsky [100] derived a homogenized macroscopic ion transport model in nanoporous electrode that captures dynamics of electrical double layer.

The heat generation in battery is closely related to energy conversion efficiency. Rao and Newman [101] estimated heat generation from thermodynamics and electrochemical processes. Pesaran [102] used a lumped capacitance thermal model to predict temperature changes according

to battery usage cycles, cooling, and battery types. Saw et al. [103] used a 1D electro-thermal model to predict temperature changes in charging and discharging cycles.

Coupled with the main electrochemical processes, irreversible intercalation and side reactions at SEI, where loss of ions and active materials, as well as impedance increase occur which cause capacity fade and degradation of battery performance, were also modeled. Fu et al. [104] extended electrochemical modeling to capture the lost ions and active anode materials so the capacity fade is predicted. Kupper and Bessler [105] extended 1D thermos-electrochemical model to simulate the aging effect. Kakimoto and Goto [106] developed an electrical circuit model of capacity fade. Mesoscale multi-physics approaches to predict electrochemical-thermal effects [107, 108, 109], electrochemical-mechanical effects [110, 111, 112, 113], or electrochemical-thermal-mechanical coupled effects [114] have also been developed and widely used.

## **2.8. Application of Commercial Simulation Packages**

Using commercial simulation software tools, Jeon and Baek [115] studied the transient thermal property of batteries during discharge with ABAQUS. Samba et al. [116] developed 2D transient battery thermal models and solved with ANSYS. Zhang et al. [117] studied electrical-mechanical-thermal properties of cells using LS-DYNA. Kindermann et al. [118] developed a SEI model to predict aging effects due to capacity and power fade using COMSOL.

## **2.9. Atomistic Modeling**

Different from continuum schemes, atomistic models capture atomic movement explicitly. Newman et al. [119] applied molecular dynamics (MD) simulations to predict diffusion coefficients for continuum models, and showed that reduction of conductivity and the increase of salt concentration in liquid electrolytes are caused by ion association. Kim et al. [120] used MD to

simulate the formation and growth of SEI with different types of electrolyte. Takenaka et al. [121] combined Monte Carlo with MD to study the sensitivity of electrolyte types on SEI formation.

Compared to MD for nanosecond scale simulation, kinetic Monte Carlo (kMC) [122] is able to simulate much longer time scales in the electrochemical reactions and diffusions. Methkar et al. [123] applied kMC to simulate the formation of SEI layer at a graphite anode. Yu et al. [124] used kMC to simulate the ion and electron-polaron diffusions in electrodes. Blanquer et al. [125] used kMC to model the oxygen reduction reaction in porous electrodes and diffusion of  $O_2$  and  $Li^+$  in electrolyte.

At quantum level, density functional theory (DFT) was also applied to study battery material properties. For instance, Bedrov et al. [126] combined DFT and MD with reactive force field (ReaxFF) to study the formation of SEI. Wu et al. [127] applied DFT to study the electrochemical, thermal, and mechanical properties of  $LiCoO_2$  for thin film battery. Xu et al. [128] studied the diffusivity of ion and electrical conductivity for  $Cr_2C$  and  $V_2C$  as potential anode materials. First-principles molecular dynamics has also been applied to study reaction and diffusion behaviors in batteries [129, 130].

## **2.10. Equivalent Circuit Model**

Equivalent circuit model (ECM) can predict the battery performance and service life. In the ECM approach, it is common that data obtained from electrochemical impedance spectroscopic (EIS) are used when making an equivalent circuit. However, finding resistance values for the circuit is time consuming in practical applications and the circuit is mostly state-of-charge (SOC) dependent. From the experimental data, the experimental resistance can be derived as a function of SOC by using the Ohmic law. For instance, Dubarry et al. [131] used ECM to capture the conditions of the cell operation and simulate the battery performance characteristics. The

resistance curves at different rates showed abrupt changes, which means that there are some phase transformations such as staging of the anode material. However, these were expected because those regions are locations where staging was expected to occur. The integration of the ECM tool with cell testing to enhance the battery performance. The integrated testing and simulation would lead to a new method to design a sophisticated battery model without the need to understand the chemistry.

## **2.11. Design Optimization**

For battery design and optimization, the best combination of design parameters need to be obtained so that battery performance can be optimized. Therefore, battery design is an iterative searching process. The major research challenges of design optimization include the selection of several quantitative measures as objective functions for optimization and trade-off between them, as well as the consideration of multiple significant parameters in higher dimensional spaces. Here, we provide a review of existing work on design optimization of batteries.

### *2.11.1. Optimization Methods with Multiple Design Parameters*

Various optimization algorithms and methods have been applied to optimize battery performance, where the best combination of design parameters is sought. Both gradient-based and gradient-free algorithms have been applied. The most commonly used objective is energy density of battery cell, where improving the performance is the most important goal. Another one is the mass or weight of battery, where reducing weight is important for applications. If multiple design objectives are involved, multi-objective optimization methods are needed.

### *2.11.2. Sensitivity Informed Optimization*

De et al. [132] maximized the specific energy of the battery by optimizing design parameters simultaneously by first optimizing the most sensitive parameters and then subsequently performing optimization on lesser sensitive parameters to speed up the simulation. Through simultaneous optimization, one could check if the potential benefits of optimized electrode thickness would be limited given fixed porosity values. For a single one-parameter optimization, the thickness of the positive electrode was optimized. Neither improvement nor degradation of energy density could be noticed as compared to the battery with base conditions due to the discharge time constraint. The specific energy decreased with increased applied current density at the same rate as the base case. The authors denote that it is advantageous to have reduced thickness because it leads to less weight, which is desirable in my applications, but it is disadvantageous because it decreases capacity. Moreover, increase in thickness results in increased capacity but causes underutilization. For a two-parameter optimization, cathode porosity was included as a design parameter in addition to thickness. While minimum discharge duration was maintained, up to a 25% energy density increase was observed at higher current density. For a three-parameter optimization, the porosity of the anode was included to the list of design parameters and the results showed a much higher energy density at lower current density levels but no improvements at higher current levels. This indicates that the discharge time constraint prevents improvements beyond a certain limit. Lastly, the thickness and porosity of both electrodes were optimized in a four-parameter optimization that showed some more improvement in energy density at higher applied current. The results showed that if there are more number of design parameters that are optimized simultaneously, increased energy densities could be achieved. This study is noteworthy because this procedure could be further applied in many other applications such as managing

charging/discharging capacity and thermal behavior to meet various energy and power requirements accordingly.

### *2.11.3. Sequential Quadratic Programming*

For energy density optimization, Xue et al. [133] implemented a gradient-based algorithm called Sequential Quadratic Programming (SQP) on a 2D battery model. The model consists of a full sandwich cell with porous electrodes, and the active materials are modeled as uniformly-sized spherical particles. Since both morphological and material transport properties are closely related, various discharge rates have been applied to determine corresponding optimal morphology of electrode. SQP optimization algorithm is applied to the framework in which gravimetric energy density is minimized with respect to bounded variables such as thickness, porosity and particle size. Because SQP is gradient-based, the gradients are derived to find the search direction and the step size toward an optimal design and in this case, a complex-step approximation method was used. To maximize energy density, twelve design variables have been selected with their respective lower and upper bounds between which the variables can vary freely in nine different optimization runs. The design variables include the cycling rate, separator thickness and five variables for each electrode.

Without having any electrochemical reactions, separators do not contribute to the physical model of the cell, and the ions in the separators only serve to transport charges. It would be desirable to remove the separator completely as a whole as it contributes to the cell weight that must be ideally minimized. Therefore, the minimum amount of separator was used such that the separator does not cause any short circuit between the electrodes. As the specific power density is increased, the thickness of the electrodes tends to become thinner while the porosity is increased simultaneously. It can also be interpreted that this same combination of a thinner and more porous

electrodes lead to reduced energy capacity. It can be noticed that the positive electrode is relatively thicker and more porous than the negative electrode in the optimal cell design due to higher volumetric coulombic capacity of the positive electrode. Higher porosity is necessary to supply sufficient iron transport rate. Diffusivities and conductivities that are both transport parameters of the electrodes have been considered in the optimization, but having a low sensitivity up to an order of magnitude, they were shown to have minimal effect on the energy density.

#### *2.11.4. Direct Search Method*

Dai et al. [ 134 ] investigated porosity and thickness of both electrodes in a  $\text{LiMn}_2\text{O}_4/\text{graphite}$  cell using Direct Search Method to determine how the current can be optimized with discharge time being maintained. Because the objective function is not continuous, it is not suitable for a gradient-based optimization. Since only the small number of variables were computed in the study, the direct search method was suitable, otherwise it would take longer time. The optimization tool was applied to compare the two designs with constant and varying porosity. However, both designs behaved similarly, and authors believe it is because of a trade-off between energy density and discharge time on the optimized designs. On the other hand, the authors have found that more ideal energy density can be obtained by decreasing tortuosity, which they believe to be the important design parameter to investigate further.

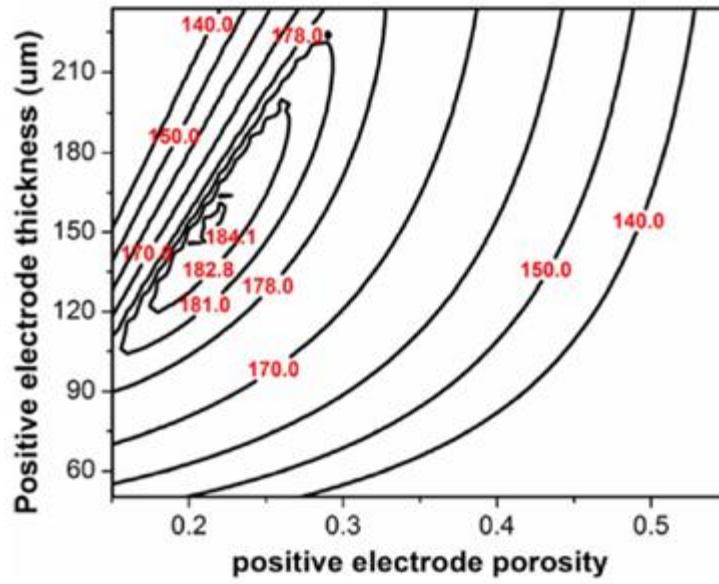


Figure 2.18. Energy density as a function of positive electrode thickness and porosity [134].

#### 2.11.5. Particle Swarm Optimization

Particle Swarm Optimization (PSO) is a widely used optimization tool that provides the effectiveness and accuracy as it iteratively searches for optimal solutions by updating prime candidates. PSO is similar with the method of Genetic Algorithm which seeks an updated optima in each generation among a population of random solutions. However, what differentiates PSO from Genetic Algorithm is that PSO does not perform crossover and mutation operators and that the potential solutions referred to as particles perform the search in design space using the current optimum particles. Similar to lithium-ion batteries, lead-acid batteries also require optimization due to its characteristics of low energy content, high dimension and weight. Increasing the energy content through experimental trial and error method is simply not feasible and very time consuming. In fact, Pourmirzaagha et al. [135] implemented PSO on a 1D non-isothermal lead-acid battery.

Two single-objective scenarios were considered. In the first scenario. The objective of optimizing the four components of the battery to achieve the maximum energy was considered under the constraint of same total thickness. It was shown that the positive electrode thickness increased 67% while negative electrode thickness was reduced by 38.3% while the electrolyte and separator also decreased. This has resulted in an overall increase of energy content by 27.6%. In the second scenario in which the energy and the cut off voltage was kept constant, the total thickness of the cell decreased 23.8% or by 0.0451 mm.

Furthermore, to achieve an optimal solution while achieving two objectives of energy content and thickness simultaneously through multi-objective optimization, a Multi-Objective PSO (MOPSO) was used on 50 particles in 100 iterations. Multi-objective optimization is a process that finds countless solution points that contain a trade-off between the objectives. Among these solution points, the best trade-off was determined by Pareto optimality. The best trade-off on the lead-acid battery cell was a 16.3% increase in energy content and 13.7% decrease in the cell size. This study shows that a definite trade-off between energy content and dimension exists that must be determined through optimization for optimized battery performance.

#### *2.11.6. Surrogate Based Optimization*

A combination of a gradient-based optimizer with a surrogate model was suggested by Du et al. [136] in which raising power density and gravimetric energy simultaneously was the goal. The optimization process started with the design of experiments to select design points to generate simulations of P2D model. The surrogate model was then constructed based on the cell model simulations, and global sensitivity analysis (GSA) was applied to the surrogate model to simplify the process by adjusting variable bounds. With reduced problem complexity, a new refined surrogate model was constructed and the rough optimization design points were identified. On the

other hand, the gradient-based model was constructed directly from the cell model simulations. The main concern of the study was with thickness and porosity because the authors were interested in investigating how optimal thickness and porosity would change with respect to different design parameters, not just under a specific condition. Therefore, with the two optimization methods, the effect of cycling rate, particle size and diffusivity on the optimal thickness and porosity were studied through two different cases. In Case 1, a thick electrode with low porosity is desired for high diffusion and low C-rate. In Case 2, the optimum is a thick electrode is desired with higher porosity to keep a low diffusivity and high C-rate. Unlike Case 1, Case 2 could have two optimization models with only a 2.5% difference in the final energy density between the two models. Although the authors observed less than 5% of prediction error with the surrogate model in many design cases, they were concerned that it is possible for prediction error to be more than 10% in few isolated cases. Under any combination of variables, the surrogate model maps the entire design space while the gradient-based model is very focused on finding maximum or minimum. Therefore, the authors make a significant suggestion that combining the two approaches would benefit each other because the surrogate model would eliminate any discontinuities or local max/min. In addition, the gradient-based model could reduce the prediction error caused by the surrogate model.

Although the above study was able to optimize based on a physical model, the study was done on a cell-level model which does not include any packaging or microstructure particles, which may lack details to be used on real applications. Du et al. [137] further performed the microscopic simulation with a surrogate-based multi-scale model to analyze interfacial electrochemical kinetics. First, the microscopic model was created with a representative elementary volume (REV), which represents a part of 3D electrode as a cluster of particles, and a

Cartesian voxel method was used to create mesh of REV. In order to study microscopic transport and electrochemical properties in a macroscopic level, a kriging surrogate model was built. However, it was shown that the developed kriging surrogate model would lose some of the microstructure information. Therefore, GSA was applied to limit the problem size effectively. It was shown that the kriging model is still not a satisfying solution because its gradients are not clearly defined. As a result, a polynomial response surface (PRS) surrogate model was introduced to enhance the GSA generated kriging model. The variables in a PRS surrogate model were solid-phase ion concentration and overpotential. In their work, 2463 REV realization cases were simulated to observe the relationship between tortuosity and porosity in a microscopic level, and the Bruggeman equation was generated based on the simulation results. After, the generated Bruggeman relationship was compared with the common Bruggeman equation used in the macroscopic model. It was illustrated that the Bruggeman equation in a macroscopic level over predicts the cell performance such as the effective diffusivity and conductivity due to under prediction of the tortuosity. In addition, the PRS surrogate model was proved to account both macroscopic and microscopic model as it behaved similarly during discharge in terms of electrochemical reaction flux. When the PRS surrogate model was compared with macroscopic model in terms of cell voltage profile during discharge, a significant difference was not observed. This finding denotes that cell performance is differentiated by number of ions and electrons transferred, not by how they are distributed. However, it is important to note that degradation mechanisms were not considered, which the authors believe to have a strong dependency on the conditions of electrodes.

### 2.11.7. Optimization via Sensitivity Analysis

Sensitivity analysis provides the information of dependency between input variables and output responses, which can be used in optimization. Particularly, local sensitivity is gradient information that can be applied directly in searching optimum. Golmon et al. [138,139] solved the battery design optimization problem based on multi-physics models of electrochemical and mechanical properties. Especially, the study focused on manipulating the scales of porosities and particle radii to maximize the usable capacity of a cell, subject to the constraint of mechanical strength. When a total of 120 variables were analyzed, including 40 macroscale uniform porosities in 100  $\mu\text{m}$  and 80 microscale particle radii between 1 nm and 10  $\mu\text{m}$ , adjoint sensitivity analysis method was applied, which is more efficient with increased number of variables. It was shown that the initial variables result in 17.19  $\text{Ahr}/\text{m}^2$  of usable capacity, while optimized variables result in 29.27  $\text{Ahr}/\text{m}^2$  of usable capacity. For optimization, a Globally Convergent Method of Moving Asymptotes (GCMMA), which is a variant of the Method of Moving Asymptotes (MMA) algorithm [140], was applied. In this algorithm, a convex approximating subproblem is generated in each iteration step and is solved by a primal-dual method, with convergence to a Karush-Kuhn-Tucker optimal point. GCMMA can be effectively used in applications that involve many design parameters but with fewer constraints. Parameters in algorithm include step size, initial adaptation of asymptotes, adaptation of asymptotes, maximum sub cycle number, and the convergence criterion.

The authors took a multiscale modeling approach where macroscale models are obtained from homogenization of microscale ones to improve computational efficiency. Although the optimization did not include microscale reactions such as strain effects between particles, having found that either maximum or minimum porosity and particle size cause higher stresses in the

electrode, the authors studied the optimal layout of electrodes by varying porosity and particle size distribution to achieve the maximum battery potential at the end of discharge with the maximum tensile tangential stress set at 50 MPa. It was illustrated that relatively lower porosity was optimal to increase diffusivity in the front cathode while increasing voltage at the end. It was also demonstrated that smaller particle size in the front cathode was optimal to control the stress levels caused by higher lithium fluxes in that region, while larger particle size at the end was optimal to decrease the rate of lithium insertion so that the battery potential is constant. The optimal design successfully controlled the lithium concentration within the cathode through well distributed porosity and particle size.

In addition to local sensitivity analysis, variance based global sensitivity analysis can provide information of improvement based on available data. Kim et al. [141] investigated the importance of electrode thickness and porosity in the application of Hybrid Electric Vehicles (HEV). This study involved a numerical 1D electrochemical battery model based on nine design parameters, which include porosity, thickness, volume fraction of fillers of both electrodes, porosity and thickness of the separator, as well as conductivity of electrode. In order to simplify the optimization process, Analysis of Variance (ANOVA) was chosen as a screening technique to determine which parameters weigh more than others in importance. A three-level orthogonal array was implemented as a design of experiment to embed nonlinearity and global sensitivity of each parameter. Throughout ANOVA, the contribution ratio, which is the variation of response of one variable to the total variation of response for every other variable, of the nine variables were measured and compared. It was determined that the porosity of anode, the thickness of anode, the volume fraction of fillers of anode and the porosity of cathode each contributed approximately 60.4%, 17.9%, 13.4% and 3.8%, respectively, to maximize battery energy. As the four most

important variables, they were used to make kriging surrogate model that enables the study of electrochemical properties at a macroscopic level [142]. When the optimization was performed using the kriging surrogate model, a 5.12% increase in total energy of battery under mass constraint was observed. In addition, when the HEV model with optimized battery was simulated under a Highway Fuel Economy Test (HWFET) cycle, the final state of charge was improved.

ANOVA was also applied by Hosseinzadeh et al. [143] to develop a statistical analysis of a 1D electrochemical-thermal battery model that optimizes specific energy and specific power. Four variables in the positive electrode were varied in this study, which include particle size (30-100 nm), electrode thickness (20-100  $\mu\text{m}$ ), active material volume fraction (0.3-0.7) and C-rate (1-5). The order of significance of battery design variables could be determined by using Fisher variation ratio of ANOVA. If a factor has a high F-value and is within 5% of  $p$ -values on the confidence level of 95%, it indicates that it is relatively more significant than other variables. It was determined that the electrode thickness and C-rate have the highest F-value for the objective of specific energy and specific power, respectively. In addition, the impact of interactions between two design variables on battery performance was also considered in ANOVA. In fact, the interaction between thickness and volume fraction and the interaction between thickness and C-rate were found to be the most significant factor among the different interactions for maximizing specific energy and specific power, respectively. Optimum energy could be achieved with thicker electrode and lower C-rate, while optimum power could be achieved with thinner electrode and higher C-rate. This demonstrates that both objectives cannot be achieved at the same time. The author claims that a trade-off should be made between specific energy and specific power in order to optimize between two objectives. This study could be further applied with other variables that affect specific power and specific energy such as operating temperature and porosity distribution.

### 2.11.8. Hybrid Optimization

Xue et al. [144] used a unique hybrid optimization method which incorporates a gradient-free optimizer followed by a gradient-based optimizer to investigate on a battery pack design applied in plug-in hybrid electric vehicles (PHEVs). An approximate estimate of optimal design values are achieved using the gradient-free optimizer, then using gradient-based optimization, the estimate value is further refined. Gradient-free optimization methods do not require design space to be continuous or smooth, thus enabling easier coupling with mixed-integer problems. The main objectives were to reduce the mass, volume, as well as material cost of a battery pack. The basic outline of the optimization process starts from the gradient-free optimization that uses augmented Lagrangian particle swarm optimization algorithm, and the results from that are used as starting points for gradient-based optimization to achieve a refined battery model.

The model consisted of  $n$  modules in series while each module consisted of  $m$  layers in parallel. The variables that were used are thickness, porosity, cut-off voltage which controls the number of modules, and number of layers. Overall, 13.9%, 18.7%, and 18.0% of reductions were observed in model's mass, volume and cost respectively, while the power requirement was constant. The optimized parameters were put into the real drive cycle simulations, and they showed a significant improvement on vehicle's efficiency. Since the model used in this study was ideal, more detailed studies are expected with other objectives included such as a capacity fade.

## 2.12. Other Design Objectives

Energy density is an obvious and commonly used design objective for battery. Other properties such as capacity fade, thermal behavior, underutilization and thermal runaway, and charging/discharging profiles are equally important in the process of optimizing battery

performance with desirable efficiency and safety. Here, the objectives of capacity fade and cell temperature distribution are summarized. It should be emphasized that multi-objective optimization is essential for battery design since trade-offs are needed among the objectives.

### *2.12.1. Capacity Fade*

One interesting factor to reduce capacity fade is the charging/discharging profile. Suthar et al. [145,146] focused on intercalation-induced stresses to idealize the charging profile of lithium-ion batteries in a single-particle model (SPM) and a P2D model. While the P2D model can be used to study electrochemical kinetics at higher complexities, the SPM model simplifies the P2D model in a way that porous electrode is treated as a large number of single particles. This is due to the fact that properties such as current are assumed to be distributed uniformly in a SPM [147]. To optimize the amount of transferred charge under the time constraint, the model is used with a reformulation methodology to perform better convergences of properties at higher charging and discharging rates. There are other factors such as side reactions [148] and thermal degradation [149]. The P2D model has focused on the mechanical degradation with emphasis on the stresses within the anode.

It is known that relatively higher stresses are observed in the area where anode touches the separator. A study was performed by Suthar et al. with different sets of constraint placed on radial and tangential stresses. Peak tangential stresses occur on particle surface while peak radial stresses are found in the particle center. Two cases were studied, where in the first case the peak radial stress was restricted at 0.199, whereas it was set at 0.146 in the second case. The derived optimal charging profiles showed a good agreement with stress profiles derived with CC-CV of 3C and 2C. Using the derived charging profiles, peak radial stresses are restricted as expected. It was proved that even a small compromise in charge stored in CC-CV with 4C can optimize the safe

charging profiles that are similar to CC-CV with 2C. Because the anode-separator interface experiences more stresses than other part of the anode, charging profiles could be improved to reduce this stress. Fathy and colleagues [150] conducted similar studies using a MATLAB-based computational tool that combines dynamic programming [151], genetic algorithm [152, 153], direct transcription [154], and pseudo spectral optimization [155]. Such model-based control that constrains properties such as side reaction overpotential to prevent lithium plating was known to perform better than the standard CC-CV charging.

However, in most of these studies isothermal models are applied and the possible impacts of thermal properties are not assessed. It is very challenging to address thermal properties in the models because those properties can contribute more complexity such as domino effects of materials selection on the performance. Therefore, nonlinear thermal properties as well as other capacity fade factors to be applied. In fact, minimizing the SEI layer formation by Model Predictive Control (MPC) [156] and managing thermal behavior by Hybrid Model Predictive Control (HMPC) [157] were investigated to develop optimal charging profiles.

In addition, the focus on capacity fade was addressed by Suthar et al. [158] as the authors believe that managing the capacity fade can directly make the approach to maximize energy density with thicker parameters impractical. Therefore, the study was further developed to observe how porosity and anode thickness at different Bruggeman coefficient and temperature affect the capacity fade mechanisms that include intercalation induced stresses, side reactions at solid electrolyte interface and lithium plating with fixed capacity. The Bruggeman was related to tortuosity that higher Bruggeman coefficient means higher tortuosity. It was demonstrated that smaller Bruggeman coefficients do not affect the capacity fade mechanisms at different porosities and different porosity gradients, but the higher Bruggeman coefficient led the capacity fade

mechanisms to vary at each porosity and porosity gradient. In fact, the thinner electrode with less porosity took longer time to charge at higher Bruggeman coefficient. Also, when the models of different porosity gradients were compared, the design of the negative porosity gradient resulted in more energy density, less maximum peak tangential stress and less peak radial stresses, which indicates that the capacity fade was reduced. Since only the anode was considered, more studies would be necessary to take more design parameters with fixed anode to cathode capacity ratio to observe better capacity fade behavior for each fixed ratio.

### 2.12.2. Cell Temperature Distribution

Thermal behavior in batteries has always been a challenge in the development of hybrid electric vehicle batteries because lithium-ion batteries require a complex and costly thermal management system. The optimization has been applied by Dandurand et al. [159], who tried to find the optimal operating cell temperature distribution on the cell layout, especially on cell spacing. The concept of Pareto optimality was refined in this study to minimize the cell temperature while keeping the evenness of temperature distribution as a multi-objective optimization. The concept of equitability, the case when criterial have common meaning and units, was introduced because it generates an improved design through an even redistribution of the outcomes. For example, two battery packs can have the same overall average temperature while the temperature distributions can be different between two packs. Therefore, the refined Pareto optimality preserves the equity among the criteria of anonymity, comparability, and the Pigou-Dalton principle of transfers, which are the equitable preferences [160]. The term *comparability* indicates equal physical properties among each objective, and the term *anonymity* means that the distribution of temperature is important and not the temperature of a specific battery cell. By the Pigou-Dalton principle, an evenly distributed temperature design is more important than having

the same average temperature. This is a great approach to reduce the number of optimal designs because Pareto itself cannot restrict the available design choices.

Northrop et al. [161] investigated the thermal effects of a cell by varying the temperature boundary conditions based on a 2D model that consists of cathode, separator, and anode. It was demonstrated that each model with a different height could have different temperature, and the positions with more heat generation leads to increased current density. It was also observed that some positions can experience different discharge rate, although the same discharge rate is applied throughout the cell. The authors suspect that if higher discharge rate is observed in a position, then it could result the increase in local capacity and heat generation.

### **2.13. Topology Optimization**

Similar to the geometric factors associated with each component of the lithium-ion battery, topological optimization has been introduced for battery design. This includes different choices of materials for each battery component, and their spatial relationships in the architecture design. It was found that the concept of topological optimization can enhance the battery performance based solely on material choices. In this section, a glimpse review of the concept of topology optimization for battery design, particularly on electrodes, is proposed.

Similar to lithium-ion batteries, components of solid oxide fuel cells (SOFC) also experience ohmic losses. Song et al. [162] optimized the topology of cathode within SOFC by minimizing cathode resistance. The 2D domain is subdivided into small rectangular elements and different materials are assigned to those elements. Simulation runs are applied to predict properties so that the best material assignment is found. The optimal result tends to have larger surfaces or perimeters, which allow more current to come from the ionic transfer boundary condition and more material allows lesser resistance to the current. By having an electrocatalyst material with lower

performance, the surface resistance dominates the cathode's scaffold resistance that results in larger perimeter and longer branches. When the performance of the electrocatalyst material is higher, the focus shifts towards the body of the scaffold. In this range, the performance is improved by emphasizing the ion paths through the scaffold. The cathode shape is more important for larger footprints. For some material properties, it was demonstrated that a larger perimeter itself does not necessarily promise higher performance. The topologically optimized designs have shown nearly 50% improvement as compared to the one-column design, but were very complex and difficult to realize. However, the study provides a guidance of what features to emphasize in the cathode design.

Song et al. [163] continued the study further into the 3D topology optimization of SOFC to idealize the current generation. Specifically, the channel of SOFC where the air flows is topologically optimized in this study. To calculate the air flow field, a modified momentum equation was applied using the Darcy flow term. Then the air flow field is used to calculate the oxygen gas transport, which is essential in converting chemical energy into electrical power within the SOFC. For the SOFC to be optimized, there has to be a trade-off between the air flow and the oxygen exchange interface. Therefore, the design domain tends to form a shape of a ring in order to have a larger interface with sufficient air flow. With higher ratio of oxygen exchange distance to overall air flow distance, it was shown that the interfacial area reaches maximum but the total volume air flow reaches minimum. This explains the significance of optimization between two objectives, as the ratio of 0.3 and 0.5 showed about 9% improvement in current generation. Also, the area of the cathode becomes larger in the bottom part to prevent ohmic resistance from impeding the current. This study has proved that there needs to be a balance between the air flow and the interface area when designing a SOFC, and this combination can be optimized using the

topology optimization method. If this study were to be conducted with more variances in geometry, more improvements could be observed.

A different approach of optimizing a SOFC was studied by Hasanabadi et al. [164]. The authors focused on investigating the microstructure of a SOFC in 3D, which is generated by two-point correlation functions (TPCFs). The objective is maximizing the interfacial area, which is to minimize the cathode impedance and solid-phase tortuosity. The concept of TPCFs comes from the statistical approach of n-point correlation functions that calculates the probability of arrangement of n points. The optimization process is established by first calculating the TPCFs with two independent variables and using a phase recovery algorithm to model in three dimensions. In the study, two control parameters  $b$  and  $q$  were used. The variable  $b$  is a positive characteristic parameter that indicated a coarser microstructure phase when larger. The variable  $q$ , on the other hand, determines the oscillations of the function. It is important to note that intervals of  $0 < b \leq 51.2$  and  $0 < q \leq 40$  were used in modeling in order to satisfy the volume fraction constraint. From Figure 2.19, it can be inferred that the pathways become finer as variable  $q$  increases. This also means that as the active interfacial area increases, both the efficiency of the cathode and tortuosity increases. This study was remarkable in the fact up to 99% of interfacial area within the microstructure is active. With optimal designs, it can be concluded that tortuosity increases when the size of the void channels decreases with increased interfacial area. Lastly, a balance between tortuosity and interfacial area can be obtained under objective of minimizing impedance.

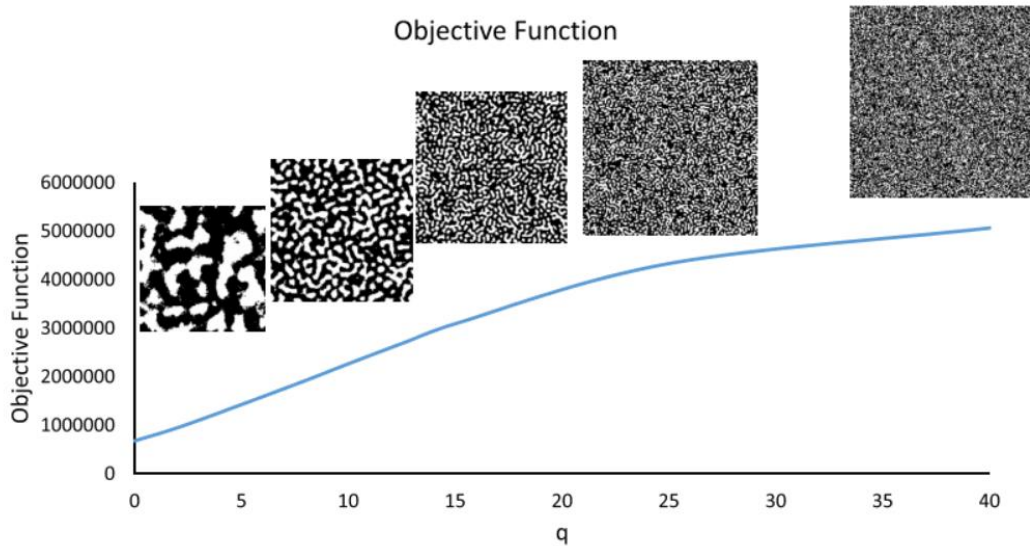


Figure 2.19. Design objective for different microstructures:  $b=1.6$ ,  $q=2.5, 7.5, 15, 25, 40$  [164].

In the lithium-ion battery industry, the need for replacing the traditional graphite anode with silicon has been much desired. However, while having 10 times higher theoretical specific capacity than that of graphite, silicon can experience up to 310% of volume transformation when it reacts with lithium. Topology optimization methods can be applied to prevent detrimental effects. Mitchell et al. [165] applied the density methods and multi-objective optimization in silicon anode design for battery. Optimal designs for good structural integrity and electrical conductivity are sought. First, the optimization was performed for the structural design objective with 30% volume fraction. The filter radius, which is used as regularization and for manufacturing consideration, was varied. The larger filter radius showed more concise and larger structural features. This design is suitable for batteries with both liquid and polymer electrolytes because it can accommodate the large volume due to lithiation and lower state of stress. The lower filter radius showed worse performance and severe manufacturing limitations, so the paper has concluded that an optimal structural design should be simple as possible to realize the manufacturability of the design. For

the objective of optimizing electronic conduction, higher electric conduction was observed in the design with more conductive material. The paper addresses that there is a trade-off between structural and conduction designs to satisfy both design objectives as seen in Figure 2.20. By assigning the weights as 0 and 1, for full conduction objective and full structural objective respectively, the combined objective optimization was performed. The paper concludes that the intermediate frame structure is desired in any volume fraction as it provides solid structure that allows good pathways for reactions. In addition, the authors point out that the structure with lower volume fraction that is just enough to provide durable structure and produce sufficient electrochemical reaction is needed to optimize the design that overcomes the mechanical degradation.

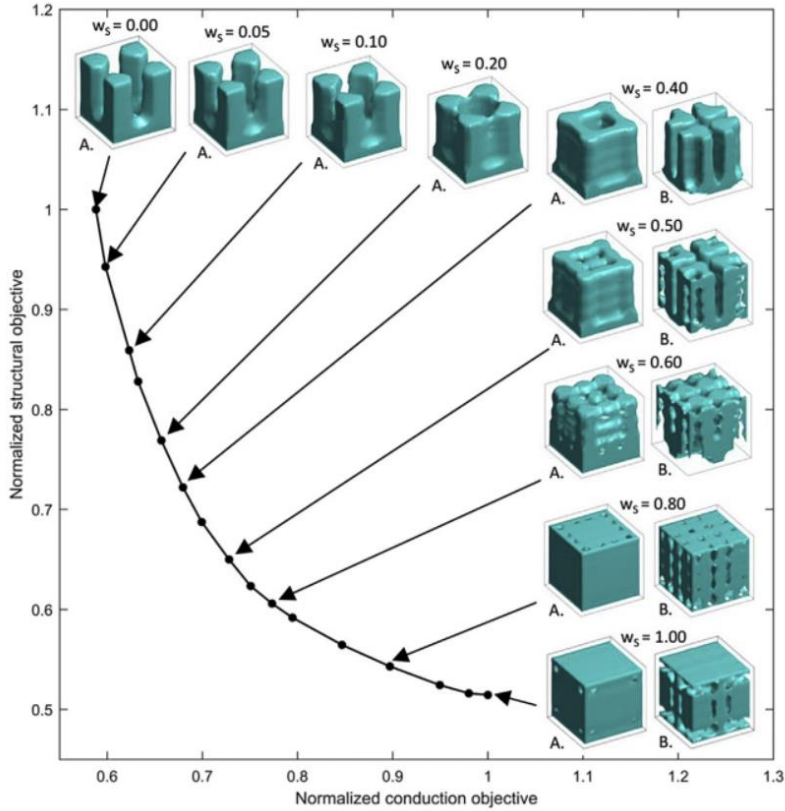


Figure 2.20. The Pareto front for the multi-objective optimal topologies for volume fraction of Base cell (A) and shifted base cell with higher Pareto weights (B) [165].

## 2.14. Multi-Objective Optimization

Hong and Lee [166] focused on various anode thickness and porosity to realize optimization between the objectives of achieving higher energy and lower mass. A reaction zone model was used to analyze the Pareto optimal front of the multi-objective functions in lithium-ion batteries. A reaction zone model is a simplified 2D model that assumes there is a certain constantly shifting 2D zone through the electrodes where the reactions occur in that specific zone only. In this study by Hong et al., Genetic Algorithm (GA) was implemented on the MATLAB-built reaction zone model in order to estimate the Pareto optimal set. GA is a process that iterates each generation that contains a population of individual solutions until the Pareto optimal set is found.

GA is not a biased tool because each generation is modified with a set of non-dominated solutions instead of a single solution for multi-objective optimization. Eventually, such diverse non-dominated solutions lead to Pareto optimal set through each generation. Only thickness and porosity of the positive electrode were changing except that the thickness of negative electrode was adjusted accordingly to maintain the capacity ratio. The authors made an important observation that the objective to find the largest specific energy only gives a single solution while the whole Pareto front provides many set of points that could be useful for other applications in which objectives may need modification. In addition, two more cases, one that requires minimization of area and mass and the other that maximizes the unit area energy and specific energy, were studied. It was concluded that the Pareto front for the first case can be used to obtain results for other cases. In addition, similar shapes of the Pareto front would appear even when additional design variables are added to the study because it is obvious that specific energy of Li-ion battery would start to fall whenever there is significant contradiction between the objectives. It is clear that multi-objective optimizations have more flexibility, but due to limitations of the reaction zone model, the paper was able to optimize two design variables.

Liu et al. [167] focused on multi-objective optimization to maximize discharge specific power and specific energy of lithium-ion batteries, as well as to minimize the capacity loss for long term use. The design parameters included thickness, particle size and porosity for both electrodes and cathode conductivity. In this study a modified Elitist Non-Dominated Sorting Genetic Algorithm (NSGA-II) is implemented for multi-objective optimization, in which all equations, including lithium ion transport, potential variation and kinetics, are computed through finite difference method. The idea is to discretize the computational domain into uniform grids, both design parameters and time, and simulate over time. The NSGA-II reduces the computational

cost of optimization by applying elite-preserving operators that pass on good results until next better results are found. When the stop criterion of 300 generations was met, the process produced Pareto-optimal solutions. The optimized model exhibits a less SEI thickness in anode and improved residual capacity, which is the percentage of capacity remained at the 750th cycle. In addition, more uniformed SEI growth and residual capacity along electrodes were observed. Such uniformity leads to increased battery effectiveness as the authors suggested. In fact, the optimized cell resulted in about 95 nm less in SEI thickness than the non-optimized cell. In addition, the optimized cell has a less degradation and a larger capacity over long-term cycles than the cell that is not optimized. The study improved the battery performance successfully through a reduction of degradations.

Furthermore, Liu et al. [168] expanded the concept of multi-objective optimization using NSGA-II to achieve fast charging. It was aware of that degradation and potential damage to the battery are most likely to occur when fast charging is applied. Therefore, the objectives in this study were to reduce charging time, side reactions, and temperature increase. Particularly, the pulse current parameters were optimized, which include the amplitude of charging pulse and rest pulse, nonlinear decay coefficient and cycle duty. After optimization, the results demonstrated that the charging pulse amplitude and the decay coefficient have decreased to reduce side reactions, while the rest pulse amplitude increased to reduce the battery charging time. As expected, the decay coefficient decreased in order to prevent a battery from current saturation. The study showed that constant current followed by constant voltage (CC-CV) charging takes about 4.3 hours to fully charge a battery model while pulse charging requires only 0.35 hours to charge completely that corresponds to 98% efficiency. The main advantage of pulse charging is that a high current could be supplied while alternating with the rest pulse to prevent concentration saturation without

damaging a battery. This study proved the successful usage of NSGA-II system to optimize the battery design as well as faster charging with minimal side reactions. It is expected to be applied in many different applications of battery usage with many variables included. The authors also applied their system to investigate the optimal porosity-graded electrodes design, where the two objectives were to achieve higher specific energy and lower capacity loss by varying the porosity and thickness in both porosity-grading electrodes. Their simulations showed that the conventional cell with constant optimal porosity is possible to behave a large specific energy as much as the porosity-graded cell, but the porosity-graded cell has advantage on less capacity loss. More experiments are planned in the future to investigate advantages and disadvantages of developing optimal porosity-graded electrodes over a constant optimal porosity cell.

## CHAPTER 3. SIMULATION-BASED DESIGN OPTIMIZATION

### METHODOLOGY

#### 3.1. Battery Electrochemistry

An all solid-state lithium ion battery uses solid electrodes and solid electrolyte while a typical lithium ion or lithium polymer battery uses liquid or polymer electrolytes. Considered as potential alternatives to traditional liquid electrolyte lithium batteries, the solid-state batteries have a greater margin of safety without having any liquid components that are prone to leakages and flammability. Also in terms of recyclability, the potential of releasing noxious gases upon disposal is also eliminated with the use of solid state batteries.

A solid-oxide electrolyte with high lithium ion conductivity is used in a solid-state battery, typically with electrodes of cobalt (Co), nickel (Ni) or manganese (Mn) oxides. At the negative electrode and electrolyte interface, the lithium metal reacts to produce a lithium ion and a negative electron that can be expressed in a simple chemical reaction as follows:



The charge transfer process at the interface of the electrode and the electrolyte is expressed using the Butler-Volmer kinetic expression:

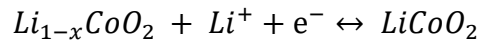
$$J = i_0 \left[ e^{\left( F \alpha_a \frac{\eta}{RT} \right)} + e^{\left( -F \alpha_c \frac{\eta}{RT} \right)} \right]$$

where  $i_0$  is the exchange current density and  $\alpha_a$  and  $\alpha_c$  are the anodic and cathodic transfer coefficient, respectively.  $\eta$  represents the surface overpotential that can be determined using the overpotential equation  $\eta = \phi_1 + \phi_2 - E_{eq}$ , where  $\phi_1$  is the potential in the electrode,  $\phi_2$  is the potential in the electrolyte and  $E_{eq}$  is the open circuit or equilibrium potential of the reaction. For

the negative electrode, the equilibrium potential is set to zero while for the positive electrode, the equilibrium potential is dependent on the lithium concentration inside the electrode. From the Butler-Volmer equation,

$$i_{neg} = Fk_{neg} \left( \frac{c_{Li^+}}{c_{Li^+,0}} \right)^{\alpha_{neg}} \left[ e^{\left( \frac{\alpha_{neg}F\eta}{RT} \right)} + e^{-\left( \frac{(1-\alpha_{neg})F\eta}{RT} \right)} \right]$$

can be obtained in order to determine the reaction kinetics at the negative electrode. At positive electrode and electrolyte interface, lithium ions and electrons react with positive electrode material to form solid lithium and can be expressed as

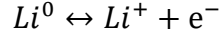


At the positive electrode, the Butler-Volmer equation is again used to determine reaction kinetics, where  $i_{0,pos}$  is expressed as

$$i_{pos} = i_{0,pos} \left[ e^{\left( \frac{\alpha_{pos}F\eta}{RT} \right)} + e^{-\left( \frac{(1-\alpha_{pos})F\eta}{RT} \right)} \right]$$

$$i_{0,pos} = Fk_{pos} \left[ \frac{(c_{Li,max} - c_{Li})c_{Li^+}}{(c_{Li,max} - c_{Li,min})c_{Li_0^+}} \right]^{\alpha_{pos}} \left( \frac{c_{Li} - c_{Li,min}}{c_{Li,max} - c_{Li,min}} \right)^{1-\alpha_{pos}}$$

where  $F$  and  $R$  represents the Faraday's constant with a value of 96485 C/mol and the molar gas constant with a value of 8.3145 J/mol·K, respectively.  $k_{neg}$  is the rate constant of the reaction,  $c_{Li^+,0}$  is the total concentration of lithium ion the electrolyte, and  $\alpha_{neg}$  is the charge transfer coefficient.  $T$  is the temperature, while the  $c$  values,  $c_{Li,max}$  and  $c_{Li,min}$ , represent the maximum level of lithium and minimum level of lithium in the solid electrode. In the electrolyte, the ionization reaction that occurs in which oxygen-bonded lithium becomes lithium ions and negative charges can be expressed as:



The transport of lithium,  $Li^+$ , and the negative ions,  $n^-$ , can be determined using the Nernst-Planck equation, as

$$N_i = -D_i \nabla c_i + \left( \frac{z_i F}{RT} \right) D c_i \nabla \phi_i$$

where  $D_i$  is diffusion coefficient of the species and  $z_i$  is species charge.

The electroneutrality was assumed so that  $c_{Li^+} = c_{Li^-}$  at all times. Faraday's law was then implemented to couple the flux on the interfaces of the electrolyte. While the transport of lithium and negative ions are determined using Nernst-Planck equation, the transport of solid lithium in the positive electrode is represented by Fick's law:

$$N_{Li} = -D_{Li} \nabla c_{Li}$$

The flux of lithium ions on the electrolyte boundary and solid lithium on the electrode-electrolyte boundary are coupled to the electrochemical reactions using Faraday's law.

### 3.2. Bayesian Optimization

There has been increased efforts to develop better techniques in global optimization. Bayesian optimization is a powerful tool that is used for optimizing objective functions which are very computationally expensive or slow to evaluate. It is regarded as an efficient optimization technique that is able to optimize problems of bounded difficulty in a short amount of time with efficiency. Such optimization methods have been applied in areas of robotics [169], environmental monitoring [170] as well as machine learning [171]. In this work, the application of this optimization in the area of lithium ion battery simulation is investigated. Any problem that consists of an objective function and requires minimization or maximization can be said to be a global

optimization problem that can be optimized using Bayesian optimization. In mathematical terms of determining the maximum of an undetermined function can be expressed as

$$\mathbf{x}^* = \arg \max_{\mathbf{x} \in \mathcal{S}} f(\mathbf{x})$$

where  $\mathcal{S}$  can generally be understood as a design space of interest or a search space and  $f(\mathbf{x})$  is the unknown or the black-box function that is calculated at random point  $\mathbf{x}$ .

To achieve global optimum, whether it is a minimum or a maximum, a random-sampling can be used, perhaps, until an optimum is reached. Regardless of efficiency and speed, random-sampling will eventually solve the problem and present the optimum at the end. However, because this sampling is random, it is not efficient. By going through each and every value through random sampling until an optimum is achieved without any optimization procedure, it is extremely inefficient, time-consuming and computationally expensive.

The Bayesian optimization is a unique nonlinear optimization that the algorithm determines the subsequent points to explore based on the distribution analysis of the current function that has been generated previously. Based on what is known already, which is referred to as a prior or prior belief over the function, subsequent values called the posterior are generated while the model is updated after every iteration.

### 3.3. Gaussian Process

Gaussian process is a distribution over functions that is defined by mean function and by covariance function. It is a commonly used stochastic process for modeling dependent data that is favored due the fact that the Gaussian process is determined only by mean and covariance. It is basically an extension of multivariate Gaussians to infinite-sized arrays of real-valued variables. For any length vector that is finite in length and expressed as  $x = [x_1, x_2, \dots, x_n]^T$ , there is a

corresponding vector  $F_x = [F_{x_1}, F_{x_2}, \dots, F_{x_n}]^T$  with Gaussian distribution. This can be simply expressed as

$$F_x \sim N\{\mu(x), k(x, \hat{x})\}$$

In the expression above,  $\mu(x)$  is the mean function,  $k$  is the kernel or the variance function that characterizes correlations between different points in the process. If  $x \approx x'$ , then  $k(x, \hat{x})$  approaches this maximum, meaning  $F_x$  is nearly perfectly correlated with  $F_{x'}$ . If  $x$  is far from  $x'$ , then  $k(x, \hat{x})$  approaches zero, meaning  $F_x$  is very far from  $F_{x'}$ . In a simple linear regression, consider a function  $y$  of an independent variable  $x$ . Because the function is linear, the slope and the intercept of the line can be set as parameters  $\theta_0$  and  $\theta_1$ , respectively, to formulate the equation form of  $y = \theta_0 + \theta_1 x + \epsilon$ , where  $\epsilon$  is the irreducible error. The Bayesian linear regression uses a probabilistic approach by finding a distribution over the parameters after every newly observed data point. However, the Gaussian process is a non-parametric approach to find a distribution of possible functions rather than parameters, using a prior distribution of known values to produce a posterior distribution.

Characterized by prior mean function  $\mu$  and its covariance function  $k$ , Gaussian process regression assumes that  $f = f_{1:n}$  are jointly Gaussian and their respective observations are normally distributed. Given that  $x$  is a set of observation points and  $F_x$  is resulting real-valued observation, the posterior distribution of a new point  $\hat{x}$  can be computed as

$$\mu(\hat{x} | x) = \mu(\hat{x}) + k(\hat{x}, x)k(x, x)^{-1}(F_x - \mu(x))$$

$$\sigma^2(\hat{x} | x) = \mu(\hat{x}) + k(\hat{x}, x)k(x, x)^{-1}(F_x - \mu(x))$$

### 3.4. Acquisition Functions

Once the Bayesian optimization determines the probabilistic belief about the unknown function  $f$  through the distribution  $\mathbb{R}^N$  from the set of points  $\{x_n \in \mathcal{X}\}_{n=1}^N$ , an acquisition function is necessary to determine the location of where to evaluate next. An acquisition function for Bayesian optimization is an inexpensive function that is evaluated at a given point that is equivalent to where the next  $\mathbf{x}$  is expected to be in a minimization or a maximization problem. This acquisition function is then optimized to select the next location. The acquisition function is a balance between exploration and exploitation. Exploration is the act of searching regions or points in the surrogate model with high uncertainty and exploitation is the act of searching in the regions in the model where the value is already estimated to be high, hence they are points with low mean. It is important to determine a tradeoff between exploration and exploitation. The Bayesian optimization algorithm is designed to choose the next point or query by maximizing the selected. acquisition function.

There are three different kinds of acquisition function that are commonly used. These acquisition functions depend completely on the predictive mean function  $\mu(x; \{x_n, y_n\}, \theta)$  and the variance function  $\sigma^2(x; \{x_n, y_n\}, \theta)$ . An improvement-based acquisition function called Probability of Improvement (PI) evaluates the function  $f$  at a point that is most likely to improve from the already determined value. This acquisition function determines the probability that a point  $x$  leads to an improvement. Let's assume that  $f'$  is the minimum point of function  $f$  determined so far, and therefore,  $f' = \min f$ . This acquisition function then evaluates  $f$  at this point as the minimum point of the function is the point that has the most chance of improving as compared to other points that are greater. A utility function, or simply a negative loss function, assigns a reward

of value 1 if the evaluated function is less than the current minimum  $f'$ , and no reward of value 0 if it is greater. The utility function  $u(x)$  can be expressed as the following:

$$u(x) = \begin{cases} 0 & f(x) > f' \\ 1 & f(x) \leq f' \end{cases}$$

Because it is known that the posterior distribution of the function is Gaussian, the equation below for the acquisition function  $\alpha_{PI}$  can be used to calculate this probability.  $\Phi$  is the standard normal cumulative distribution function and in order to maximize  $\alpha_{PI}$ . The point with the highest probability of improvement or with the maximal expected utility is chosen.

$$\alpha_{PI}(x; D_n) = \Phi\left(\frac{\mu_n(x) - \tau}{\sigma_n(x)}\right)$$

The Probability of Improvement performs satisfactorily when the target is known but when the target is unknown, this acquisition function loses efficiency. There are cases when the acquisition function is lost in a local optimal value and exploration efficiency decreases. Improving on this drawback, another acquisition function known as Expected Improvement (EI) can be used.

The Expected Improvement acquisition function differs from the Probability of Improvement that instead of being based on the chance that an improvement will exist, it accounts for how great the magnitude of improvement is. As seen in the utility function below, an award will be received which has a value of the improvement that is the difference between the current function and the minimal value.

$$u(x) = \max(0, f' - f(x))$$

$$\alpha_{EI}(x; D_n) = (\mu_n(x) - \tau) \Phi\left(\frac{\mu_n(x) - \tau}{\sigma_n(x)}\right) + \sigma_n(x) \varphi\left(\frac{\mu_n(x) - \tau}{\sigma_n(x)}\right)$$

Just as the name suggests, the expected value of the gain from the sampling of the new point is computed through this acquisition function. There are two components in expected

improvement. The first part of the equation with the mean function  $\mu_n(x)$  can be increased by decreasing the mean function. The second part of the equation can be increased instead if the variance  $\sigma_n(x)$  is increased. These two parts can be adjusted as a tradeoff between evaluating points with low mean and high uncertainty. This is a tradeoff or a balance between exploitation and exploration that the expected improvement considers. Expected improvement is commonly used in practice because it works well, it is easy to implement and it is easy to understand.

An alternate acquisition function is called the Upper Confidence Bound (UCB). Usually, the Upper Confidence Bound is used in applications where function  $f$  is maximized rather than minimized. When maximizing  $f$ , the equation can be as follows:

$$\alpha_{\text{UCB}}(\mathbf{x}; D_n) = \mu_n(x) + \beta_n \sigma_n(x)$$

When minimizing  $f$ , the equation can be expressed by reversing the sign of the second component to a negative sign.

$$\alpha_{\text{LCB}}(\mathbf{x}; D_n) = \mu_n(x) - \beta_n \sigma_n(x)$$

The Upper/Lower Confidence Bound acquisition function has been a popular method of determining a tradeoff between exploration and exploitation that corresponds to the mean  $\mu_n(x)$  and variance  $\sigma_n(x)$ , respectively. The tradeoff parameter  $\beta_n$  must be greater than zero while  $\sigma_n(x)$  is the marginal standard deviation of  $f$ . The idea is that an iterative application of this acquisition function will result in a convergence of the global minimum value. In other words, points where there is high mean or points where there is high variance can be sampled by varying the value of tradeoff parameter.

### 3.5. Parallelization of Bayesian Optimization

The parametric sweep function in COMSOL Multiphysics is useful when modifying a few parameters within the provided range of numbers. However, because it has to go through each and every provided numbers for each iteration, this is not efficient and because it low dimensional, it is not a good method of optimization. It is oftentimes desirable to send batches of parameter values to explore, especially when large parallel processing capabilities are available.

The Bayesian optimization is used to optimize an unknown function  $f$  with the goal of finding an appropriate solution of the minimum or the maximum. It is conventionally considered as a sequential problem when each experiment or iteration is completed before going on to the next one. For complex functions, evaluating function  $f$  can be expensive or time-consuming, thus it is necessary to carefully calibrate the exploration-exploitation tradeoff. When an experiment is considered costly, it means that it takes a long time to evaluate and resources such as time and computational power is limited. Hence, it is desirable to conduct multiple experiments in parallel instead of in sequential. Through parallelization, it is possible conduct many experiments simultaneously, resulting in more evaluations within a given amount of time. To achieve parallelization, “batches” of runs or experiments must be set up that will run simultaneously to explore and exploit the function on regions of high estimated value.

The algorithm enables the input of the exploit and explore size, after which a hallucination loop is conducted. The term ‘hallucination’ means observations when the prior mean is used instead of a function evaluation, which is used to update the posterior mean and variance. With absence of information to update the posterior mean, function evaluations are approximated using prior or points from information about posterior variance. During the ‘hallucination’ process, the  $\mu_{\text{predict}}$  is set equal to  $\mu_{\text{actual}}$  for one iteration according to GP-UCB. Then pure exploration is

conducted to explore the most unknown region. The Bayesian optimization algorithm is modified to enable parallel simulations once the posterior mean and variance are determined.

## CHAPTER 4. DEMONSTRATION AND OPTIMIZATION RESULTS

The simplest lithium ion battery model can be demonstrated as a one dimensional geometry as shown in Figure 4.1. The goal is to optimize the thickness of each of the battery components within a fixed length, which would be the battery's total thickness.

### 4.1. One-Dimensional (1D) Model Simulation

In solid state batteries, the liquid electrolyte is replaced with a solid electrolyte that is advantageous since it eliminates the necessity of a container that can hold the liquid electrolyte in place. Moreover, the difference between traditional lithium ion battery and solid state battery is that solid batteries do not use porous electrode. The solid state battery will be simulated using the Tertiary Current Distribution interface to simulate the transport and potential of the electrolyte. The performance factors that are of interest are the electrolyte potential, electrolyte concentration of lithium ions and electric potential of positive electrolyte-electrode interface.

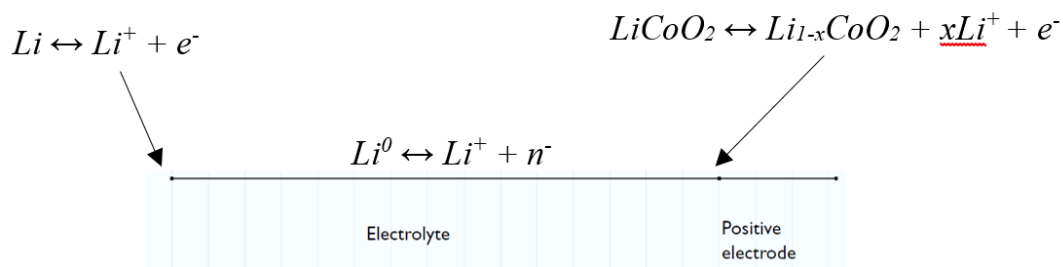


Figure 4.1 One-dimensional solid-state lithium battery showing the electrolyte, positive electrode and the interfaces in between

The simulations that are conducted are time-dependent and are completed using COMSOL Multiphysics. Between the negative electrode and electrolyte, the lithium metal reacts to generate lithium ion and electrode as follows:  $Li \leftrightarrow Li^+ + e^-$ . Between the positive electrode and the

electrolyte, lithium ions and electrons react according to  $Li_{1-x}CoO_2 + Li + e^- \leftrightarrow LiCoO_2$ . The Butler-Volmer equation is used at both electrodes in two different forms. Prior to conducting optimization on the model, a few cases of variable electrode-electrolyte interface have been demonstrated for a lithium battery cross section of width 1.3 mm and 0.2 mm to observe any impacts on performance. The source of electric current is located at the top boundary of the battery and it covers a distance of exactly half of the battery length. The total current is -0.05 [A] with a boundary electric potential initial value of 1 [V]. The positive electrode that consists of  $LiMn_2O_4$  spinel is the domain that is in contact with the electric current. The negative electrode is assigned to a material of a lithium metal for the electrode kinetics, which has an anodic and cathodic transfer coefficient of 0.5 and an anodic and cathodic rate constant of 0.001 [m/s]. The electrolyte reference concentration is 1 [mol/m<sup>3</sup>]. These initial values must be assigned before any simulation. The electrolyte and electric potential are both set to 0 V and the electrolyte salt concentration is set to 1000 mol/m<sup>3</sup>.

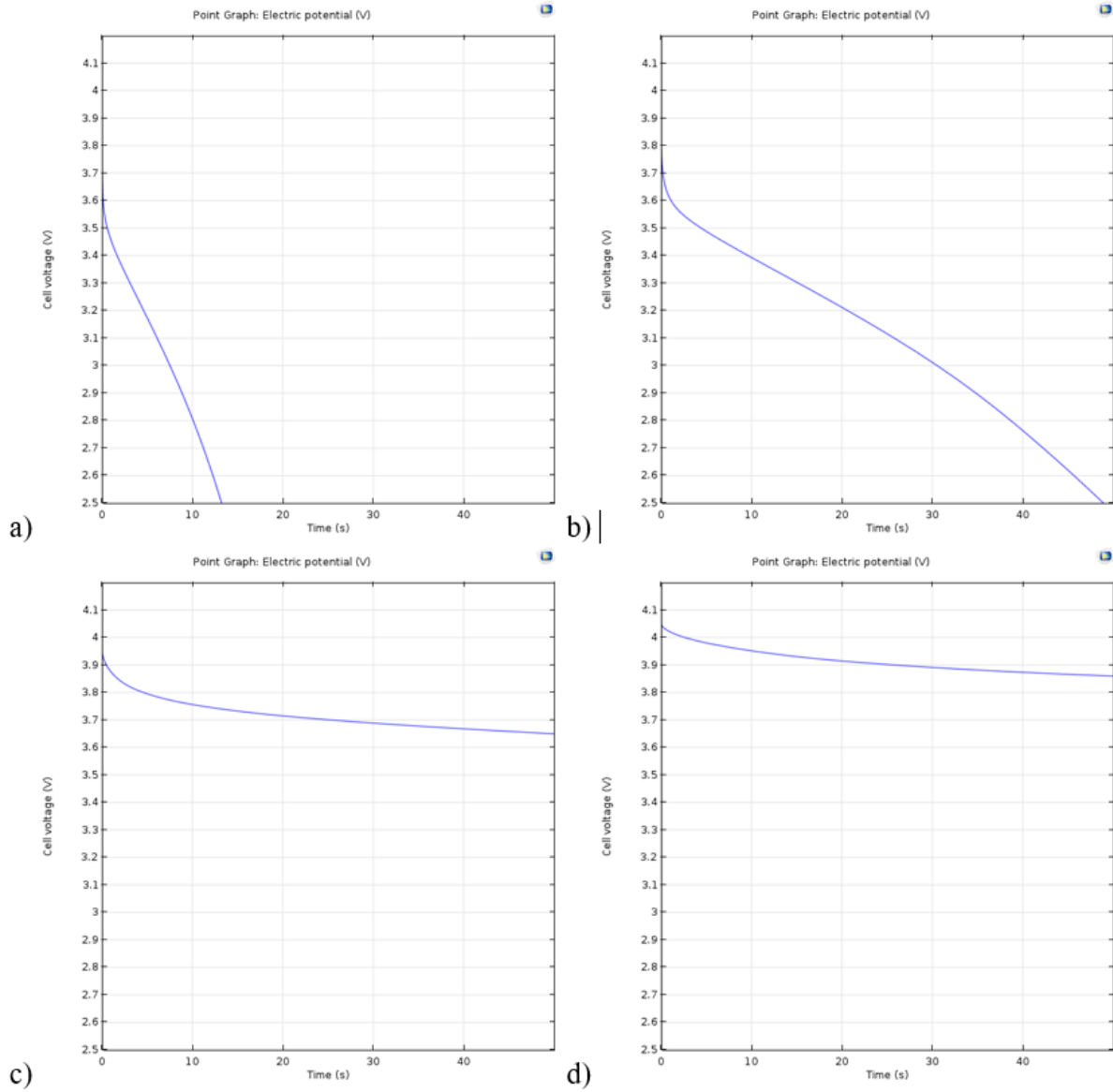
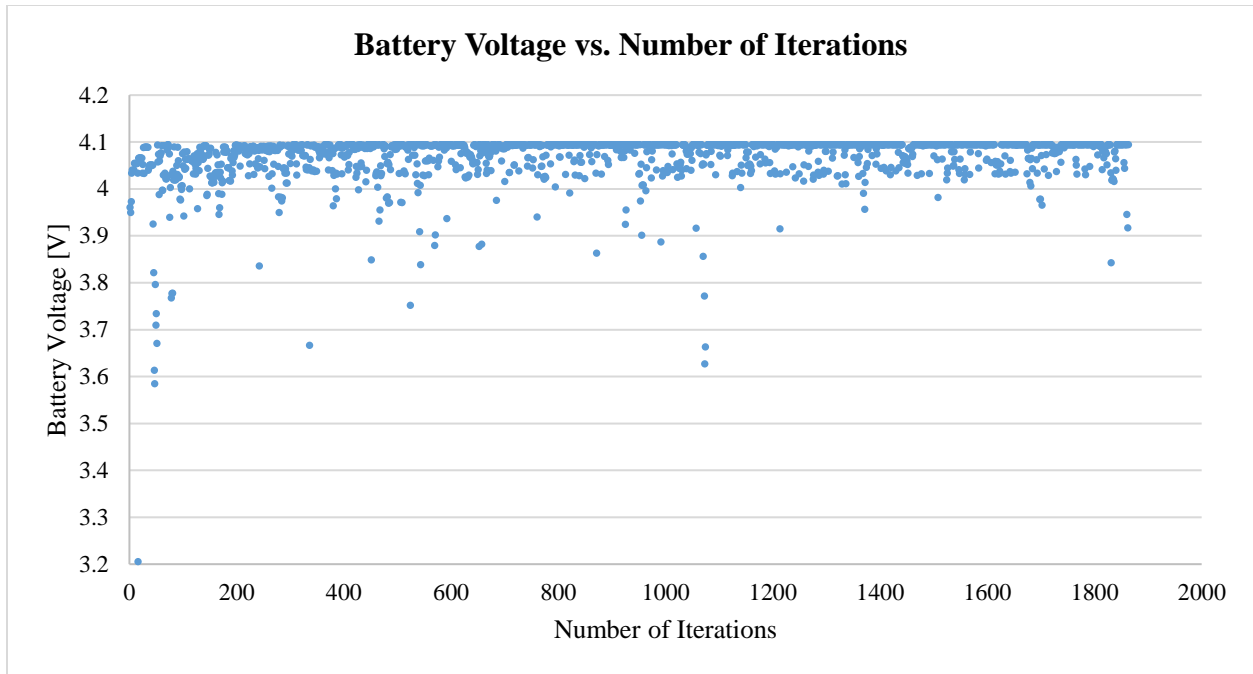


Figure 4.2. Four battery models discharged for  $t=50s$  with different thicknesses are compared as initial study of thickness parameter effects: a)  $L_{negative}=2.5\mu m$ ;  $L_{separator}=135\mu m$ ;  $L_{positive}=2.5\mu m$  (1.79% : 96.4% : 1.79%); b)  $L_{negative}=5\mu m$ ;  $L_{separator}=130\mu m$ ;  $L_{positive}=5\mu m$  (3.57% : 92.86% : 3.57%); c)  $L_{negative}=20\mu m$ ;  $L_{separator}=100\mu m$ ;  $L_{positive}=20\mu m$  (14.3% : 71.4% : 14.3%); d)  $L_{negative}=55\mu m$ ;  $L_{separator}=30\mu m$ ;  $L_{positive}=55\mu m$  (39.3% : 21.4% : 39.3%)

For a discharge duration of  $t=50s$ , four battery models with different thicknesses for the electrodes and electrolyte are generated before optimization to study the effect of thickness on the

cell voltage, as shown in Figure 4.2. The geometry in Figure 4.2a) has  $2.5 \mu\text{m}$  thickness for positive electrode and negative with a  $135 \mu\text{m}$  for the separator, which results in a  $L_{\text{negative}} : L_{\text{separator}} : L_{\text{positive}}$  ratio of  $1.79 : 96.4 : 1.79$ . The geometry in Figure 4.2b) has  $5 \mu\text{m}$  thickness for positive electrode and negative with a  $130 \mu\text{m}$  for the separator, which corresponds to a  $L_{\text{negative}} : L_{\text{separator}} : L_{\text{positive}}$  ratio of  $3.57 : 92.86 : 3.57$ . The geometry in Figure 4.2c) has  $20 \mu\text{m}$  thickness for positive electrode and negative with a  $100 \mu\text{m}$  for the separator, which corresponds to a  $L_{\text{negative}} : L_{\text{separator}} : L_{\text{positive}}$  ratio of  $14.3 : 71.4 : 14.3$ . The geometry in Figure 4.2d) has  $55 \mu\text{m}$  thickness for positive electrode and negative with a  $30 \mu\text{m}$  for the separator, which translates to a  $L_{\text{negative}} : L_{\text{separator}} : L_{\text{positive}}$  ratio of  $39.3 : 21.4 : 39.3$ . It can be seen that the discharge time is longer for the model with thinner electrolyte thickness. However, these four samples are not sufficient and cannot confirm whether making the electrolyte thickness smaller always results in better performance. In the case for one-dimensional battery model, the thickness of the three battery components are the input parameters for the Bayesian optimization. Each of the three components are given a bound of 0 to  $1000 \mu\text{m}$ , hence setting the lower bound of the input parameter as  $0 \mu\text{m}$  and the upper bound of the input parameter as  $1000 \mu\text{m}$ .



*Figure 4.3. Battery voltage vs. Number of Iterations scatter plot for 1D lithium battery model using Bayesian Optimization*

Figure 4.3 shows the scatter plot with the number of iterations in the  $x$ -axis and the output battery voltage in the  $y$ -axis. After 1860 iterations, the optimization code was terminated, at which the scatter plot converges. According to Figure 4.3, it can be seen that the scatter plot converges to a battery voltage value of 4.0947 V and further number of optimization iterations does not result in a greater value. To graph a convergence plot to determine how quickly the optimization results in this maximum value of 4.0947, Figure 4.4 truncates Figure 4.3 up to 200 iterations. At iteration number 198, the value of 4.0947 V is reached. Figure 4.5 to Figure 4.7 show how the three parameters are related with respect to the output battery voltage. While the thickness of the electrodes must be maximized within the battery size limit, the electrolyte through which the lithium ions must travel through must be reduced to a bare minimum thickness at which the two electrodes are separated.

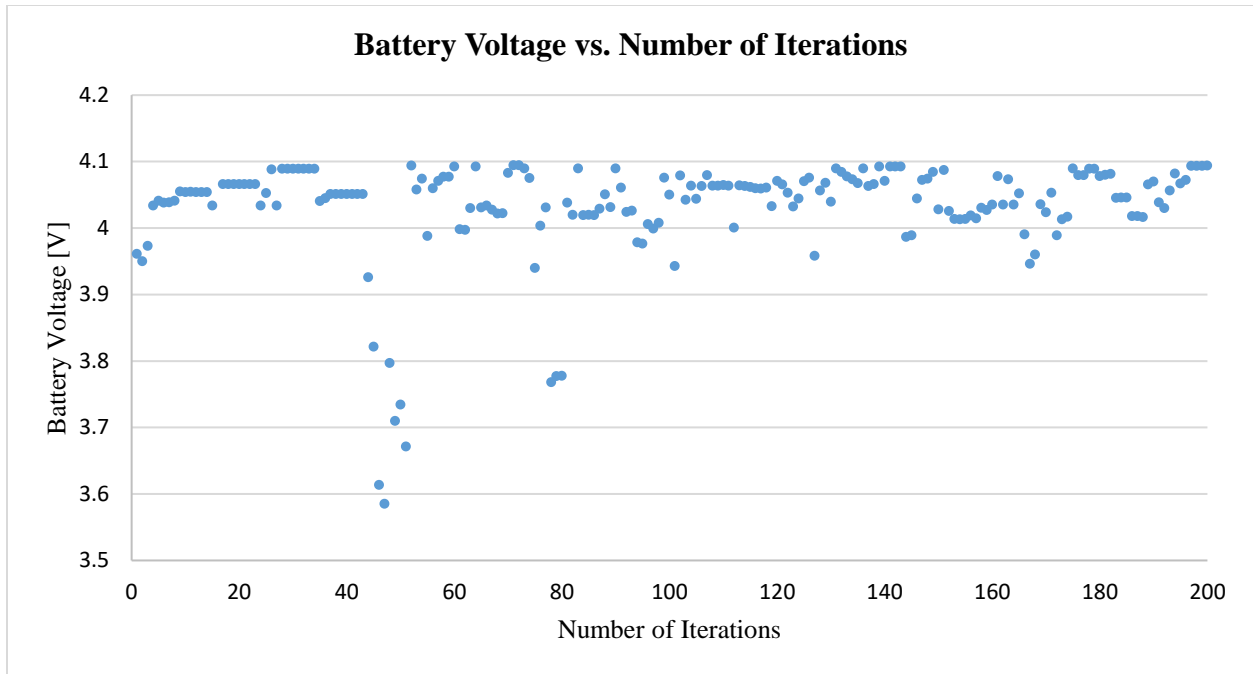


Figure 4.4. Truncated Bayesian Optimization plot for Figure 4.3 upto 200 iterations

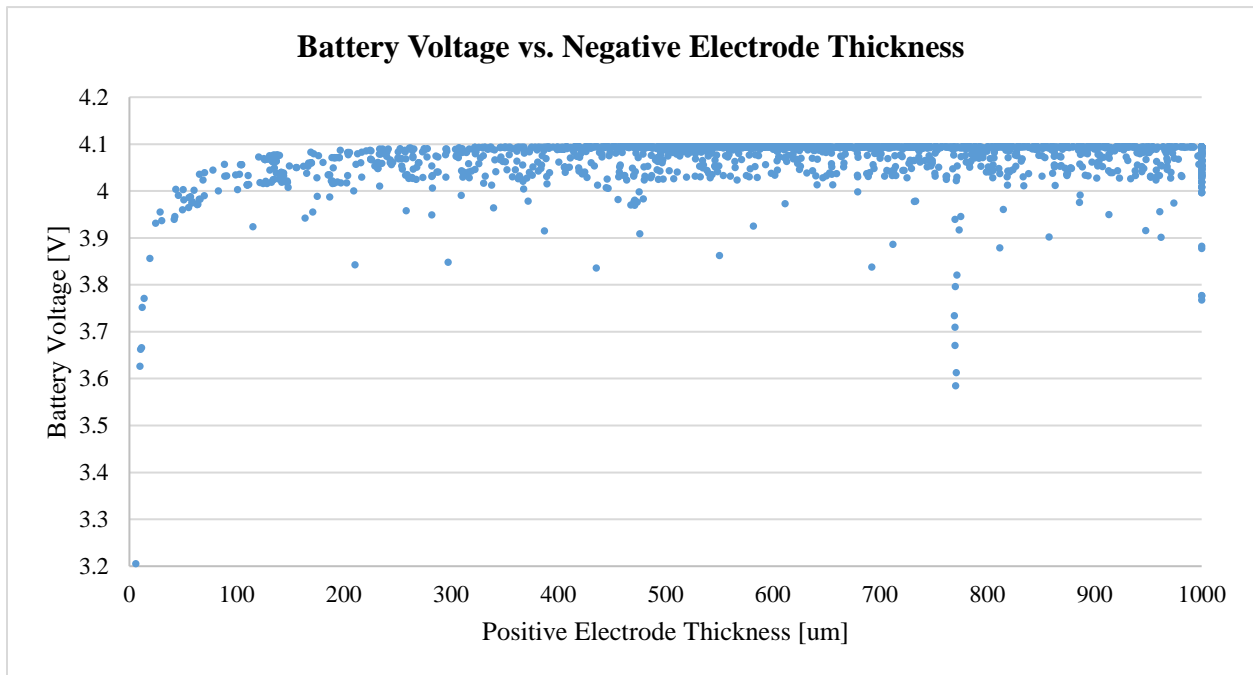


Figure 4.5. Battery voltage vs. negative electrode thickness scatter plot for 1D lithium battery model using Bayesian Optimization

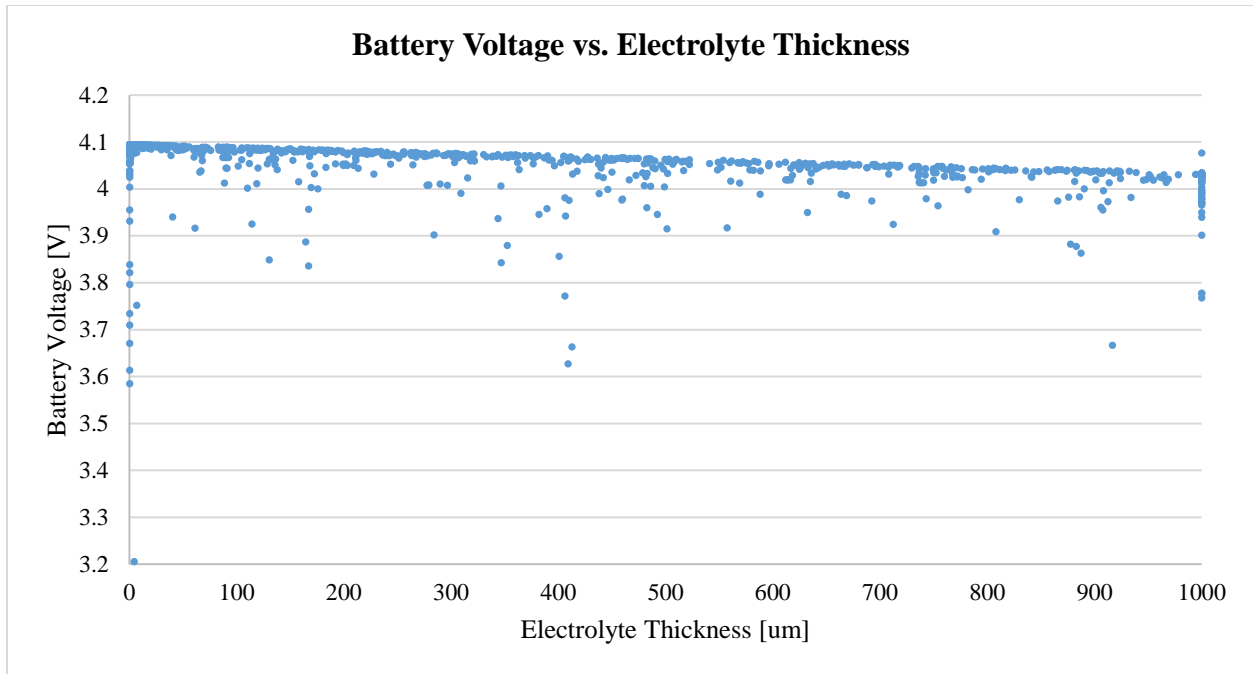


Figure 4.6. Battery voltage vs. electrolyte thickness scatter plot for 1D lithium battery model using Bayesian Optimization

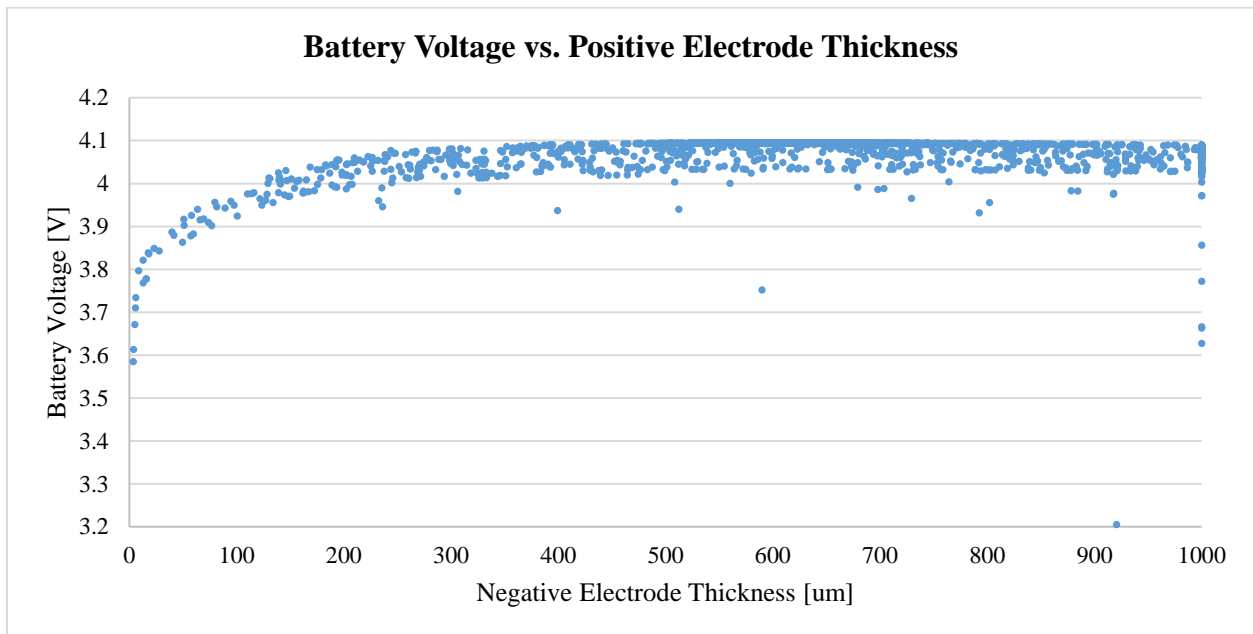


Figure 4.7. Battery voltage vs. positive electrode thickness scatter plot for 1D lithium battery model using Bayesian Optimization

## 4.2. Two-Dimensional (2D) Model Simulation

Having investigated the viability of applying Bayesian optimization in a one-dimensional model and observing the convergence of objective function, the same methodology can be applied to a lithium ion battery model of increased dimensions. While the one-dimensional battery could only express the thickness of the battery, a two-dimensional model can be defined by more parameters such as length and width in addition to the thickness parameter.

In simulation studies conducted by Bates et al [38], electrochemical reaction, heat transfer, lithium ion and electron diffusion and electrons in electrolyte, as well as solid lithium diffusion in the positive electrode were all simulated with a 2D battery model by using COMSOL Multiphysics using a solid state battery model. Sensitivity studies were conducted with different parameter values of lithium ion diffusion rate, lithium diffusion rate, electrolyte thickness, and electrode thickness. Variables such as electrolyte potential and electric potential are examples of primary dependent variables that are results of the simulations. Particularly, while the lithium ion diffusion, lithium diffusion and electrolyte thickness were kept constant, the positive electrode thickness was reduced from 500 nm to 250 nm at multiple C-rates. When measured in terms of the discharge curve in which the electric potential declines over time, the reduced thickness resulted in the maximal activity or complete discharge to be reached much quicker at each C-rate. In terms of lithium ion concentration over the distance along the electrolyte, the concentration gradient rapidly increased at higher C-rates but the concentration was adjusted to 3000~19000 mol/m<sup>3</sup> from 2000~20000 mol/m<sup>3</sup> of the control case. At a low C-rate of 6.4, the reduction in thickness of the positive electrode had little effect. When positive electrode thickness was halved, a complete discharge was reached much faster than other cases. Higher C-rates results in solid lithium polarization in the positive electrode. Also, only at higher C-rates, the reduction of electrode

thickness influences solid lithium concentration range to have higher minimum concentration, mostly due to reduced diffusion distance in the electrode. However, it is suggested that the lithium-ion solid state battery should be operated under lower discharge currents due to the possibility of high internal heating and poor rechargeability. Bates et al. concluded that the concentration of polarization is high at higher C-rates, and this would result in a lower performance as lithium would stack up at the positive electrode and less lithium ions would be present between electrode and electrolyte.

Bates et al. [38] implemented five test cases with changes in thicknesses and diffusion rates. Having set the first test case at 1500 nm electrolyte thickness and 500 nm electrode thickness, case 2 halved the electrolyte thickness while case 3 reduced electrode thickness by half. For case 4 and case 5, the lithium ion diffusion rate was increased to  $4.58 \times 10^{-12}$  and lithium diffusion rate was reduced to  $1.5 \times 10^{-16}$ , respectively. Using Bayesian optimization, the interface layer or the region between the electrodes and the electrolyte can be optimized for improved output voltage, cut-off voltage and cut-off time. Prior to applying optimization, the impact of varied thickness of the battery components has been investigated. While the thickness of the complete battery is fixed at 0.2 mm or 200  $\mu\text{m}$ , the thickness along the length of the battery is varied. Beyond the typical battery with fixed total thickness, the boundaries of the battery is then made irregular.

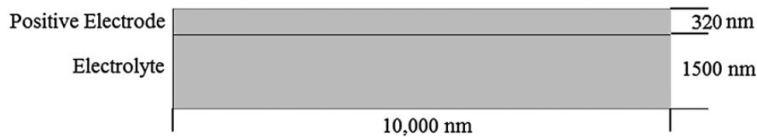


Figure 4.8. Geometry of solid-state battery: 10,000 nm in length and 1820 nm in thickness [38].

Table 4.1. For each case, different values have been assigned for the above parameters [35].

Case	Li-ion Diffusion (m <sup>2</sup> /s)	Lithium Diffusion (m <sup>2</sup> /s)	Electrolyte Thickness (nm)	Electrode Thickness (nm)
1	$0.9 \times 10^{-15}$	$1.76 \times 10^{-15}$	1500	500
2	$0.9 \times 10^{-15}$	$1.76 \times 10^{-15}$	750	500
3	$0.9 \times 10^{-15}$	$1.76 \times 10^{-15}$	1500	250
4	$4.58 \times 10^{-15}$	$1.76 \times 10^{-15}$	1500	500
5	$0.9 \times 10^{-15}$	$1.5 \times 10^{-16}$	1500	500

While liquid electrolytes are commonly used, solid state electrolytes allow for more variations and complexities in geometric configurations of the battery cell. Notten et al. [172] used solid state electrolyte for a new lithium battery concept in which thin film silicon intercalated electrodes are covered with solid state electrolyte. The geometry has trenches and holes with a high aspect ratio. The silicon material is etched using a reactive ion etching technique to increase surface area 25 times and this increased surface area overcomes the limitations that are inherent in planar solid-state thin film batteries with insufficient energy densities. Such batteries are suitable for low-loss decoupling that suppresses cross-talk in high frequency circuits. The cycle-life of a thin film electrode in conventional organic lithium-ion battery electrolyte and in solid-state electrolyte are compared. In the case with the liquid electrolyte, the storage capacity starts to decline approximately after thirty cycles and solid electrolyte interphase gradually forms on the electrode surface due to electrolyte decomposition.

#### 4.2.1. 2D Model with Variable Electrode-Electrolyte Interface

With the introduction of additive manufacturing in the battery manufacturing industry, there is potential for further improvement in battery performance. Current manufacturing techniques that are implemented in battery production plants manufacture lithium ion batteries with uniform cross sectional thicknesses. The thickness of each battery component, when observed through a cross section, does not change across the width or length of the complete battery. Thin films of electrodes and electrolytes are placed in a form of a sandwich, layer by layer, in order to reduce the manufacturing time per finished battery. However, as proven by Sun et al. [173], lithium ion batteries can be produced using additive manufacturing, specifically through the use of 3D printers.

With the use of 3D printers that can deposit materials not only in the  $x$  and  $y$  direction but also in the vertical  $z$  direction, more complex battery shapes can be generated. Sun et al. used 3D printing to produce a novel three dimensional lithium battery, complete with computer-controlled deposition of electrodes and electrolyte, in a interdigitated pattern. Although interdigitated, the battery can be interpreted as a 2.5 dimensional rather than a complete three-dimensional. No literature has investigated the potential of using Bayesian optimization to optimize a geometric parameter of a lithium ion battery.

For the case of a two-dimensional battery model, a rectangular geometry of  $1300\ \mu\text{m}$  in length and  $250\ \mu\text{m}$  in thickness will be used. Within the bounds between  $250\ \mu\text{m}$  and  $1300\ \mu\text{m}$  geometry, the domains of the electrolyte and electrodes will be varied by altering the interface boundary between the cathode and electrolyte. The anode is assigned with a lower boundary and is assumed to be a thin lithium foil, hence no domain region is assigned. The cathode domain is the region that is in contact with the upper boundary as well as the electric current source which is

upper boundary that is highlighted in blue. The electrolyte is assigned to the remaining region in between the cathode and the anode.

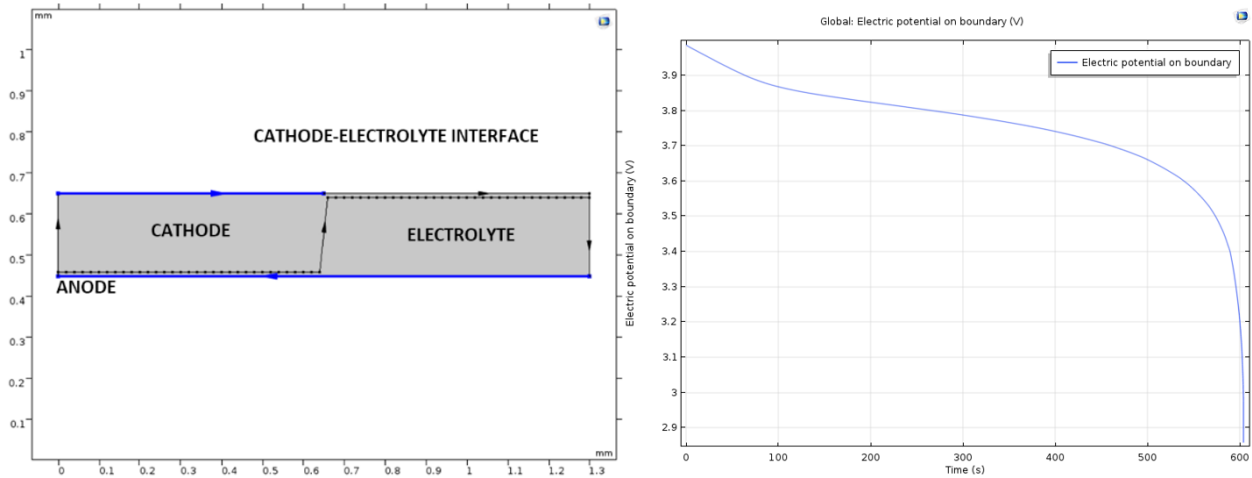


*Figure 4.9. A 2D lithium ion battery geometry with uneven cathode-electrolyte interface and its corresponding discharge curve.*

Given the geometry of having the current source assigned to half of the upper boundary, the two interface geometries display a small difference. Figure 4.10 shows a modified cathode-electrolyte interface that results in a shorter distance between the interface and the anode on the left half of the battery geometry while Figure 4.11 shows the opposite case where the distance is shorter in the right half of the battery geometry. The result would have been identical given the boundary associated with the current source extends fully across the upper boundary in a symmetrical way, but because the upper boundary is asymmetrical with the current source extending across half of the upper boundary from the far left, there is a difference in the result.

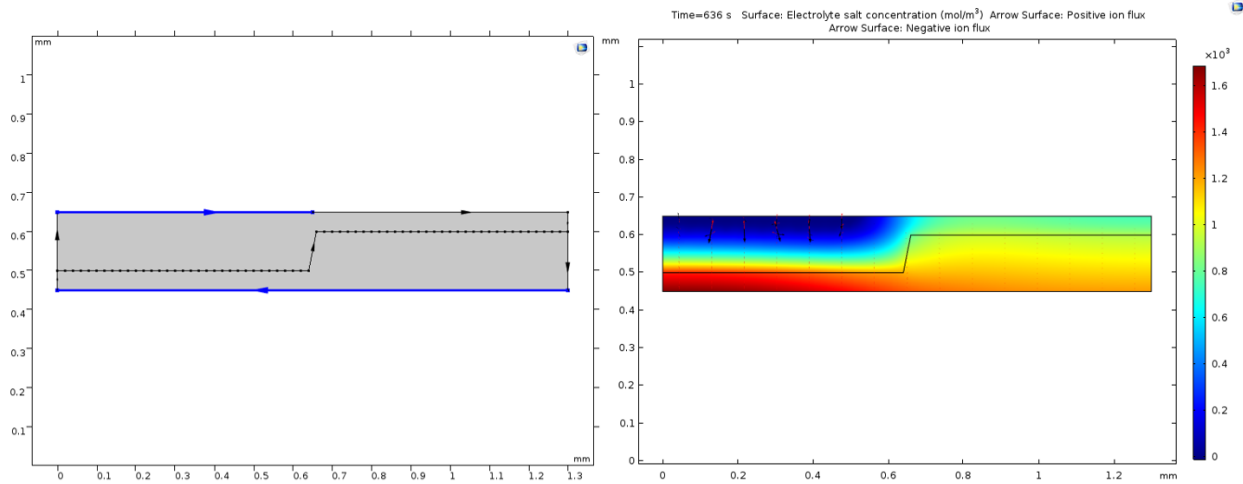


Figure 4.10. A 2D lithium ion battery geometry with uneven cathode-electrolyte interface (left) and surface electrolyte salt concentration contours (cut-off at  $t=636$ s)

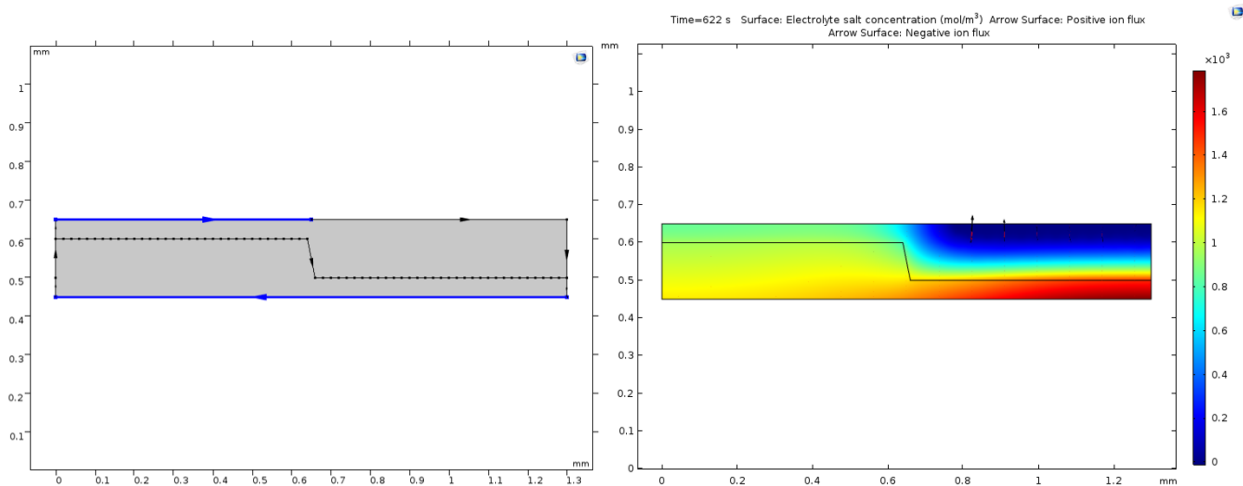


Figure 4.11. A 2D lithium ion battery geometry with uneven cathode-electrolyte interface (left) and surface electrolyte salt concentration contours (cut-off at  $t=622$ s)

The difference is shown at the discharge termination time. The battery model in Figure 4.10 terminates or cuts off at time  $t=638$ s while the battery model in Figure 4.11 cuts off at time  $t=622$ s as shown by the discharge curve in Figure 4.12. When discharging, lithium ions migrate from anode to cathode through the electrolyte and because the electrolyte thickness is shorter in

the battery shown in Figure 4.10 relative to its counterpart in Figure 4.11 in a region closer to the current source boundary, the latter model shows a shorter discharge duration.

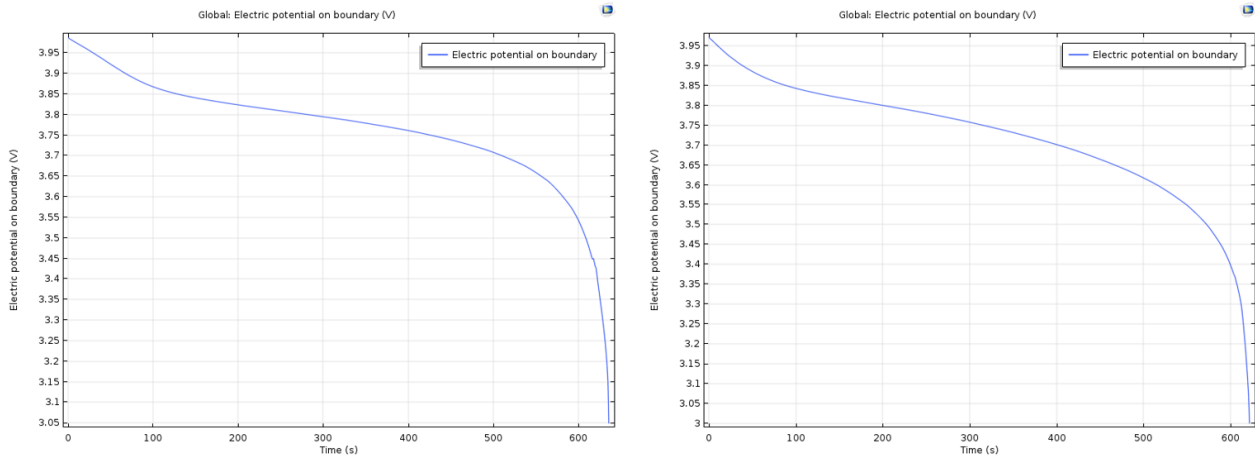


Figure 4.12. Electric potential discharge curves for Figure 4.10 (left) and Figure 4.11 (right)

The boundaries of the two-dimensional battery model is made more complex by employing an irregular cathode boundary. Figure 4.13 shows a ‘cut’ in the middle of the upper boundary with two boundary regions that are assigned the material and electrochemistry of a cathode. Through this base geometry, interface between cathode and electrolyte will be varied to observe improvements or degradation in the output voltage.

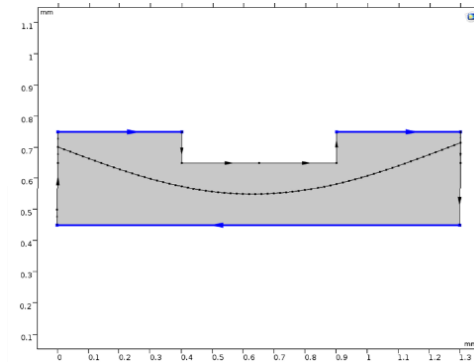


Figure 4.13. 2D battery geometry with uneven positive electrode boundary

Three models of the same overall battery geometry but with different cathode-electrolyte interface are observed. The boundaries of the cathode, anode remain consistent while interfaces change in terms of the average distance from the anode decreases.

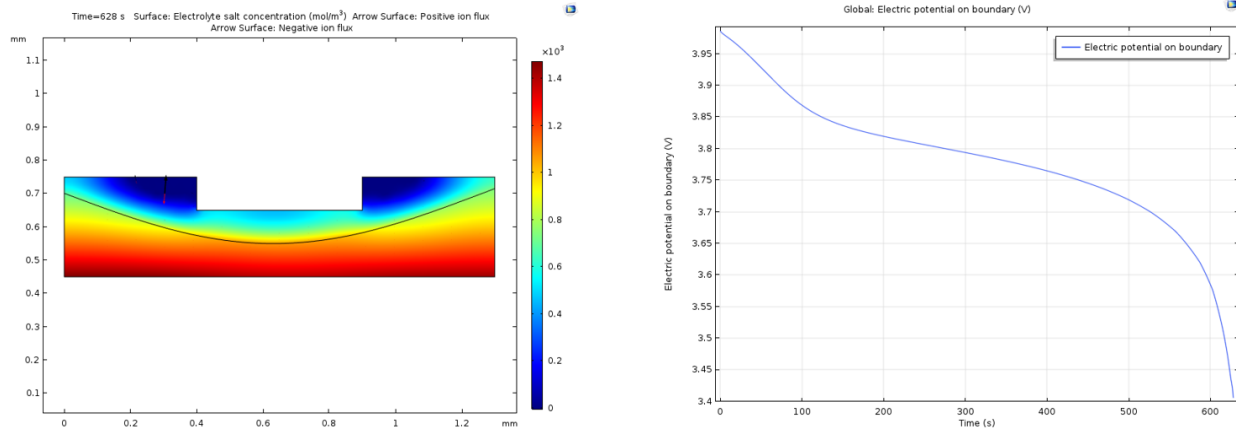


Figure 4.14. Electrolyte Salt Concentration and Electrical Potential (cut-off at  $t=628\text{ s}$ )

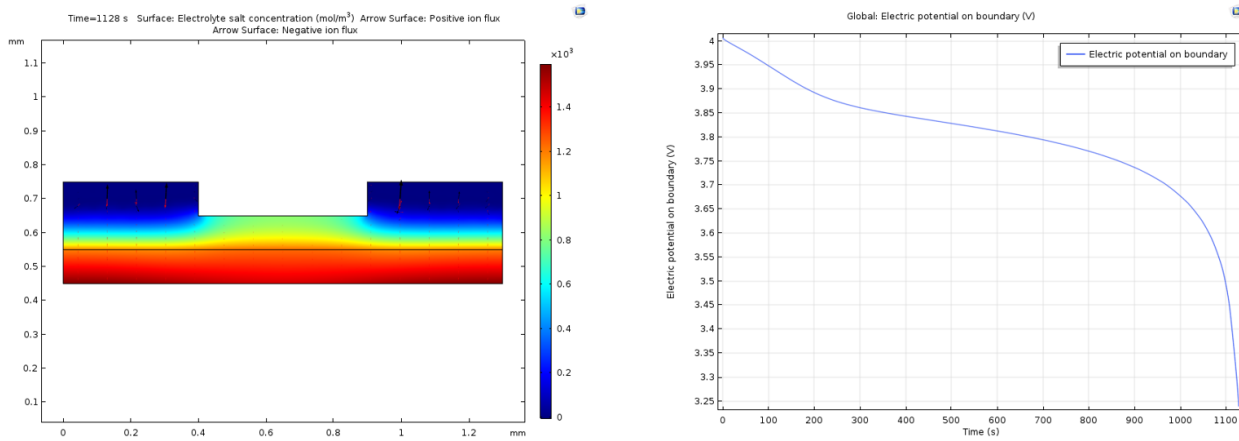


Figure 4.15. Electrolyte Salt Concentration and Electrical Potential (cut-off at  $t=1128\text{ s}$ )

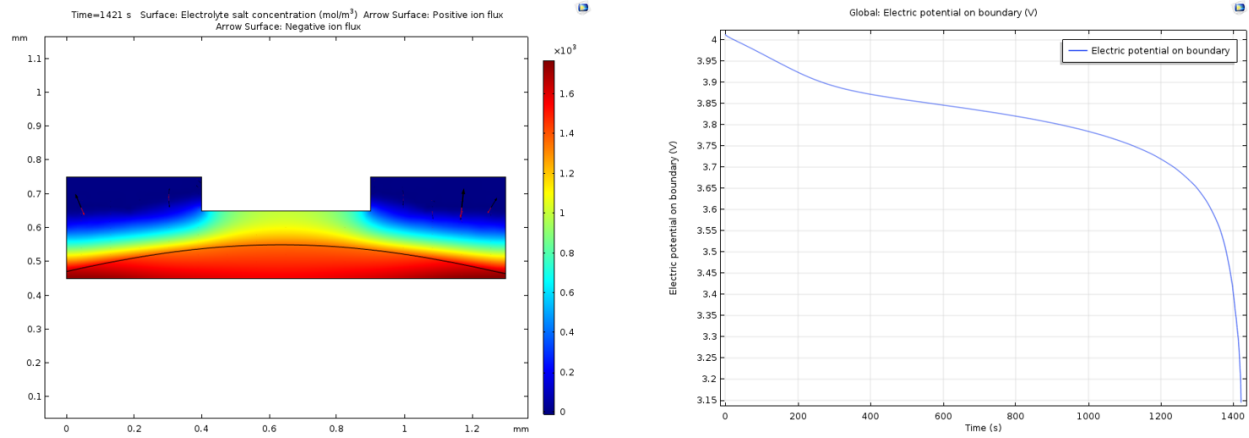


Figure 4.16. Electrolyte Salt Concentration and Electrical Potential (cut-off at  $t=1421s$ )

Figure 4.14 shows not only the lowest starting battery voltage of 3.98 V, but cuts off after a discharge time of  $t=628s$  that is shortest among the three battery models. The second battery model with consistent electrolyte thickness throughout the length of the battery showed a discharge time of  $t=1128s$  while the last model with the shortest average distance between the interface and the anode show the longest duration of  $t=1421s$ . During the discharge process, in accordance with the results from the one-dimensional battery model, it is shown that the electrolyte thickness should be minimized for longest discharge time and highest starting battery voltage. Figure 4.17 also shows three cases of an identical battery geometry but with varying interface shape that clearly has an effect on the discharge cut-off time. Figure 4.17a) is displaying the greatest electrolyte area while it has a cut-off time of  $t=477s$ . Figure 4.17b) and Figure 4.17c) with thinner electrolyte thickness have displaying cut-off times of  $t=984s$  and  $t=1571s$ , respectively.

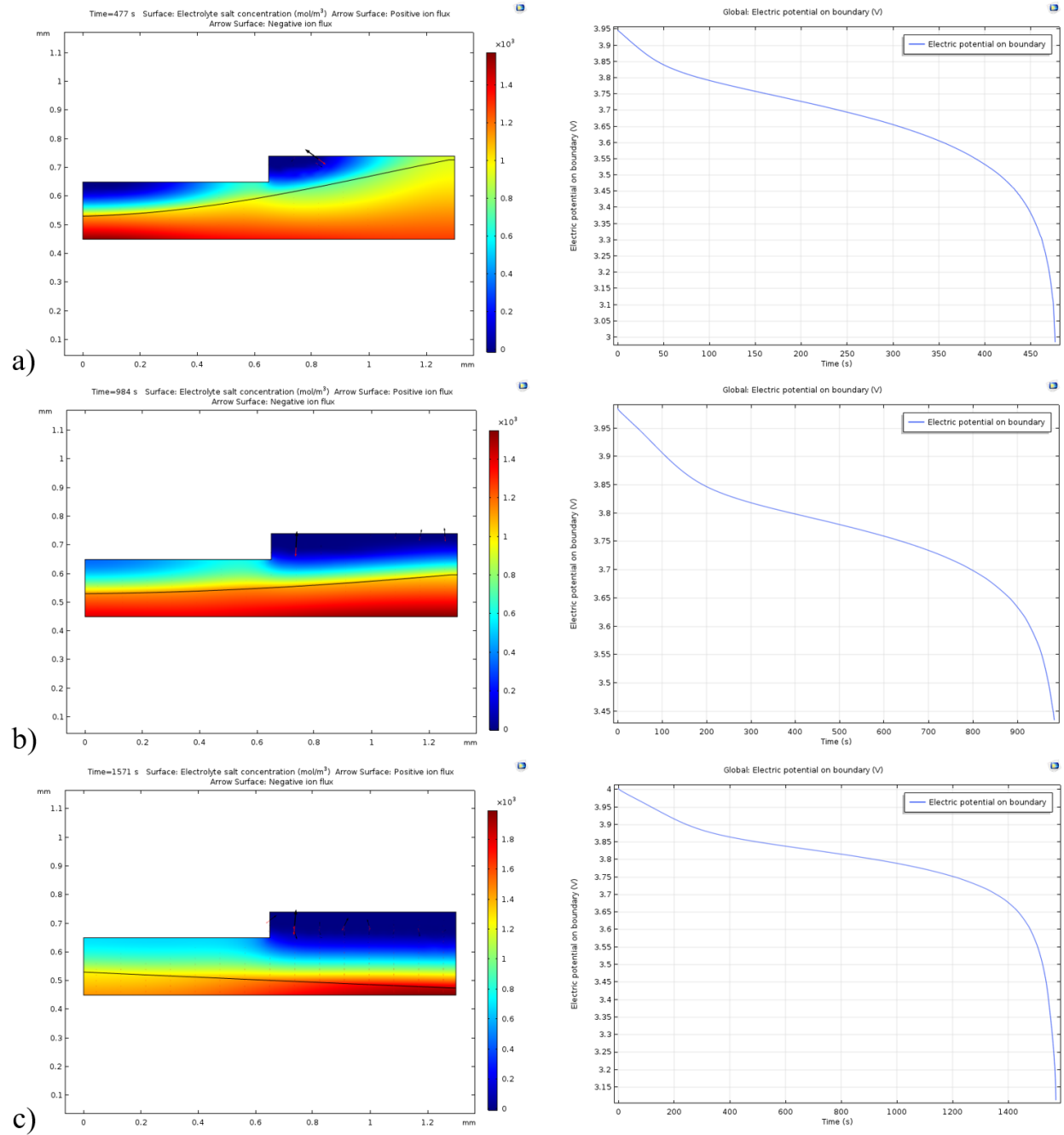


Figure 4.17. a) Electrolyte Salt Concentration and Electrical Potential with cut-off time at  $t=477s$ ; b) Electrolyte Salt Concentration and Electrical Potential with cut-off time at  $t=984s$ ; c) Electrolyte Salt Concentration and Electrical Potential with cut-off time at  $t=1571s$

Similarly, three-dimensional (3D) batteries can achieve higher power density than batteries with two-dimensional (2D) geometries [174]. The development of 3D batteries is important as research in semiconductors and microelectromechanical systems progresses. Simply making the electrodes thicker is not a promising option because the mechanical integrity and power density decrease with the increased electrode thickness. On the other hand, simply making the electrodes thinner is not a viable option either, because as the electrodes are made thinner, the amount of materials that contribute directly to the energy density or simply, active materials, will decrease, causing the battery to fail and unable to satisfy application requirements [175]. In addition, because thin electrodes are also difficult to manufacture, they increase manufacturing expenses and material costs [176]. The battery's 3D architecture has the advantage of introducing height as an additional design parameter that could increase the relative areal capacity. Unfortunately, this higher surface area could possibly result in undesirable side reactions that could potentially be detrimental to battery performance.

Arthur et al. [177] investigated several types of 3D architectures, which include a build-up or skyscraper design that amplifies the area of a thin-film battery in which the electrode becomes a 3D structure, as well as a concentric design and an inverse opal structure. Rechargeable thin-film batteries have been proved feasible by Bates et al. [178] using Li-V<sub>2</sub>O<sub>5</sub> cells. When designing 3D structures, two aspects must be considered. One is the limitation of height due to ohmic resistance of the element. The other is the volume of electrolyte which should be minimized to maximize energy density. Increasing the curvature of the electrode tip can produce more evenly distributed current. In addition, it was shown that power density depends on lithium ion diffusivity, as time of diffusion reduces in quadratic order with respect to the reduction of electrolyte thickness.

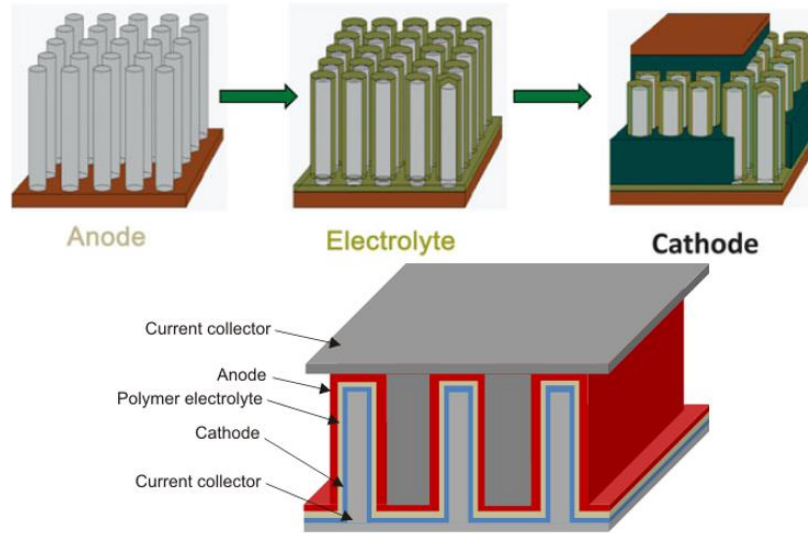


Figure 4.18. A three-dimensional representation of an interdigitated battery model [177].

The geometries such as the interdigitated designs as above used by Arthur et al. that are applied to the anode and cathode are not from a rigorous optimization process. The parameters that determine the pattern such as the height, width, curvature of the edge all have the potential of being optimized further. The 3D interdigitated model in Figure 4.18 can be simplified into a variable-interface model as shown in Figure 4.19, where the blue area signifies the electrolyte layer and the grey area above it signifies the positive electrode. The negative electrode is simplified as the bottom boundary, which is assumed to be a thin lithium metal.

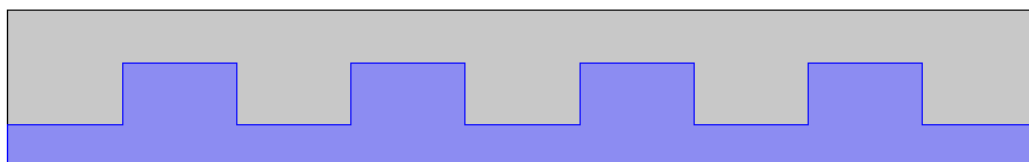


Figure 4.19. Variable-interface model with inconsistent electrolyte thickness

The heights of each of the four interdigitated pattern were set as an input parameter, hence making it a four parameter Bayesian optimization model. The scatter plot of the objective function

output that is the battery voltage is shown in Figure 4.20. After 100 iterations, the optimization code was terminated at which the scatter plot converges. It can be seen that the scatter plot converges to a battery voltage value of 3.824 V and further number of optimization iterations does not result in a greater value. At iteration number 29, the value of 3.824 V is reached.

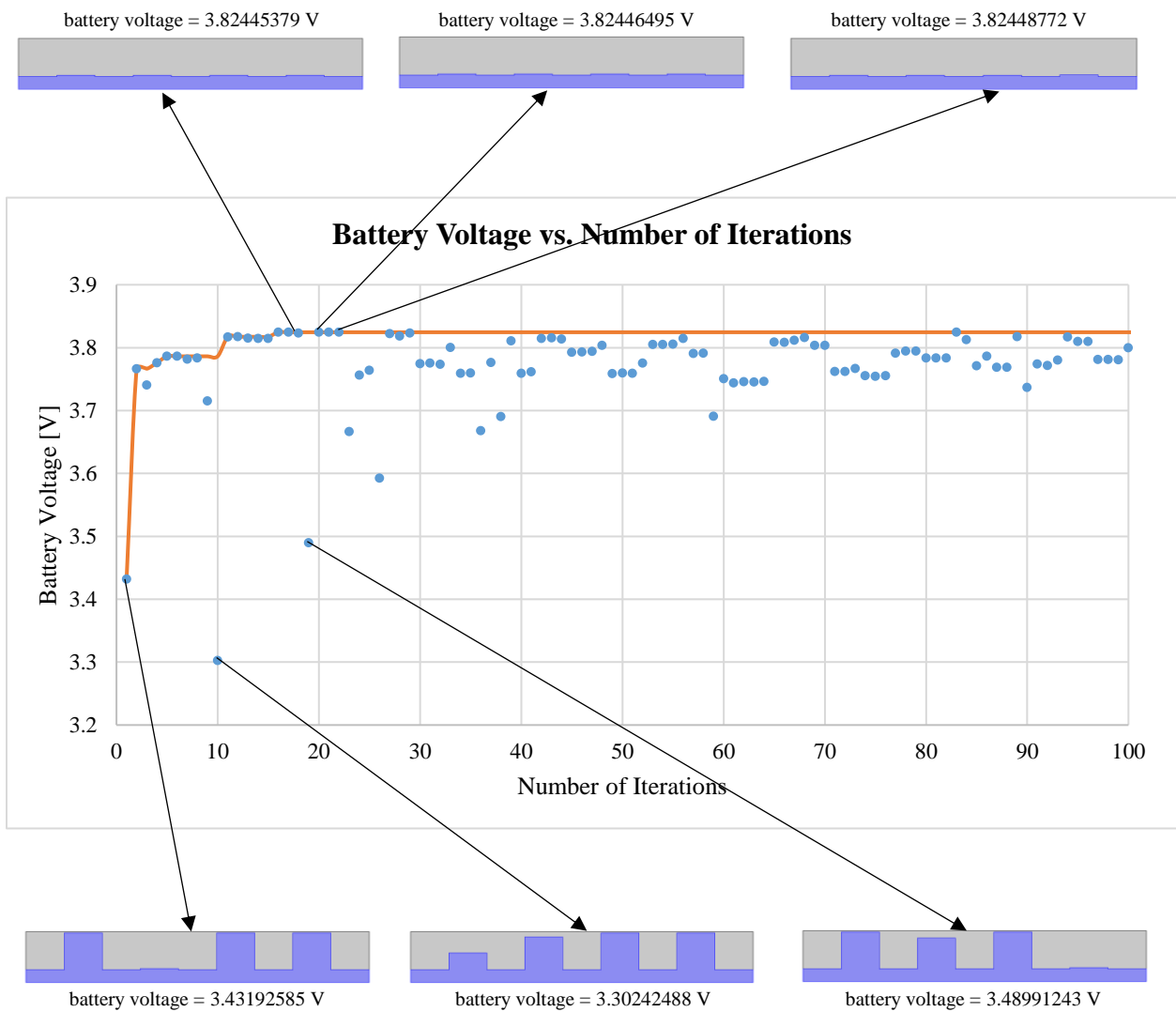


Figure 4.20. Battery voltage vs. Number of Iteration scatter plot for the Bayesian optimization of a 2D lithium battery model with variable electrode-electrolyte interface. The geometries indicate the models that generated the three highest and lowest battery voltages.

#### 4.2.2. 2D Model with Multiple Electrodes

Traditionally, whether cylindrical or pouch in terms of design, the internal battery components consist of a single cathode and single anode and a single electrolyte. Depending on the usage and battery demands, the dimensions of each of these components have been reduced or increased to achieve the desired performance. However, there is a lack of research which investigated more than one of each component. If the number of each positive and negative electrode as well as their individual geometries can be optimized, better performance could be possibly reached.

Besides optimizing the thickness in a simple 1D lithium battery model and the electrode-electrolyte interface geometry in a 2D model, another form of a two-dimensional model was developed for optimization. Instead of visualizing a typical pouch shaped lithium battery, the following model is modeled assuming that the point of view is from the top and is looked down upon. A domain with a square geometry of 2 mm by 2 mm is assumed to be the external boundary of a single cell lithium ion battery that consists of electrolyte. Using COMSOL Multiphysics, this geometry would be generated and within the electrolyte boundaries, the cathodes and anodes would be included in the form of additional geometrical shapes.

Usually, the location where the battery is implemented is very limited. For example, the lithium battery for an electric vehicle must fit inside the vehicle chassis. In mobile electronics such as smartphones, the battery size must be compact enough to be placed within the plastic casing of the phone. Virtual reality devices or goggles require batteries that are small enough to blend inside the goggle legs but with enough power to support the device usage. Hence, it can be concluded that the internal components of a battery must be modified for improved performance while the dimensions of the outer geometry are set constant. Using COMSOL, a square geometry with 0.002

m, or 2 mm, on each side is created and is assumed to be the external boundaries of the whole battery. The remaining other battery components such as electrodes will be bound within the boundary of this square electrolyte. For this study,  $\text{LiMn}_2\text{O}_4$  spinel material is used as positive electrode and graphite  $\text{Li}_x\text{C}_6$  is used for the negative electrode.  $\text{LiPF}_6$  in 1:2 p(VdF-HFP) polymer is used as electrolyte. Each of the domains and boundaries are assigned certain properties that contribute to the performance of the battery.

The model with parameters assigned to each geometric component that will be optimized can be understood as a model for a ‘black box’, which is an objective function that the selected optimization algorithm will optimize. In this case, it is the optimization of the location coordinates of the individual electrodes to maximize the terminating battery voltage after a given discharge duration. Although the algorithm can query the value  $f(x)$  for a point  $x$ , it does not have the gradient data and cannot determine how the form of the whole  $f(x)$ . It can be assumed as a function  $f(x)$  that one knows nothing about, and the goal is to determine either the minimum or the maximum of this unknown function. In the cases when the gradient is known, a gradient descent with restarts can be used and in the case when gradient is unknown, for example, the gradient can be numerically estimated. If the function is not differential, a grid search or random search can be used.

Initially, a model consisting of a single cell with one positive and one negative electrode is simulated and optimized using Bayesian optimization as shown in Figure 4.21. Figure 4.21 suggests that the highest electric potential can be achieved when two electrodes are positioned very close to each other. The three battery geometries that are displayed above the scatter plot represent the three models displaying the three highest battery voltage values after a discharge duration of 60 seconds for each of the 150 iterations. It clearly shows that the positive and negative electrodes tend to move close to each other to decrease the electrolyte region in between them which will in

turn decrease the distance which the lithium ion travels. The opposite is the case for the three models below the plot that have displayed the three lowest battery voltage values. As the positive and negative electrodes move farther apart, the generated voltage decreases along with increased electrolyte thickness region between the electrodes. This makes sense because the distance between electrodes greatly influences the distance through which lithium ions must travel.

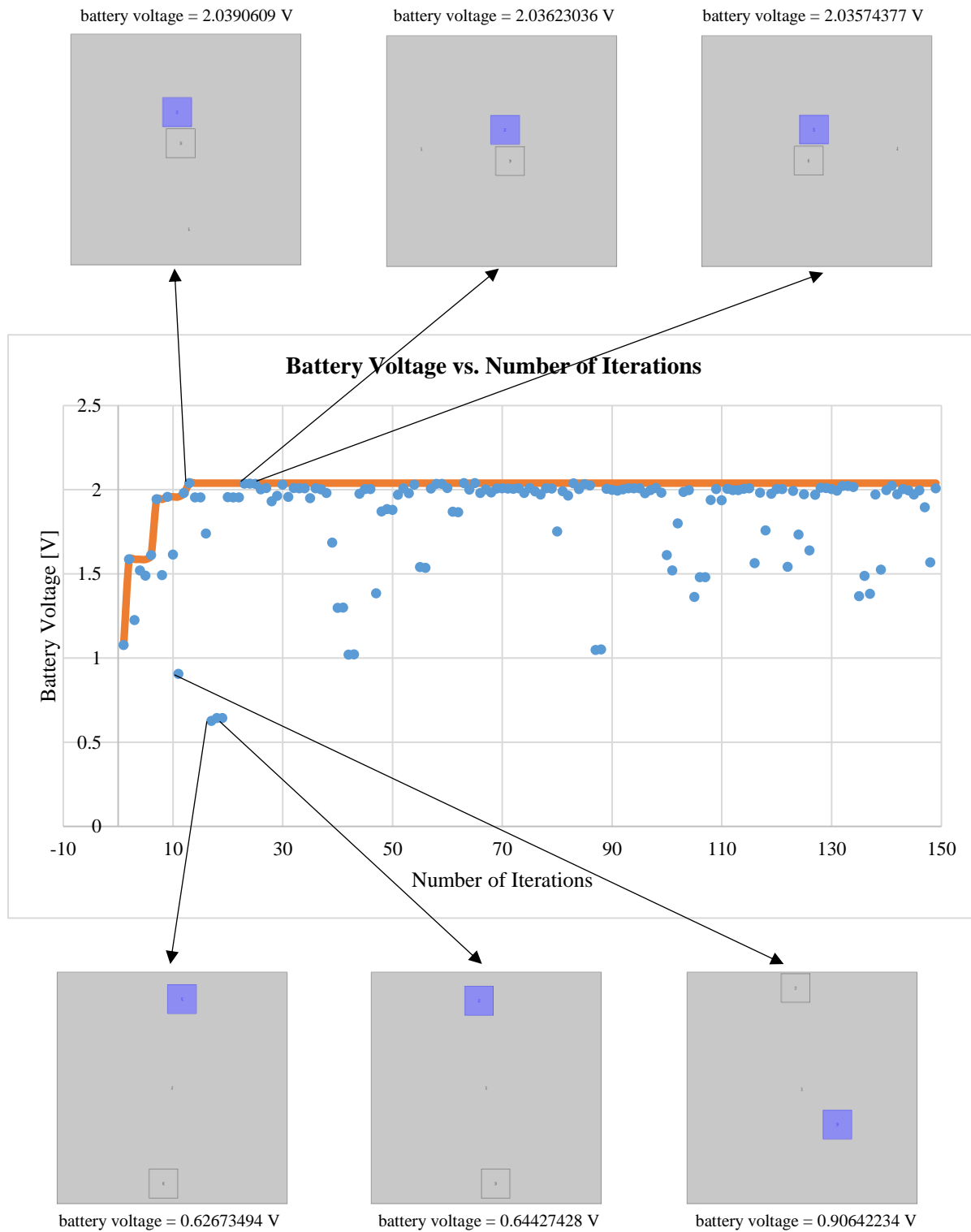


*Figure 4.21. Battery Voltage vs. Number of Iterations scatter plot for 2D lithium battery model with two electrodes using Bayesian Optimization. The geometries indicate the models that generated the three highest and lowest battery voltages*

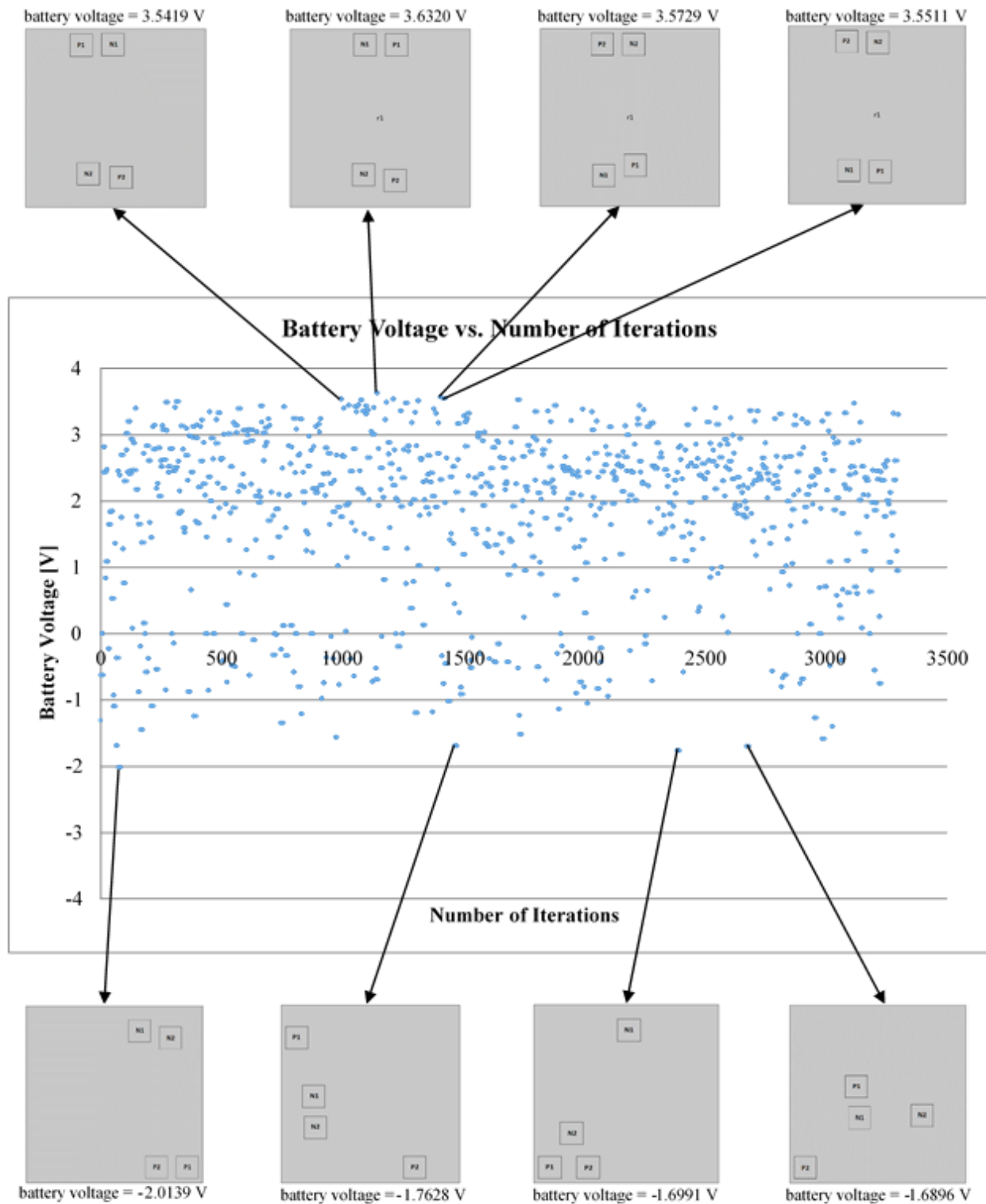


Figure 4.22. Battery voltage vs. Number of Iterations scatter plot for 2D lithium battery model with four electrodes using Bayesian Optimization. The geometries indicate the models that generated the four highest and lowest battery voltages.

Then, as shown in Figure 4.22, one more of each electrode is placed within the same electrolyte boundary. Now, the relation among the electrodes is not as simple as the case when there was just one of each positive and negative electrode. With each electrode affecting all the other existing electrodes in the vicinity in terms of electrochemistry, their positions are difficult to predict. Each electrode has an effect on each of the other electrodes and the one-dimensional model that is applied to the initial geometry cannot sufficiently express their relationships. An improved two-dimensional battery model must be used in such geometries. Because a one-dimensional battery electrochemistry model was used for a 2D model, this has led to some simulated geometries displaying negative battery voltages, which is impossible in reality. It can be suspected that there is a certain distance or a distance threshold which exists between two electrodes of opposite charges, and once the actual distance exceeds this, the displayed battery voltage turns negative. While the one-dimensional battery model is sufficient when there is one positive and one negative electrode because they are considered as one and only electrode pair in the electrolyte, once more electrodes of each type are introduced, the pair formation is difficult as each electrode has an impact on other electrodes.

## CHAPTER 5. CONCLUSION AND FUTURE WORKS

### 5.1. Accomplishments and Contribution

This thesis has effectively demonstrated the application of a Bayesian optimization algorithm to determine which value of a specific geometric parameter of interest will result in improved performance of the battery given the boundary conditions or limitations of provided dimensions and properties.

Plenty of research efforts have been made to simulate lithium-ion batteries with 2D or 3D models to predict how design parameters affect the battery performance and how they could improve the discharging process. Simulation is an efficient tool that allows us to quickly verify battery designs, observe results and improve on existing models. After three decades of efforts, battery simulation tools have become mature and easy-to-use commercial packages are readily available. Through simulation, the design optimization of lithium-ion batteries can be easily performed. Optimizations of electrode thickness and porosity have been widely studied while the importance of multi-objective optimization has been recognized. It is important to seek trade-offs between different design goals. Depending on different weights assigned to objectives according to designers' preferences, different optimum designs can be obtained.

Most of the existing work in battery structural design did not apply optimization methods to systematically search the best designs. Among the relatively limited studies of design optimization, only a few design parameters were considered. Battery design is a multi-faceted systems engineering process where all parameters of anode, cathode, electrolyte, and current collector, as well as the spatial configurations of them, need to be considered simultaneously in order to find true optimum. The complexity of optimization increases as the dimension of design

space increases with the simultaneous considerations of all design parameters, both continuous and discrete. This itself imposes a challenge for optimization algorithms. Furthermore, existing geometry and topology optimization studies did not consider constraints of materials properties, manufacturing limitations, costs, and others. In order to physically realize optimum designs, such constraints have to be considered in searching optimum. Through the literature review part of this thesis paper, the impact of each battery component with geometric parameters on different battery design objectives have been reviewed. Studies show that important geometric parameters include the size, shape, texture of electrodes, as well as configurations between electrodes, electrolyte, and current collectors.

In the battery manufacturing industry today, most of the produced batteries come in forms of a pouch or a cylinder shape that share very similar manufacturing processes until packaging state where the battery stack is cut into desired shapes for the pouch type while it is rolled into a cylindrical shape for the latter type. Being an industry driven by cost-effectiveness and mass production, the battery manufacturers have been producing batteries with consistent thicknesses regardless of the fact that it is the best or optimized geometry or not. With recent advancements in battery production that apply additive manufacturing techniques such as 3D printing, improved levels of performance can be achieved through complex battery designs and geometries that were once thought to be impossible to fabricate. Through this thesis paper, it has been investigated that the geometry of the electrode-electrolyte interface has an influence on the overall performance of the lithium ion battery. The key output parameters that are of interest include the electrode potential and salt concentration have been investigated. When the thickness of the overall battery is fixed or when the boundary of the battery is irregular, the interface seems to have an impact. Especially when the boundaries that are assigned the purpose of a current source or electric ground is not

parallel to one another, the cross-sectional shape of the curve that represents the electrode-electrolyte interface is further significant. Given its significance after a few simulations on extremely irregular and random boundary cases, it was decided that Bayesian Optimization were to be used to determine the optimal interfae for 1D and 2D cases. Different applications provide different space for the battery and the battery must perform its best performnace within that available volume space.

## **5.2. Future Work**

This research has developed a methodology to determine the extent of how big or small a specific parameter can be for a given battery in the form of a maximization and minimization problem, respectively. Although the demonstration of this possibility is done only simulation models in COMSOL where Bayesian optimization is applied, given the optimal geometric parameter as an output at the end of the optimizatoin iteration, this value can be applied to an experimental study where an actual lithium battery is fabricated using the geometrical parameter values used in the simulation. Once successfully fabricated, the components of the battery can be assembled to produce electrochemical results that can be compared to the simulation data generated in COMSOL. After an experimental discharge test, the discharge time and battery voltage before and after the experiment can possibly compared to the simulation results. A comparison with theoretical and experimental results may be utilized to further optimize simulation models to develop a model that correlates to the experimental results better.

In addition, more parameters can be optimized using the Bayesian Optimization approach. Perhaps paremeters other than geometrical parameters may be optimized to observe the possibility of further improving the voltage output or any other imporant output. Most previous studies focused on optimizing electrochemical properties of battery, especially on energy density. Other

performance factors such as heat generation and dissipation, capacity fade, life expectancy, and mechanical reliability should also be considered in a multi-objective optimization approach. To consider all properties, multi-physics simulation tool such as COMSOL is particularly important to predict these properties simultaneously. There are still plenty of research opportunities to develop high-fidelity multi-physics simulation tools to efficiently predict mechanical, thermal, and electrochemical properties. Furthermore, the robustness of optimality also needs to be considered. Since variability is inherent in materials and manufacturing processes, uncertainty is inevitably associated with the final system. Obtaining a suboptimal but more robust design is more meaningful in engineering practice.

## REFERENCES

- 
- [1] Scrosati, B. (2005). Power sources for portable electronics and hybrid cars: lithium batteries and fuel cells. *The Chemical Record*, 5(5), 286-297.
- [2] Dyer, C. K. (1999). Replacing the battery in portable electronics. *Scientific American*, 281(1), 88-93.
- [3] Broussely, M., & Archdale, G. (2004). Li-ion batteries and portable power source prospects for the next 5–10 years. *Journal of Power Sources*, 136(2), 386-394.
- [4] Ritchie, A., & Howard, W. (2006). Recent developments and likely advances in lithium-ion batteries. *Journal of Power Sources*, 162(2), 809-812.
- [5] Scrosati, B., & Garche, J. (2010). Lithium batteries: Status, prospects and future. *Journal of Power Sources*, 195(9), 2419-2430.
- [6] Tarascon, J. M., & Guyomard, D. (1991). Li Metal-Free Rechargeable Batteries Based on  $\text{Li}_{1+x}\text{Mn}_2\text{O}_4$  Cathodes ( $0 \leq x \leq 1$ ) and Carbon Anodes. *Journal of The Electrochemical Society*, 138(10), 2864-2868.
- [7] Fergus, J. W. (2010). Recent developments in cathode materials for lithium ion batteries. *Journal of Power Sources*, 195(4), 939-954.
- [8] Marom, R., Amalraj, S. F., Leifer, N., Jacob, D., & Aurbach, D. (2011). A review of advanced and practical lithium battery materials. *Journal of Materials Chemistry*, 21(27), 9938-9954.
- [9] Zhang, S. S. (2007). A review on the separators of liquid electrolyte Li-ion batteries. *Journal of Power Sources*, 164(1), 351-364.
- [10] Cheng, X. B., Zhang, R., Zhao, C. Z., & Zhang, Q. (2017). Toward safe lithium metal anode in rechargeable batteries: A review. *Chemical Reviews*, 117(15), 10403-10473.
- [11] Ye, J., Baumgaertel, A. C., Wang, Y. M., Biener, J., & Biener, M. M. (2014). Structural optimization of 3D porous electrodes for high-rate performance lithium ion batteries. *ACS nano*, 9(2), 2194-2202.
- [12] Scrosati, B. (2000). Recent advances in lithium ion battery materials. *Electrochimica Acta*, 45(15), 2461-2466.
- [13] Nitta, N., Wu, F., Lee, J. T., & Yushin, G. (2015). Li-ion battery materials: present and future. *Materials today*, 18(5), 252-264.
- [14] Goriparti, S., Miele, E., De Angelis, F., Di Fabrizio, E., Zaccaria, R. P., & Capiglia, C. (2014). Review on recent progress of nanostructured anode materials for Li-ion batteries. *Journal of Power Sources*, 257, 421-443.
- [15] Fergus, J. W. (2010). Recent developments in cathode materials for lithium ion batteries. *Journal of Power Sources*, 195(4), 939-954.
- [16] Xu, B., Qian, D., Wang, Z., & Meng, Y. S. (2012). Recent progress in cathode materials research for advanced lithium ion batteries. *Materials Science and Engineering: R: Reports*, 73(5), 51-65.
- [17] Yang, S., Feng, X., & Müllen, K. (2011). Sandwich-Like, Graphene-Based Titania Nanosheets with High Surface Area for Fast Lithium Storage. *Advanced Materials*, 23(31), 3575-3579.
- [18] Zhou, G., Pei, S., Li, L., Wang, D. W., Wang, S., Huang, K., Yin, L.-C., Li, F., & Cheng, H. M. (2014). A graphene-pure-sulfur sandwich structure for ultrafast, long-life lithium-sulfur batteries. *Advanced materials*, 26(4), 625-631.

- 
- [19] Yan, Y., Yin, Y. X., Guo, Y. G., & Wan, L. J. (2014). A Sandwich-Like Hierarchically Porous Carbon/Graphene Composite as a High-Performance Anode Material for Sodium-Ion Batteries. *Advanced Energy Materials*, 4(8).
- [20] Zhao, L., Gao, M., Yue, W., Jiang, Y., Wang, Y., Ren, Y., & Hu, F. (2015). Sandwich-structured graphene-Fe<sub>3</sub>O<sub>4</sub>@ carbon nanocomposites for high-performance lithium-ion batteries. *ACS applied materials & interfaces*, 7(18), 9709-9715.
- [21] Botte, G. G., Subramanian, V. R., & White, R. E. (2000). Mathematical modeling of secondary lithium batteries. *Electrochimica Acta*, 45(15), 2595-2609.
- [22] Thomas, K. E., Newman, J., & Darling, R. M. (2002). Mathematical modeling of lithium batteries. In *Advances in lithium-ion batteries* (pp. 345-392). Springer US.
- [23] Abada, S., Marlair, G., Lecocq, A., Petit, M., Sauvant-Moynot, V., & Huet, F. (2016). Safety focused modeling of lithium-ion batteries: A review. *Journal of Power Sources*, 306, 178-192.
- [24] Effat, M. B., Wu, C., & Ciucci, F. (2016). Modeling efforts in the key areas of thermal management and safety of lithium ion battery cells: a mini review. *Asia-Pacific Journal of Chemical Engineering*, 11(3), 399-406.
- [25] Grazioli, D., Magri, M., & Salvadori, A. (2016). Computational modeling of Li-ion batteries. *Computational Mechanics*, 58(6), 889-909.
- [26] Gaikwad, A. M., Steingart, D. A., Nga Ng, T., Schwartz, D. E., & Whiting, G. L. (2013). A flexible high potential printed battery for powering printed electronics. *Applied Physics Letters*, 102(23), 104\_1.
- [27] Gaikwad, A. M., Whiting, G. L., Steingart, D. A., & Arias, A. C. (2011). Highly Flexible, Printed Alkaline Batteries Based on Mesh-Embedded Electrodes. *Advanced materials*, 23(29), 3251-3255.
- [28] Gaikwad, A. M., Arias, A. C., & Steingart, D. A. (2015). Recent progress on printed flexible batteries: mechanical challenges, printing technologies, and future prospects. *Energy Technology*, 3(4), 305-328.
- [29] Singh, N., Galande, C., Miranda, A., Mathkar, A., Gao, W., Reddy, A. L. M., ... & Ajayan, P. M. (2012). Paintable battery. *Scientific reports*, 2, 481.
- [30] Zhao, R., Zhang, S., Liu, J., & Gu, J. (2015). A review of thermal performance improving methods of lithium ion battery: electrode modification and thermal management system. *Journal of Power Sources*, 299, 557-577.
- [31] Zhao, R., Liu, J., & Gu, J. (2015). The effects of electrode thickness on the electrochemical and thermal characteristics of lithium ion battery. *Applied Energy*, 139, 220-229.
- [32] Zheng, H., Li, J., Song, X., Liu, G., & Battaglia, V. S. (2012). A comprehensive understanding of electrode thickness effects on the electrochemical performances of Li-ion battery cathodes. *Electrochimica Acta*, 71, 258-265.
- [33] Xu, M., & Wang, X. (2017). Electrode Thickness Correlated Parameters Estimation for a Li-Ion NMC Battery Electrochemical Model. *ECS Transactions*, 77(11), 491-507.
- [34] Singh, M., Kaiser, J., & Hahn, H. (2016). A systematic study of thick electrodes for high energy lithium ion batteries. *Journal of Electroanalytical Chemistry*, 782, 245-249.
- [35] Du, Z., Wood, D. L., Daniel, C., Kalnaus, S., & Li, J. (2017). Understanding limiting factors in thick electrode performance as applied to high energy density Li-ion batteries. *Journal of Applied Electrochemistry*, 47(3), 405-415.
- [36] Jeong, J., Lee, H., Choi, J., Ryou, M. H., & Lee, Y. M. (2015). Effect of LiFePO<sub>4</sub> cathode density and thickness on electrochemical performance of lithium metal polymer batteries prepared by in situ thermal polymerization. *Electrochimica Acta*, 154, 149-156.

- 
- [37] Wang, J. S., Liu, P., Sherman, E., Verbrugge, M., & Tataria, H. (2011). Formulation and characterization of ultra-thick electrodes for high energy lithium-ion batteries employing tailored metal foams. *Journal of Power Sources*, 196(20), 8714-8718.
- [38] Bates, A., Mukherjee, S., Schuppert, N., Son, B., Kim, J. G., & Park, S. (2015). Modeling and simulation of 2D lithium-ion solid state battery. *International Journal of Energy Research*, 39(11), 1505-1518.
- [39] Yu, S., Chung, Y., Song, M. S., Nam, J. H., & Cho, W. I. (2012). Investigation of design parameter effects on high current performance of lithium-ion cells with LiFePO<sub>4</sub>/graphite electrodes. *Journal of Applied Electrochemistry*, 42(6), 443-453.
- [40] Shim, J., & Striebel, K. A. (2003). Effect of electrode density on cycle performance and irreversible capacity loss for natural graphite anode in lithium-ion batteries. *Journal of power sources*, 119, 934-937.
- [41] Shim, J., & Striebel, K. A. (2004). The dependence of natural graphite anode performance on electrode density. *Journal of power sources*, 130(1), 247-253.
- [42] Smekens, J., Gopalakrishnan, R., Steen, N. V. D., Omar, N., Hegazy, O., Hubin, A., & Van Mierlo, J. (2016). Influence of electrode density on the performance of Li-ion batteries: experimental and simulation results. *Energies*, 9(2), 104.
- [43] Alaboina, P. K., Cho, J. S., & Cho, S. J. (2017). Engineering and Optimization of Silicon–Iron–Manganese Nanoalloy Electrode for Enhanced Lithium-Ion Battery. *Nano-Micro Letters*, 9(4), 41.
- [44] Srinivasan, V., & Newman, J. (2004). Design and optimization of a natural graphite/iron phosphate lithium-ion cell. *Journal of the Electrochemical Society*, 151(10), A1530-A1538.
- [45] Chen, Y. H., Wang, C. W., Zhang, X., & Sastry, A. M. (2010). Porous cathode optimization for lithium cells: Ionic and electronic conductivity, capacity, and selection of materials. *Journal of Power Sources*, 195(9), 2851-2862.
- [46] Bitsch, B., Gallasch, T., Schroeder, M., Börner, M., Winter, M., & Willenbacher, N. (2016). Capillary suspensions as beneficial formulation concept for high energy density Li-ion battery electrodes. *Journal of Power Sources*, 328, 114-123.
- [47] Choi, J., Son, B., Ryou, M. H., Kim, S. H., Ko, J. M., & Lee, Y. M. (2013). Effect of LiCoO<sub>2</sub> Cathode Density and Thickness on Electrochemical Performance of Lithium-Ion Batteries. *Journal of Electrochemical Science and Technology*, 4(1), 27-33.
- [48] Das, S., Li, J., & Hui, R. (2014, October). Impact of Electrode Surface/Volume Ratio on Li-ion Battery Performance. In *Proceedings of the COMSOL Conference*, Boston, MA, USA (pp. 8-10).
- [49] Suthar, B., Northrop, P. W., Rife, D., & Subramanian, V. R. (2015). Effect of Porosity, Thickness and Tortuosity on Capacity Fade of Anode. *Journal of The Electrochemical Society*, 162(9), A1708-A1717.
- [50] Liu, L., & Guan, P. (2017). The Role of Porosity-Graded Electrode in Mitigating Performance Degradation of High Voltage Lithium-Ion Battery. *ECS Transactions*, 77(11), 321-329.
- [51] Dai, Y., & Srinivasan, V. (2016). On graded electrode porosity as a design tool for improving the energy density of batteries. *Journal of The Electrochemical Society*, 163(3), A406-A416.
- [52] Lu, C. H., & Lin, S. W. (2001). Influence of the particle size on the electrochemical properties of lithium manganese oxide. *Journal of power sources*, 97, 458-460.
- [53] Botte, G. G., Johnson, B. A., & White, R. E. (1999). Influence of Some Design Variables on the Thermal Behavior of a Lithium-Ion Cell. *Journal of the Electrochemical Society*, 146(3), 914-923.

- 
- [54] Sheu, S. P., Yao, C. Y., Chen, J. M., & Chiou, Y. C. (1997). Influence of the LiCoO<sub>2</sub> particle size on the performance of lithium-ion batteries. *Journal of power sources*, 68(2), 533-535.
- [55] Taleghani, S. T., Marcos, B., Zaghbi, K., & Lantagne, G. (2017). A Study on the Effect of Porosity and Particles Size Distribution on Li-Ion Battery Performance. *Journal of The Electrochemical Society*, 164(11), E3179-E3189.
- [56] Newman, J. (1995). Optimization of porosity and thickness of a battery electrode by means of a reaction-zone model. *Journal of the Electrochemical Society*, 142(1), 97-101.
- [57] Shen, L., & Chen, Z. (2007). Critical review of the impact of tortuosity on diffusion. *Chemical Engineering Science*, 62(14), 3748-3755.
- [58] Thorat, I. V., Stephenson, D. E., Zacharias, N. A., Zaghbi, K., Harb, J. N., & Wheeler, D. R. (2009). Quantifying tortuosity in porous Li-ion battery materials. *Journal of Power Sources*, 188(2), 592-600.
- [59] Shearing, P. R., Howard, L. E., Jørgensen, P. S., Brandon, N. P., & Harris, S. J. (2010). Characterization of the 3-dimensional microstructure of a graphite negative electrode from a Li-ion battery. *Electrochemistry communications*, 12(3), 374-377.
- [60] Kehrwald, D., Shearing, P. R., Brandon, N. P., Sinha, P. K., & Harris, S. J. (2011). Local tortuosity inhomogeneities in a lithium battery composite electrode. *Journal of The Electrochemical Society*, 158(12), A1393-A1399.
- [61] Lim, C., Yan, B., Yin, L., & Zhu, L. (2014). Geometric characteristics of three dimensional reconstructed anode electrodes of lithium ion batteries. *Energies*, 7(4), 2558-2572.
- [62] Son, B., Ryou, M. H., Choi, J., Kim, S. H., Ko, J. M., & Lee, Y. M. (2013). Effect of cathode/anode area ratio on electrochemical performance of lithium-ion batteries. *Journal of Power Sources*, 243, 641-647.
- [63] Xue, R., Huang, H., Li, G., & Chen, L. (1995). Effect of cathode anode mass ratio in lithium-ion secondary cells. *Journal of power sources*, 55(1), 111-114.
- [64] Kim, C. S., Jeong, K. M., Kim, K., & Yi, C. W. (2015). Effects of capacity ratios between anode and cathode on electrochemical properties for lithium polymer batteries. *Electrochimica Acta*, 155, 431-436.
- [65] Kohler, R., Proell, J., Ziebert, C., Ulrich, S., Przybylski, M., & Pfleging, W. (2011). Laser processing of SnO<sub>2</sub> electrode materials for manufacturing of 3D micro-batteries. In *Proc. of SPIE* Vol. 7921, pp. 79210P-1.
- [66] Lim, D. G., Chung, D. W., Kohler, R., Proell, J., Scherr, C., Pfleging, W., & García, R. E. (2014). Designing 3D conical-shaped lithium-ion microelectrodes. *Journal of the Electrochemical Society*, 161(3), A302-A307.
- [67] Ikeshita, K., Inoue, G., & Kawase, M. (2017). Electrode Designs of Lithium Ion Batteries Utilizing the Simulation of Porous Structures. *ECS Transactions*, 75(20), 165-172.
- [68] Hart, R. W., White, H. S., Dunn, B., & Rolison, D. R. (2003). 3-D microbatteries. *Electrochemistry Communications*, 5(2), 120-123.
- [69] Zadin, V., Kasemägi, H., Aabloo, A., & Brandell, D. (2010). Modelling electrode material utilization in the trench model 3D-microbattery by finite element analysis. *Journal of Power Sources*, 195(18), 6218-6224.
- [70] Miranda, D., Costa, C. M., Almeida, A. M., & Lanceros-Méndez, S. (2016). Computer simulations of the influence of geometry in the performance of conventional and unconventional lithium-ion batteries. *Applied Energy*, 165, 318-328.

- 
- [71] Miranda, D., Costa, C. M., Almeida, A. M., & Lanceros-Méndez, S. (2016). Computer simulation evaluation of the geometrical parameters affecting the performance of two dimensional interdigitated batteries. *Journal of Electroanalytical Chemistry*, 780, 1-11.
- [72] Chabot, V., Farhad, S., Chen, Z., Fung, A. S., Yu, A., & Hamdullahpur, F. (2013). Effect of electrode physical and chemical properties on lithium-ion battery performance. *International Journal of Energy Research*, 37(14), 1723-1736.
- [73] Kennell, G. F., & Evitts, R. W. (2012). Two-dimensional lithium-ion battery modeling with electrolyte and cathode extensions. *Advances in Chemical Engineering and Science*, 2(04), 423.
- [74] Zadin, V., Brandell, D., Kasemägi, H., Aabloo, A., & Thomas, J. O. (2011). Finite element modelling of ion transport in the electrolyte of a 3D-microbattery. *Solid State Ionics*, 192(1), 279-283.
- [75] Miranda, D., Costa, C. M., Almeida, A. M., & Lanceros-Méndez, S. (2015). Modeling separator membranes physical characteristics for optimized lithium ion battery performance. *Solid State Ionics*, 278, 78-84.
- [76] Kosch, S., Rheinfeld, A., Erhard, S. V., & Jossen, A. (2017). An extended polarization model to study the influence of current collector geometry of large-format lithium-ion pouch cells. *Journal of Power Sources*, 342, 666-676.
- [77] Yang, G. F., Song, K. Y., & Joo, S. K. (2015). Ultra-thick Li-ion battery electrodes using different cell size of metal foam current collectors. *RSC Advances*, 5(22), 16702-16706.
- [78] Yao, M., Okuno, K., Iwaki, T., Kato, M., Tanase, S., Emura, K., & Sakai, T. (2007). LiFePO<sub>4</sub>-based electrode using micro-porous current collector for high power lithium ion battery. *Journal of Power Sources*, 173(1), 545-549.
- [79] Wang, Q., Wang, D., & Wang, B. (2012). Preparation and electrochemical performance of LiFePO<sub>4</sub>-based electrode using three-dimensional porous current collector. *Int J Electrochem Sci*, 7, 8753-8760.
- [80] Yang, G. F., Song, K. Y., & Joo, S. K. (2014). A metal foam as a current collector for high power and high capacity lithium iron phosphate batteries. *Journal of Materials Chemistry A*, 2(46), 19648-19652.
- [81] Yang, G. F., Song, J. S., Kim, H. Y., & Joo, S. K. (2013). Metal Foam as Positive Electrode Current Collector for LiFePO<sub>4</sub>-Based Li-Ion Battery. *Japanese Journal of Applied Physics*, 52(10S), 10MB13.
- [82] Yang, G. F., & Joo, S. K. (2015). Calendering effect on the electrochemical performances of the thick Li-ion battery electrodes using a three dimensional Ni alloy foam current collector. *Electrochimica Acta*, 170, 263-268.
- [83] Yu, S., Kim, S., Kim, T. Y., Nam, J. H., & Cho, W. I. (2013). Transportation properties in nanosized LiFePO<sub>4</sub> positive electrodes and their effects on the cell performance. *Journal of Applied Electrochemistry*, 43(3), 253-262.
- [84] Palomares, V., Goñi, A., De Muro, I. G., De Meazza, I., Bengoechea, M., Cantero, I., & Rojo, T. (2010). Conductive additive content balance in Li-ion battery cathodes: Commercial carbon blacks vs. in situ carbon from LiFePO<sub>4</sub>/C composites. *Journal of Power Sources*, 195(22), 7661-7668.
- [85] Denis, Y. W., Donoue, K., Inoue, T., Fujimoto, M., & Fujitani, S. (2006). Effect of electrode parameters on LiFePO<sub>4</sub> cathodes. *Journal of The Electrochemical Society*, 153(5), A835-A839.
- [86] Qi, X., Blizanac, B., DuPasquier, A., Oljaca, M., Li, J., & Winter, M. (2013). Understanding the influence of conductive carbon additives surface area on the rate performance of LiFePO<sub>4</sub> cathodes for lithium ion batteries. *Carbon*, 64, 334-340.

- 
- [87] Zhang, J., Lu, B., Song, Y., & Ji, X. (2012). Diffusion induced stress in layered Li-ion battery electrode plates. *Journal of Power Sources*, 209, 220-227.
- [88] Kwon, K. H., Shin, C. B., Kang, T. H., & Kim, C. S. (2006). A two-dimensional modeling of a lithium-polymer battery. *Journal of Power Sources*, 163(1), 151-157.
- [89] Santhanagopalan, S., Guo, Q., Ramadass, P., & White, R. E. (2006). Review of models for predicting the cycling performance of lithium ion batteries. *Journal of Power Sources*, 156(2), 620-628
- [90] Park, M., Zhang, X., Chung, M., Less, G. B., & Sastry, A. M. (2010). A review of conduction phenomena in Li-ion batteries. *Journal of Power Sources*, 195(24), 7904-7929.
- [91] Zhang, C., Li, K., Mcloone, S., & Yang, Z. (2014). Battery modelling methods for electric vehicles-A review. In *Proc. IEEE Control Conference (ECC)*, June 24-27, 2014. Strasbourg, France, pp. 2673-2678.
- [92] Bandhauer, T. M., Garimella, S., & Fuller, T. F. (2011). A critical review of thermal issues in lithium-ion batteries. *Journal of the Electrochemical Society*, 158(3), R1-R25.
- [93] Zhao, R., Zhang, S., Liu, J., & Gu, J. (2015). A review of thermal performance improving methods of lithium ion battery: electrode modification and thermal management system. *Journal of Power Sources*, 299, 557-577.
- [94] Franco, A. A. (2013). Multiscale modelling and numerical simulation of rechargeable lithium ion batteries: concepts, methods and challenges. *Rsc Advances*, 3(32), 13027-13058.
- [95] Doyle, M., Fuller, T. F., & Newman, J. (1993). Modeling of galvanostatic charge and discharge of the lithium/polymer/insertion cell. *Journal of the Electrochemical Society*, 140(6), 1526-1533.
- [96] Fuller, T. F., Doyle, M., & Newman, J. (1994). Simulation and optimization of the dual lithium ion insertion cell. *Journal of the Electrochemical Society*, 141(1), 1-10.
- [97] Sikha, G., White, R. E., & Popov, B. N. (2005). A mathematical model for a lithium-ion battery/electrochemical capacitor hybrid system. *Journal of the Electrochemical Society*, 152(8), A1682-A1693.
- [98] Kennell, G. F., & Evitts, R. W. (2012). Two-dimensional lithium-ion battery modeling with electrolyte and cathode extensions. *Advances in Chemical Engineering and Science*, 2(04), 423.
- [99] Arunachalam, H., Onori, S., & Battiato, I. (2015). On veracity of macroscopic Lithium-ion battery models. *Journal of The Electrochemical Society*, 162(10), A1940-A1951.
- [100] Zhang, X., & Tartakovsky, D. M. (2017). Effective Ion Diffusion in Charged Nanoporous Materials. *Journal of The Electrochemical Society*, 164(4), E53-E61.
- [101] Rao, L., & Newman, J. (1997). Heat generation rate and general energy balance for insertion battery systems. *Journal of the Electrochemical Society*, 144(8), 2697-2704.
- [102] Pesaran, A. A. (2002). Battery thermal models for hybrid vehicle simulations. *Journal of power sources*, 110(2), 377-382.
- [103] Saw, L. H., Somasundaram, K., Ye, Y., & Tay, A. A. O. (2014). Electro-thermal analysis of Lithium Iron Phosphate battery for electric vehicles. *Journal of Power Sources*, 249, 231-238.
- [104] Fu, R., Choe, S. Y., Agubra, V., & Fergus, J. (2015). Development of a physics-based degradation model for lithium ion polymer batteries considering side reactions. *Journal of Power Sources*, 278, 506-521.
- [105] Kupper, C., & Bessler, W. G. (2017). Multi-Scale Thermo-Electrochemical Modeling of Performance and Aging of a LiFePO<sub>4</sub>/Graphite Lithium-Ion Cell. *Journal of The Electrochemical Society*, 164(2), A304-A320.

- 
- [106] Kakimoto, N., & Goto, K. (2016). Capacity-fading model of lithium-ion battery applicable to multicell storage systems. *IEEE Transactions on Sustainable Energy*, 7(1), 108-117.
- [107] Wang, C. Y., & Srinivasan, V. (2002). Computational battery dynamics (CBD)—electrochemical/thermal coupled modeling and multi-scale modeling. *Journal of power sources*, 110(2), 364-376.
- [108] Fang, W., Kwon, O. J., & Wang, C. Y. (2010). Electrochemical–thermal modeling of automotive Li-ion batteries and experimental validation using a three-electrode cell. *International journal of energy research*, 34(2), 107-115.
- [109] Lee, K. J., Smith, K., Pesaran, A., & Kim, G. H. (2013). Three dimensional thermal-, electrical-, and electrochemical-coupled model for cylindrical wound large format lithium-ion batteries. *Journal of Power Sources*, 241, 20-32.
- [110] Khateeb, S. A., Farid, M. M., Selman, J. R., & Al-Hallaj, S. (2006). Mechanical–electrochemical modeling of Li-ion battery designed for an electric scooter. *Journal of Power Sources*, 158(1), 673-678.
- [111] Snyder, J. F., Carter, R. H., & Wetzel, E. D. (2007). Electrochemical and mechanical behavior in mechanically robust solid polymer electrolytes for use in multifunctional structural batteries. *Chemistry of materials*, 19(15), 3793-3801.
- [112] Golmon, S., Maute, K., & Dunn, M. L. (2009). Numerical modeling of electrochemical–mechanical interactions in lithium polymer batteries. *Computers & Structures*, 87(23), 1567-1579.
- [113] Angulakshmi, N., Thomas, S., Nahm, K. S., Stephan, A. M., & Elizabeth, R. N. (2011). Electrochemical and mechanical properties of nanochitin-incorporated PVDF-HFP-based polymer electrolytes for lithium batteries. *Ionics*, 17(5), 407-414.
- [114] Fu, R., Xiao, M., & Choe, S. Y. (2013). Modeling, validation and analysis of mechanical stress generation and dimension changes of a pouch type high power Li-ion battery. *Journal of Power Sources*, 224, 211-224.
- [115] Jeon, D. H., & Baek, S. M. (2011). Thermal modeling of cylindrical lithium ion battery during discharge cycle. *Energy Conversion and Management*, 52(8), 2973-2981.
- [116] Samba, A., Omar, N., Gualous, H., Firouz, Y., Van den Bossche, P., Van Mierlo, J., & Boubekour, T. I. (2014). Development of an advanced two-dimensional thermal model for large size lithium-ion pouch cells. *Electrochimica Acta*, 117, 246-254.
- [117] Zhang, C., Santhanagopalan, S., Sprague, M. A., & Pesaran, A. A. (2015). Coupled mechanical-electrical-thermal modeling for short-circuit prediction in a lithium-ion cell under mechanical abuse. *Journal of Power Sources*, 290, 102-113.
- [118] Kindermann, F. M., Keil, J., Frank, A., & Jossen, A. (2017). A SEI Modeling Approach Distinguishing between Capacity and Power Fade. *Journal of The Electrochemical Society*, 164(12), E287-E294.
- [119] Newman, J., Thomas, K. E., Hafezi, H., & Wheeler, D. R. (2003). Modeling of lithium-ion batteries. *Journal of power sources*, 119, 838-843.
- [120] Kim, S. P., Van Duin, A. C., & Shenoy, V. B. (2011). Effect of electrolytes on the structure and evolution of the solid electrolyte interphase (SEI) in Li-ion batteries: A molecular dynamics study. *Journal of Power Sources*, 196(20), 8590-8597.
- [121] Takenaka, N., Suzuki, Y., Sakai, H., & Nagaoka, M. (2014). On electrolyte-dependent formation of solid electrolyte interphase film in lithium-ion batteries: strong sensitivity to small structural difference of electrolyte molecules. *The Journal of Physical Chemistry C*, 118(20), 10874-10882.

- 
- [122] Turner, C. H., Zhang, Z. T., Gelb, L. D., & Dunlap, B. I. (2015). Kinetic Monte Carlo Simulation of Electrochemical Systems. *Rev. Comput. Chem*, 28, 175-204.
- [123] Methekar, R. N., Northrop, P. W., Chen, K., Braatz, R. D., & Subramanian, V. R. (2011). Kinetic Monte Carlo simulation of surface heterogeneity in graphite anodes for lithium-ion batteries: passive layer formation. *Journal of The Electrochemical Society*, 158(4), A363-A370.
- [124] Yu, J., Sushko, M. L., Kerisit, S., Rosso, K. M., & Liu, J. (2012). Kinetic Monte Carlo Study of Ambipolar Lithium Ion and Electron–Polaron Diffusion into Nanostructured TiO<sub>2</sub>. *The Journal of Physical Chemistry Letters*, 3(15), 2076-2081.
- [125] Blanquer, G., Yin, Y., Quiroga, M. A., & Franco, A. A. (2016). Modeling Investigation of the Local Electrochemistry in Lithium-O<sub>2</sub> Batteries: A Kinetic Monte Carlo Approach. *Journal of The Electrochemical Society*, 163(3), A329-A337.
- [126] Bedrov, D., Smith, G. D., & Van Duin, A. C. (2012). Reactions of singly-reduced ethylene carbonate in lithium battery electrolytes: a molecular dynamics simulation study using the ReaxFF. *The Journal of Physical Chemistry A*, 116(11), 2978-2985.
- [127] Wu, L., Lee, W. H., & Zhang, J. (2014). First principles study on the electrochemical, thermal and mechanical properties of LiCoO<sub>2</sub> for thin film rechargeable battery. *Materials Today: Proceedings*, 1(1), 82-93.
- [128] Xu, Z., Lv, X., Chen, J., Jiang, L., Lai, Y., & Li, J. (2017). DFT investigation of capacious, ultrafast and highly conductive hexagonal Cr 2 C and V 2 C monolayers as anode materials for high-performance lithium-ion batteries. *Physical Chemistry Chemical Physics*, 19(11), 7807-7819.
- [129] Ferguson, G., & Curtiss, L. A. (2013). Atomic-Level Modeling of Organic Electrolytes in Lithium-Ion Batteries. In *Applications of Molecular Modeling to Challenges in Clean Energy* (pp. 217-233). American Chemical Society.
- [130] Boyer, M. J., & Hwang, G. S. (2016). Recent progress in first-principles simulations of anode materials and interfaces for lithium ion batteries. *Current Opinion in Chemical Engineering*, 13, 75-81.
- [131] Dubarry, M., & Liaw, B. Y. (2007). Development of a universal modeling tool for rechargeable lithium batteries. *Journal of Power Sources*, 174(2), 856-860.
- [132] De, S., Northrop, P. W., Ramadesigan, V., & Subramanian, V. R. (2013). Model-based simultaneous optimization of multiple design parameters for lithium-ion batteries for maximization of energy density. *Journal of Power Sources*, 227, 161-170.
- [133] Xue, N., Du, W., Gupta, A., Shyy, W., Sastry, A. M., & Martins, J. R. (2013). Optimization of a single lithium-ion battery cell with a gradient-based algorithm. *Journal of The Electrochemical Society*, 160(8), A1071-A1078.
- [134] Dai, Y., & Srinivasan, V. (2016). On graded electrode porosity as a design tool for improving the energy density of batteries. *Journal of The Electrochemical Society*, 163(3), A406-A416.
- [135] Pourmirzaagha, H., Esfahanian, V., Sabetghadam, F., & Torabi, F. (2016). Single and multi-objective optimization for the performance enhancement of lead–acid battery cell. *International Journal of Energy Research*, 40(14), 1966-1978.
- [136] Du, W., Xue, N., Gupta, A., Sastry, A. M., Martins, J. R., & Shyy, W. (2013). Optimization of LiMn<sub>2</sub>O<sub>4</sub> electrode properties in a gradient-and surrogate-based framework. *Acta Mechanica Sinica*, 29(3), 335-347.
- [137] Du, W., Xue, N., Shyy, W., & Martins, J. R. (2014). A surrogate-based multi-scale model for mass transport and electrochemical kinetics in lithium-ion battery electrodes. *Journal of the Electrochemical Society*, 161(8), E3086-E3096.

- 
- [138] Golmon, S., Maute, K., & Dunn, M. L. (2012). Multiscale design optimization of lithium ion batteries using adjoint sensitivity analysis. *International Journal for Numerical Methods in Engineering*, 92(5), 475-494.
- [139] Golmon, S., Maute, K., & Dunn, M. L. (2014). A design optimization methodology for Li+ batteries. *Journal of Power Sources*, 253, 239-250.
- [140] Svanberg, K. (1987). The method of moving asymptotes—a new method for structural optimization. *International journal for numerical methods in engineering*, 24(2), 359-373.
- [141] Kim, J., Kim, S., Kim, S., Lim, W., Jang, J., Kim, Y., Yang, W., & Lee, T. H. Design optimization of lithium-ion battery using hybrid electric vehicle simulation model. *Proc. International Electric Vehicle Symposium and Exhibition (EVS'28), Goyang, Korea, May 3-6, 2015*.
- [142] Nielsen, H. B., Lophaven, S. N., & Søndergaard, J. (2002). DACE, a MATLAB Kriging toolbox. *Informatics and mathematical modelling*. Lyngby–Denmark: Technical University of Denmark, DTU.
- [143] Hosseinzadeh, E., Marco, J., & Jennings, P. (2017). Electrochemical-Thermal Modelling and Optimisation of Lithium-Ion Battery Design Parameters Using Analysis of Variance. *Energies*, 10(9), 1278.
- [144] Xue, N., Du, W., Greszler, T. A., Shyy, W., & Martins, J. R. (2014). Design of a lithium-ion battery pack for PHEV using a hybrid optimization method. *Applied Energy*, 115, 591-602.
- [145] Suthar, B., Ramadesigan, V., De, S., Braatz, R. D., & Subramanian, V. R. (2014). Optimal charging profiles for mechanically constrained lithium-ion batteries. *Physical Chemistry Chemical Physics*, 16(1), 277-287.
- [146] Suthar, B., Northrop, P. W., Braatz, R. D., & Subramanian, V. R. (2014). Optimal charging profiles with minimal intercalation-induced stresses for lithium-ion batteries using reformulated pseudo 2-dimensional models. *Journal of The Electrochemical Society*, 161(11), F3144-F3155.
- [147] Rajabloo, B., Désilets, M., & Choquette, Y. Parameter Estimation of Single Particle Model Using COMSOL Multiphysics and MATLAB Optimization Toolbox. In *Proceedings of the 2015 COMSOL Conference in Boston*.
- [148] Klein, R., Chaturvedi, N. A., Christensen, J., Ahmed, J., Findeisen, R., & Kojic, A. (2011, June). Optimal charging strategies in lithium-ion battery. In *American Control Conference (ACC), 2011 (pp. 382-387)*. IEEE.
- [149] Suthar, B., Ramadesigan, V., Northrop, P. W., Gopaluni, B., Santhanagopalan, S., Braatz, R. D., & Subramanian, V. R. (2013, June). Optimal control and state estimation of lithium-ion batteries using reformulated models. In *American Control Conference (ACC), 2013 (pp. 5350-5355)*. IEEE.
- [150] Liu, J., Li, G., & Fathy, H. K. (2016). A computationally efficient approach for optimizing lithium-ion battery charging. *Journal of Dynamic Systems, Measurement, and Control*, 138(2), 021009.
- [151] Moura, S. J., Forman, J. C., Bashash, S., Stein, J. L., & Fathy, H. K. (2011). Optimal control of film growth in lithium-ion battery packs via relay switches. *IEEE Transactions on Industrial Electronics*, 58(8), 3555-3566.
- [152] Bashash, S., Moura, S. J., Forman, J. C., and Fathy, H. K., 2011, “Plug-In Hybrid Electric Vehicle Charge Pattern Optimization for Energy Cost and Battery Longevity,” *J. Power Sources*, 196(1), pp. 541–549.

- 
- [153] Mamun, A.-A., Narayanan, I., Wang, D., Sivasubramaniam, A., and Fathy, H. K., 2015, "Multi-Objective Optimization to Minimize Battery Degradation and Electricity Cost for Demand Response in Datacenters," ASME Paper No. DSCC2015-9812.
- [154] Rahimian, S. K., Rayman, S., and White, R. E., 2011, "Optimal Charge Rates for a Lithium Ion Cell," *J. Power Sources*, 196(23), pp. 10297–10304.
- [155] Hu, X., Li, S., Peng, H., and Sun, F., 2013, "Charging Time and Loss Optimization for LiNMC and LiFePO<sub>4</sub> Batteries Based on Equivalent Circuit Models," *J. Power Sources*, 239, pp. 449–457.
- [156] Pathak, M., Sonawane, D., Santhanagopalan, S., & Subramanian, V. R. (2016, September). Analyzing and Minimizing Capacity Fade through Model Predictive Control-Theory and Experimental Validation. In Meeting Abstracts (No. 6, pp. 912-912). The Electrochemical Society.
- [157] Torchio, M., Magni, L., Braatz, R. D., & Raimondo, D. M. (2016, December). Optimal charging of a Li-ion cell: A hybrid Model Predictive Control approach. In Decision and Control (CDC), 2016 IEEE 55th Conference on (pp. 4053-4058). IEEE.
- [158] Suthar, B., Northrop, P. W., Rife, D., & Subramanian, V. R. (2015). Effect of Porosity, Thickness and Tortuosity on Capacity Fade of Anode. *Journal of The Electrochemical Society*, 162(9), A1708-A1717.
- [159] Dandurand, B., Guarneri, P., Fadel, G., & Wiecek, M. M. (2013). Equitable multi-objective optimization applied to the design of a hybrid electric vehicle battery. *Journal of Mechanical Design*, 135(4), 041004.
- [160] Kostreva, M. M., Ogryczak, W., & Wierzbicki, A. (2004). Equitable aggregations and multiple criteria analysis. *European Journal of Operational Research*, 158(2), 362-377.
- [161] Northrop, P. W., Pathak, M., Rife, D., De, S., Santhanagopalan, S., & Subramanian, V. R. (2015). Efficient simulation and model reformulation of two-dimensional electrochemical thermal behavior of lithium-ion batteries. *Journal of The Electrochemical Society*, 162(6), A940-A951.
- [162] Song, X., Diaz, A. R., Benard, A., & Nicholas, J. D. (2013). A 2D model for shape optimization of solid oxide fuel cell cathodes. *Structural and Multidisciplinary Optimization*, 47(3), 453-464.
- [163] Song, X., Diaz, A. R., & Benard, A. (2013). A 3D topology optimization model of the cathode air supply channel in planar solid oxide fuel cell. In Proceedings of the 10th World Congress on Structural and Multidisciplinary Optimization, Orlando, Florida.
- [164] Hasanabadi, A., Baniassadi, M., Abrinia, K., Safdari, M., & Garmestani, H. (2016). Optimization of solid oxide fuel cell cathodes using two-point correlation functions. *Computational Materials Science*, 123, 268-276.
- [165] Mitchell, S. L., & Ortiz, M. (2016). Computational multiobjective topology optimization of silicon anode structures for lithium-ion batteries. *Journal of Power Sources*, 326, 242-251.
- [166] Hong, Y., & Lee, C. W. (2016). The Multiobjective Optimal Design Problems and their Pareto Optimal Fronts for Li-Ion Battery Cells (No. 2016-01-1199). SAE Technical Paper.
- [167] Liu, C., & Liu, L. (2017). Optimal Design of Li-Ion Batteries through Multi-Physics Modeling and Multi-Objective Optimization. *Journal of The Electrochemical Society*, 164(11), E3254-E3264.
- [168] Liu, C., & Liu, L. (2017). Optimizing Battery Design for Fast Charge through a Genetic Algorithm Based Multi-Objective Optimization Framework. *ECS Transactions*, 77(11), 257-271.
- [169] Lizotte, D. J., Wang, T., Bowling, M. H., & Schuurmans, D. (2007, January). Automatic Gait Optimization with Gaussian Process Regression. In IJCAI (Vol. 7, pp. 944-949).

- 
- [170] Marchant, R., & Ramos, F. (2012, October). Bayesian optimisation for intelligent environmental monitoring. In *Intelligent Robots and Systems (IROS), 2012 IEEE/RSJ International Conference on* (pp. 2242-2249). IEEE.
- [171] Snoek, J., Larochelle, H., & Adams, R. P. (2012). Practical bayesian optimization of machine learning algorithms. In *Advances in neural information processing systems* (pp. 2951-2959).
- [172] Notten, P. H., Roozeboom, F., Niessen, R. A., & Baggetto, L. (2007). 3-D integrated all-solid-state rechargeable batteries. *Advanced Materials*, 19(24), 4564-4567.
- [173] Sun, K., Wei, T. S., Ahn, B. Y., Seo, J. Y., Dillon, S. J., & Lewis, J. A. (2013). 3D printing of interdigitated Li-Ion microbattery architectures. *Advanced Materials*, 25(33), 4539-4543.
- [174] Chamran, F., Yeh, Y., Min, H. S., Dunn, B., & Kim, C. J. (2007). Fabrication of high-aspect-ratio electrode arrays for three-dimensional microbatteries. *Journal of Microelectromechanical Systems*, 16(4), 844-852.
- [175] Lu, W., Jansen, A., Dees, D., Nelson, P., Veselka, N. R., & Henriksen, G. (2011). High-energy electrode investigation for plug-in hybrid electric vehicles. *Journal of Power Sources*, 196(3), 1537-1540.
- [176] Sakti, A., Michalek, J. J., Fuchs, E. R., & Whitacre, J. F. (2015). A techno-economic analysis and optimization of Li-ion batteries for light-duty passenger vehicle electrification. *Journal of Power Sources*, 273, 966-980.
- [177] Arthur, T. S., Bates, D. J., Cirigliano, N., Johnson, D. C., Malati, P., Mosby, J. M., ... & Dunn, B. (2011). Three-dimensional electrodes and battery architectures. *Mrs Bulletin*, 36(7), 523-531.
- [178] Bates, J. B., Dudney, N. J., Lubben, D. C., Gruzalski, G. R., Kwak, B. S., Yu, X., & Zuhr, R. A. (1995). Thin-film rechargeable lithium batteries. *Journal of Power Sources*, 54(1), 58-62.